CONTINUOUS ELECTROKINETIC DEWATERING OF PHOSPHATIC CLAY SUSPENSIONS

By

RUI KONG

A DISSERTATION PRESENTED TO THE GRADUATE SCHOOL
OF THE UNIVERSITY OF FLORIDA IN PARTIAL FULFILLMENT
OF THE REQUIREMENTS FOR THE DEGREE OF
DOCTOR OF PHILOSOPHY

UNIVERSITY OF FLORIDA

2015

To my parents

ACKNOWLEDGMENTS

I would like to thank my advisor, Professor Mark Orazem, for his support and guidance. I thank Professors Saeed Moghaddam, David Bloomquist, Spyros Svoronos, and Kirk Ziegler, for their kind support in my research. I would like to thank Paul Kucera, Bryan Baylor and Charles (Yichang) Guan, of Mosaic Fertilizer, LLC, for their involvement in sponsoring this project. I would like to recognize my team members, Yuelong Huang, Han Lai, Dazhi Yu, David Horner for their significant contribution toward the completion of the research work. Finally, I would like to thank my parents, for their love, encouragement, and guidance.

TABLE OF CONTENTS

LIST OF TABLES

LIST OF FIGURES

LIST OF SYMBOLS

Roman

A	ventilation cross-sectional area, m^2
a	parameter defined in Equation 4–2
b	parameter defined in Equation 4–2
C_{ppm}	hydrogen concentration, ppm
c	parameter defined in Equation 4–2
d	distance between cathode and anode in cake formation zone, cm
E	electric field, V/cm
$E_{req,s}$	energy consumption for removal of solids, Wh/kg_{solids}
$E_{req,w}$	energy consumption for removal of water, Wh/kg_{H_2O}
F	Faraday's constant, 96487 C/equiv
I	total current, A
k	nonideal mixing factor
L	length of electrode, m
M_{H_2}	molecular weight of hydrogen gas, 2×10^{-3}kg/mol
m_{beaker}	mass of an empty beaker, kg
m_{wet}	total mass of beaker and wet clay, kg
m_{dry}	total mass of beaker and dry clay, kg
m_{total}	total mass of thickened clay in continuous operation, kg
n	parameter defined in Equation 4–2
n_e	number of electrons transferred in a reaction

P	pressure, N/m^2
P_{req}	power consumption, W
p	parameter defined in Equation 3–2
q	parameter defined in Equation 3–2
Q_{in}	influent volumetric flow rate of clay slurry, m^3/s
$Q_{m,w}$	mass flow rate of the supernatant water, kg/h
$Q_{m,f}$	mass production rate of the thickened clay, kg/h
$Q_{m,s}$	mass production rate of the dry clay, kg/h
Q_m	hydrogen evolution rate, kg/s
Q_{out}	volumetric flow rate of supernatant water, m^3/s
Q_v	ventilation rate, m^3/s
R	Universal gas constant, 8.3143 J/mol K
T	temperature, K
T_w	turbidity of supernatant water, NTU
t	operation time, hours
$\overline{u}$	average wind velocity for ventilation, m/s
V_{cell}	cell potential, V
v_{belt}	belt speed, m/h
w_f	final solids content of clay, wt%
w_{in}	initial solids content of clay, wt%
x	location on the cake dewatering zone refers to a defined point, cm

Greek

Δm_{w}	mass of water removed, kg
Δw	change in solids content of clay, wt%
δ	thickness of clay cake in cake dewatering zone, cm
ρ_{in}	density of influent clay slurry, kg/m^3
ρ_{w}	density of water, kg/m^3
τ	residence time, hours

Subscripts

1	pertaining to operation at a bench-scale in a fume hood
2	pertaining to operation at an industrial scale

Abstract of Dissertation Presented to the Graduate School
of the University of Florida in Partial Fulfillment of the
Requirements for the Degree of Doctor of Philosophy

CONTINUOUS ELECTROKINETIC DEWATERING OF PHOSPHATIC CLAY SUSPENSIONS

By

Rui Kong

May 2015

Chair: Mark E. Orazem
Major: Chemical Engineering

Many mining operations produce a dilute suspension of solids that, due to the properties of the suspended solids, take from 25 to 50 years to consolidate by hindered settling. The objective of this work was to develop an electrokinetic separation process that was applied to phosphatic clay suspensions generated by the mining and beneficiation of phosphate ores. The use of electric field to effect separation is attractive because the stability of the suspensions is caused, in part, by the charged character of the suspended particles. Previously reported work has demonstrated the feasibility of batch-wise electrokinetic separation of phosphatic clay suspensions, but the process is widely regarded to be uneconomical. The present work is predicated on the assumption that an economically feasible separation requires development of a fully-continuous electrokinetic separator.

A systematic progression of prototypes was developed and used to explore the concepts needed to develop a fully-continuous separator. The evolution of prototype design was guided by a constitutive relationship that was discovered in previous work and found to apply, with different values for adjustable parameters, to each of the prototypes. To explore the production of clarified water, a semi-continuous prototype was designed that retained thickened solids and produced a stream of low turbidity water. This process demonstrated that, when combined with gravity settling, clarified water could be produced with turbidity levels lower than 10 NTU. The residence time required for gravity settling

was less than 24 hours. The subsequent semi-continuous prototype was designed to remove solids by use of a fabric belt that moved across the anode. Design parameters for the belt were identified. The key parameter was found to be the open area of the belt, which, to minimize potential losses, should be at least 50 %. The belt design proved to be efficient, and a solids content of roughly 25 wt% was produced. The belt design was implemented in the first-generation fully-continuous prototype, in which solids were collected on the belt in a horizontal configuration and then removed from the cell by redirecting the belt to an incline. The performance of the first-generation prototype was poor. A solids content of only 20 wt% could be achieved. The second-generation fully-continuous prototype comprised a cake formation zone and a cake dewatering zone. A solids content as high as 35-40 wt% could be achieved.

The improvement in economic feasibility is evident in a comparison of benchmark values to those obtained by application of previous bench-scale experiments to estimation of power and energy requirements for batch-wise dewatering of a clay settling area. McKinney and Orazem reported that the power requirement for dewatering a clay-settling pond at the Four-Corners Mine in Bartow, Florida from a solids content of 10 wt% to 25 wt% would be 44,000 MW. The power requirement for continuous dewatering of the output of the Four-Corners Mine to a higher solids content of 35 wt% was estimated to be as low as 29 MW. The improvement of efficiency is seen in the reduction of the energy consumption from 41.3 Wh/kg_{H_2O} of reclaimed water for the batch dewatering of a clay settling pond to 6.6 Wh/kg_{H_2O} for the continuous process. These figures may be expressed in terms of dry solids produced as 248 Wh/kg_{solids} and 47 Wh/kg_{solids}, respectively. It is important to recognize that the improvement in energy efficiency was obtained while increasing the final solids content from 25 wt% to 35 wt%. The efficiency of the present configuration can be improved further by optimization of the cake formation and cake dewatering zones. While the process was developed for processing phosphatic

clay suspensions, it is anticipated that the electrokinetic dewatering may be applied as well for other mining operations such as associated with the oil sand tailings in Canada.

CHAPTER 1
INTRODUCTION

Phosphatic clay suspensions, a waste effluent from the beneficiation process of phosphate mining industry, are produced with solids content of 2-3 wt%. If allowed free-settling for several days, the solids would settle by gravity to reach the solids content of around 10 wt%. By adding polymer flocculant, the 10 wt% solids content would be achieved immediately. However, for the purpose of solids and water recovery and the land reclamation, the solids content needs to reach about 30 wt%. The process that increases solids content from 10 wt% to 30 wt%, unfortunately, would take several decades if settled by gravity only. In Florida, the phosphatic clay suspension is stored in a clay settling area, in the form of a one square mile clay settling pond near the mining site. After July 1, 1975, a Florida law mandated the restoration of all mined land, which encouraged research on the fast dewatering of phosphatic clay.

The movement of clay particles in suspension under the influence of electric field was first observed by Reuss in 1808[1]. Subsequent researchers have demonstrated the capability of electrokinetic dewatering to increase the solids content in several hours with batch experiments, but the poor economic feasibility hindered the further development of this technology. The object of this work is to develop prototypes for continuous operation of electrokinetic dewatering of phosphatic clay, which would reduce the energy consumption.

The first prototype, presented in Chapter 3, was designed to recover supernatant water. The 10 wt% clay slurry was pumped continuously into a plastic storage box used as the reservoir. A pair of mesh electrodes were suspended in the tank, and the water was removed from clay under the influence of electric field. A stream of low-turbidity water was obtained continuously from overflow during pseudo-steady-state operation. The thickened clay was accumulated in tank between the electrodes. The effluent water had the turbidity lower than 10 NTU, which could be recycled for process water.

The second prototype, presented in Chapter 4, was designed to recover solids. The modification was made based on the first prototype. A conveyor belt was implemented surrounding the anode plate. With the movement of the conveyor belt, thickened clay was removed continuously from the slurry. The clay solids content was observed to increase from 10 wt% to 25 wt% with a residence time of one hour.

The third prototype, presented in Chapter 5, was designed to remove continuously both supernatant water and thickened clay from the 10 wt% clay suspension. The system was constructed as a combination of two zones: the clay formation zone and the clay dewatering zone. The clay formation zone removed water from clay suspension and produced the thickened clay with the solids content of about 20 wt%. In the clay dewatering zone, the thickened clay was moved out of water while still under electrokinetic dewatering. The final solids content increased to 35 wt% with an electric field of 1 V/cm, and the energy consumption was only 47 Wh/kg_{solids}. An economic analysis is presented in Chapter 6.

CHAPTER 2
LITERATURE REVIEW

The phosphatic clay slurries, a waste stream with solids content of 2-3 wt% produced from beneficiation process, poses major environmental issues in phosphate mining industry. The requirement of water recycling and mined land reclamation needs a solution for fast clay settlement and consolidation. A literature review of the problem and potential dewatering technologies is presented in this chapter. The recent development of electrokinetic dewatering on different materials is also discussed.

2.1 Phosphate Mining in Florida

The element Phosphorus, as the main component in phosphate fertilizer, is extracted from phosphate rock for industrial production. China, Morocco, and United States are the leading countries of phosphate rock production, as shown in Figure 2-1. From the 2015 Mineral Commodity Summaries of U.S. Geological Survey[21], the largest phosphate production is from China, and the biggest phosphate deposit reserves are in Morocco and Western Sahara, representing 74.6 percent of the world total reserve. The United States produced an estimated 27.1 million metric tons of phosphate rock in 2014, representing 12.3 percent of the world production.

Phosphate mining in Florida began in the 1880s, conducted on river pebble or land pebble by hand pick and shovel in the Peace River area near Arcadia[22]. Since 1920s, the introduction of electric dragline excavators greatly increased the mining capacity, while at the meantime, produced a large quantity of waste streams.

Phosphate ores are mined in seven locations in Florida and represented 65 percent of domestic production in 2011[23]. The phosphatic clay suspensions, representing a major waste product of the Florida phosphate mining industry, raises environmental concerns for phosphate mining companies[24]. Under gravity, the clay settling and consolidation process requires decades to reach a solids content of 20-25 wt% for which reclamation

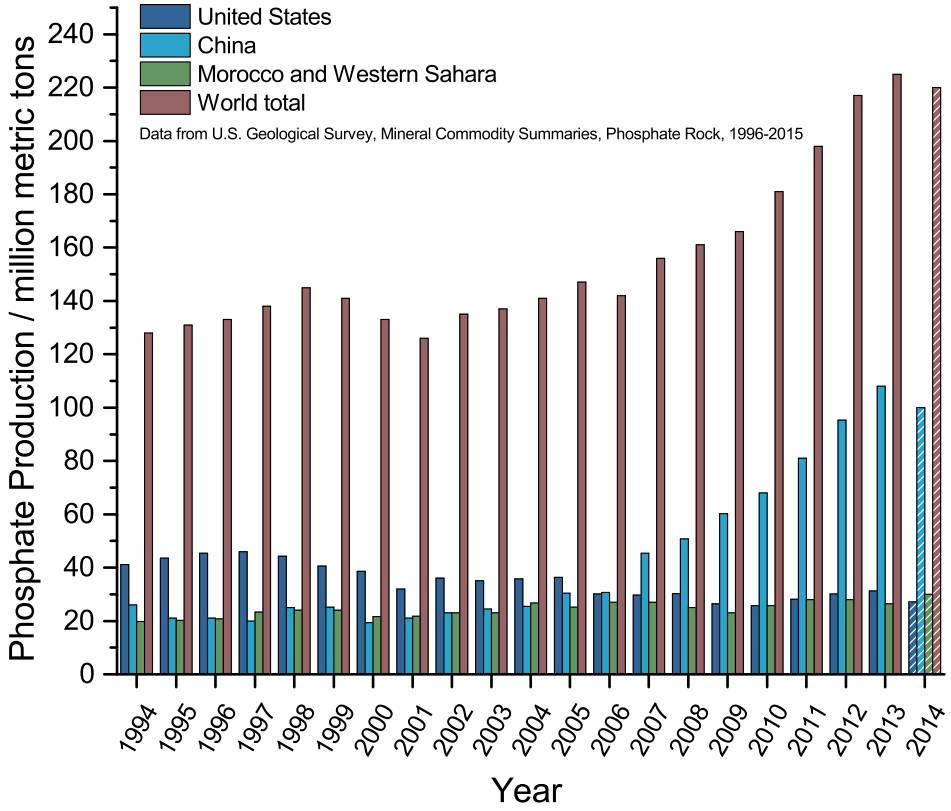

Figure 2-1. The phosphate production in major counties from 1994 to 2014. The data of year 2014 is an estimation. All data from U.S. Geological Survey, Mineral Commodity Summaries, Phosphate Rock[2–21].

becomes possible. These clay settling areas currently cover an area of over 100,000 acres in Florida, which is approximately 30% of the mined land[25].

Phosphate-deposits containing carbonate-fluorapatite (francolite), quartz, dolomite, and clay minerals[26] are the primary source of phosphoric acid, which is an intermediate in production of phosphate fertilizers. The phosphate mining operation today in Florida is a strip-mining process. Draglines are used to remove the 15-50 feet of top layer of earth (referred to as overburden) to expose the desired matrix layer that has a thickness of 10-20 feet[27]. The phosphate matrix is comprised of roughly equal mass fractions of phosphate ore, sand, and clay[28]. The matrix is mixed with a large quantity of water and sent to beneficiation plant. During the beneficiation process, phosphate rock is separated from sand and clay, and sent to a processing plant to produce the final phosphate product.

Sand is returned to fill mine pits for land reclamation. The phosphatic clay suspension, which has an initial solids content of 2-3 wt%, is pumped to large retention ponds and allowed to settle. The clay settling pond, usually in the area of one square mile, would take several decades for reclamation.

In the early years of phosphate mining in Florida, there is not mandatory regulation for restoring the Clay Settling Areas (CSAs). The number of clay settling ponds increased dramatically with the improved phosphate mining technology over the years of mining. In 1954, Tyler and Waggaman discussed the potential of recovering phosphate material from the phosphatic clay slurry[29]. In the year of 1975, a Florida state law came into effect which required reclamation of all mined land. This motivated the phosphate mining companies to discover clay dewatering technologies which would accelerate the reclamation process for mined land.

2.2 Property of Clay Particles

The properties of Florida phosphate clay lead to the difficulty of sedimentation and consolidation. The grain size of phosphate clay particles is around 10 μm, and the particle itself, because of lattices defects and ion replacement, has a negative charge on surface. The small particle size reduces the influence of gravity settling, and the big relative surface area with negative charge increases the stability of the suspension by particle repulsion. The bond between clay particle and water is very strong.

2.3 Dewatering Technologies

Numerous methods have been attempted in the search for a better clay dewatering process. Flocculation is used mainly for clarification processes, to improve water quality. Mechanical dewatering methods are mainly used for thickening.

2.3.1 Flocculation

Flocculants are widely used for solid-liquid separation. The process of flocculation is to form large agglomerates of particles by adding high molecular weight polymers such as polyethylene oxide and polyacrylamide to the clay suspension. The formed larger clusters

settle easily by gravity. A large variety of flocculating materials are used in industry for water clarification, paper making, and mineral processing[30]. The polyacrylamides was used to aid dewatering the phosphatic clay suspension followed by the hydrocyclone separation[31]. A specific type of flocculants, named Unique Molecular Architecture flocculant, was reported on the sedimentation performance of a clay suspension[32]. A methyl acrylate based flocculant with ultra high molecular weight was developed and showed good performance on sludge dewatering[33].

The flocculation method is mostly used for the clarification of wastewater to obtain a good water quality. In the phosphate mining industry flocculants are used for treatment of clay slurry to achieve a 10 wt% solids content from 3 wt%. However, the solids content could not be increased further by flocculation alone.

2.3.2 Mechanical Dewatering

Mechanical dewatering technologies are widely used for treatment of wastewater sludge. A well-accepted theory in the clay dewatering field considers water in the suspension system could be divided into four layers: free water, interstitial water, vicinal water, and the water of hydration[34]. The free water, also named bulk water, is the water that is able to move freely and is not affected by solids. The free water is the easiest to remove. The interstitial water is trapped in flocs or microbial cells, and could become free water if flocs or cells are destroyed. The vicinal water is closely attached to the solids surface without free movement. The water of hydration is chemically bound to the solids and can be removed only by thermal drying. The traditional mechanical dewatering techniques are able to remove the bulk water and part of the interstitial water. The techniques corresponding to the ability of removing identical layer of water were reviewed and discussed by Vaxelaire and Cézac for activated sludge[35].

The method of mechanical dewatering for the treatment of sewage sludge could be represented by belt filter press[36, 37] and centrifuge[37, 38]. As indicated in its name, this is the method using mechanical force to remove water from clay suspensions. It is not

easy to achieve sufficient low water content with this method as only free water can be removed with mechanical force. To achieve better separation by removing the interstitial water and vicinal water, the mechanical method is often combined with other methods. A belt filter press was made with conductive filter material to add an electric field to assist separation[39]. A centrifuge with a subsequence thermal drying was used to produce high solids content sludge[40]. The development was extended to magnetic mechanical dewatering and acoustic mechanical dewatering[41].

2.3.3 Electrokinetic Dewatering

Although there were several options available for the dewatering of phosphatic clay suspensions, none of them could completely solve the problem from both performance and economic aspects. The settling of clay by adding flocculants is convenient, but the solids content was increased to only 10 wt%. The addition of extra chemicals would also be considered a potential problem for land reclamation. Mechanical dewatering is able to achieve a considerable high clay solids content, but the energy cost is usually high and not feasible for on-site implementation. Electrokinetic dewatering is presented in this section to be an appropriate alternative technology.

2.3.3.1 Electrokinetic Phenomenon

The movement of clay particles in suspension induced by electric field was first observed and reported by Reuss in 1808[1], shortly after the world's first real battery (voltaic pile) was invented by Volta in 1800[42]. The electrokinetic phenomena was discussed using the mathematical concept of double layer theory[43]. A systematic experiment on the exploration of operation parameters was conducted in 1942, using Georgia kaolin as the clay material[44]. A detailed history of electrokinetic phenomena was reviewed by Wall[45].

The electrokinetic phenomenon was conventionally defined to include both electrophoresis and electro-osmosis, representing respectively the movement of solids in suspension and the movement of water in the porous structure. Since the clay particle has negative charge

on the surface, it tends to move towards the anode in the electric field. The electrophoresis dominates at the beginning of electrokinetic dewatering process, accumulating the clay particles at the anode. With the increase of solids content, the clay particles form a porous cake structure, the water moves to the cathode, and electro-osmosis dominates.

2.3.3.2 Applications of Electrokinetic Phenomenon

Electrokinetic concepts have been widely used in the field of soil and water treatment. Electokinetic remediation was used to extract heavy metal such as Zn, Ni[46], copper, chromium, and arsenic[47, 48] from contaminated soil. It was also used to enhance the delivering of bioremediation additives for remediation of low-permeability clay contaminated by chlorinated solvents[49].

2.3.3.3 Electrokinetic Dewatering of Mine Tailings

Electrokinetic dewatering has been considered for treatment of mine tailings world wide, including the oil sand tailings in Canada[50, 51], the tailings of ancient dunes mining in South Africa[52], the kimberlite slimes from diamond mine tailings in southern Africa[53], the West Mine tailings in Western Australia[54], and glass sand plant tailings in Turkey[55].

Johnson and Davis conducted electrophoretic clarification on colloidal suspensions of coal-washing effluent[56]. They studied the electrokinetic clarification of effluent from a coal-washing facility. An apparatus was designed to be capable of running either batch or semi-continuous operation[57]. A mathematical analysis was developed to account for the motion of charged particle in suspension and the conductivity of the suspension using the Navier-Stokes equation and finite-difference method[58].

Shang used a bench-top electrokinetic cell to evaluate the electrokinetic dewatering of three natural clay slurries: a phosphatic clay from Florida, a brown and a grey clay from Ontario, Canada[59]. The operation parameters were also evaluated on the experiment of using electrokinetic dewatering to generate engineered soil covers[60]. The electrokinetic process was concluded to be influenced by both internal and external factors. The

internal factors were associated with clay properties. The external factors were operation parameters including current density, electrode materials, and electrode configuration[61]. Thus, proper design could improve the electrokinetic dewatering efficiency by optimizing the operation parameters.

Glendinning et al. developed a polymer-based conductive material as an electrode for the electrokinetive dewatering of sewage sludge[62] and applied this material into a wide range of hydraulic applications[63]. Glendinning et al. suggested that the electroosmosis flow rate decreased with time if constant voltage was applied and was constant if constant current was applied[64].

Various designs have been attempted to optimize the process by modifying the external factors, such as a rotating anode[65], an electrokinetic belt filter press[39, 66, 67], an electrokinetic bag[63], and in-situ electrokinetic consolidation[52]. It has been pointed out that the electrokinetic dewatering power consumption tends to be reduced if applied on large-scale installation instead of lab-scale experiment. The power consumption also depends heavily on clay materials. A higher power consumption was found for smectite clays than for kaolin clays[68]. Despite these attempts, process equipment based on electrokinetics have not made the transition from lab-scale prototype to on-site industrial application due, in part, to the high energy requirement which makes it economically unfeasible.

Previous lab-scale batch experiments described by McKinney and Orazem[69] demonstrated the effects of electrokinetic dewatering. Under the influence of an electric field, the feed suspension could be separated into a water-rich phase and a solids-rich phase. A constitutive relationship was identified that related the increase of the solids content of the solids-rich phase to elapsed time and applied electric field. The solids content increased with an increasing operation time and electric field in a short period and depended only on electric field at longer times. An economic analysis, performed using boundary-element calculations and using the constitutive relationship, showed that energy

consumption for batch dewatering of a clay-settling impoundment with a one square mile Clay Settling Areas (CSAs) would be in a reasonable range, but the power consumption was too high[70].

The objective of this work was to explore the potential of fully-continuous operation as a means to effect separation at a low power consumption while maintaining a low energy consumption.

CHAPTER 3
SEMI-CONTINUOUS PROTOTYPE FOR WATER RECOVERY

The semi-continuous prototype described in this chapter represents an intermediate step in a series of prototypes for electrokinetic dewatering of phosphatic clay suspensions[71]. It serves as a transition between batch experiments and fully-continuous experiments. By helping to explore the ability of electrokinetic technology to continuously remove water, the semi-continuous prototype is expected to facilitate the design of a fully-continuous prototype.

3.1 Experimental

The experimental system allowed semi-continuous operation into which a dilute particulate suspension was continuously fed and supernatant liquid was continuously removed. The thickened solids accumulated in the tank.

3.1.1 Cell Design

A schematic representation of the deep-tank semi-continuous electrokinetic separator is presented in Figure 3-1. A plastic storage box with the dimensions of 88.9 cm $\times$ 42.5 cm $\times$ 32.7 cm was used as the container. Two mesh plate electrodes were suspended in the tank at an adjustable height. Both cathode and anode were made of titanium with an iridium oxide coating (Water Star Inc.). These electrodes had minimal surface overpotential for hydrogen evolution and oxygen evolution reactions, respectively, thus maximizing the ohmic potential drop. The use of suspended electrodes served to provide more space under the anode. This space functioned as a reservoir for solids-rich suspensions, thereby expanding the pseudo-steady-state period. The dilute feed suspensions were pumped into one end of the tank at a controlled flow rate. The fine particles moved downward under the influence of the electric field, forming a cake on the anode. When particles passed through the anode, they settled and accumulated at the tank bottom by gravity, creating a solids-rich suspension. The supernatant water, with low solids content, was removed by gravity flow through a sharp-edged weir at the other end

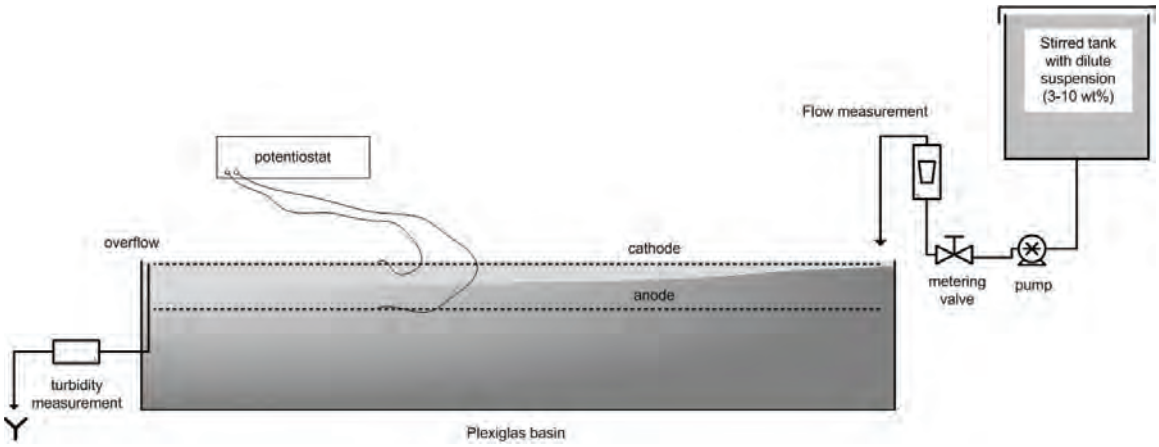

Figure 3-1. Schematic representation of the deep-tank semi-continuous electrokinetic dewatering system.

of the tank. Once the capacity of the tank to store accumulated solids was exceeded, the pseudo-steady-state operation was concluded, and the experiment was terminated.

3.1.2 Feed Suspensions

The tank was filled with suspensions provided by the Mosaic Fertilizer, LLC, from their Four Corners Phosphate Mine. These were pretreated by flocculant addition and then allowed to reach an solids content of around 10 wt%. The particle distribution analysis demonstrates that 90% of the particles had a diameter of less than 60 microns and about 65% had a diameter of less than 2 microns. The overall zeta potential of the untreated suspension was -20.1 mV. The suspended solids included silica, residual phosphate ore, and clay[69, 72].

3.1.3 Experimentation Protocol

The tank, with suspended anode and cathode, was initially filled with feed solution. At $t = 0$, the pump delivering the feed was started and the electrical potential was applied under potentiostatic conditions. To avoid unattended operation, the pump and application of electrical power were discontinued overnight and resumed in the following morning. In previous work, McKinney and Orazem[69] demonstrated that intermittent operation did not adversely influence the observed trends in batch experiments. The present results show that, for semi-continuous operation, trends were unaffected by the intermittent operation.

Supernatant water samples were collected throughout the electrokinetic separation process at 30-minute intervals. Turbidity and pH measurements were conducted on the supernatant water immediately after collection and after 24 hours of in-cell free settling. For samples with turbidity values in excess of 1000 NTU, the original sample was diluted, and the recorded turbidity value was calculated from the product of the reading value and the dilution ratio.

After the completion of the experiment, water was removed from the volume above the anode, and phosphatic clay samples were collected. A plastic cylinder of 28 cm in length and 2.6 cm in diameter was used to collect samples. The upper opening was covered after the cylinder was inserted straight into the clay such that, due to air pressure, the clay sample remained in cylinder when it was pulled out of the tank. As electrodes covered nearly the entire surface area of the tank, sampling locations were selected at an approximately 15 cm interval.

The solids content was calculated by measuring mass loss by evaporation. An empty 250 ml beaker was weighed, represented by m_{beaker}. Then the clay sample was transferred to beaker, weighed as m_{wet}. The beaker with wet clay was then put into the oven to dry. After drying, the beaker was measured again, recorded as m_{dry}. The solids content was then calculated from

$$w_{\text{f}} = \frac{m_{\text{dry}} - m_{\text{beaker}}}{m_{\text{wet}} - m_{\text{beaker}}} \times 100\% \tag{3–1}$$

Samples were taken before and after each experiment to calculate the increase of solids content.

3.1.4 Instrumentation

The potential between cathode and anode was provided by a Mastech Model HY10010EX DC Power Supply (range: potential 0-100 V, current 0-10 A). The feed flow rate of phosphatic clay suspensions was controlled by a Masterflex Model 77202-60 digital pump (Cole-Parmer Instrument Company). The turbidity of supernatant water was measured using a HACH 2100Q Portable Turbidimeter (range: 0-1000 NTU).

A B

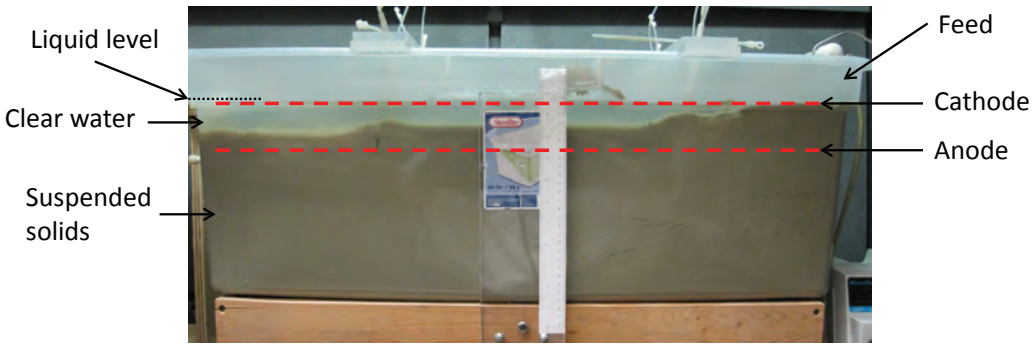

C

Figure 3-2. Results of experiments performed to establish a proof of concept: A) side-view at $t = 0$; B) side-view after a period of 15 hours without applied electric field; and C) side-view after a period of 15 hours with an applied electric field of 1 V/cm (photographs by Rui Kong).

3.2 Results

The performance of the semi-continuous electrokinetic dewatering system was examined through the measurement of changes of solids content, supernatant turbidity, and the power and energy consumption. Operation parameters, including electric field, influent flow rate, and electrode spacing, were evaluated to find optimum operation conditions.

3.2.1 Proof of Concept

One pair of experiments was conducted to prove the concept of the system configuration shown in Figure 3-1. The results are presented in Figure 3-2. Both experiments were operated under the same condition with the exception that one had an electric field of

1 V/cm and the other one did not have an applied electric field. The initial condition for both experiments is shown in Figure 3-2A. The side view of the tank in Figure 3-2B shows that, after being subjected to an electric field of 1 V/cm for 15 hours, a layer of clear water appeared that extended approximately 1/6 height of the tank. In the control experiment, as shown in Figure 3-2C, after a period of 15 hours without applied electric field a region of clear water was not formed. These experiments served to support the hypothesis that the semi-continuous electrokinetic system may be used to extract a stream of solids-free water.

3.2.2 Change of Solids Content

The solids content of the material in the cell was measured before and after every experiment. The largest change of solids content, 8.15 wt%, was achieved using an electric field of 3 V/cm and a flow rate of 40 ml/min (τ=11 h). In the experiment with electric field of 3.3 V/cm and electrode separation of 6 cm, an increase of solids content of 19.87 wt% was observed on the thickest part of clay close to the anode. Due to limitations in the sampling method and the potential for re-hydration of solids, the measurements are believed to underestimate the solids content. A fully-continuous design which would remove continuously thickened solids may be anticipated to produce a higher solids concentration. The results presented in Chapter 5 confirm this hypothesis.

3.2.3 Supernatant Turbidity and pH

Turbidity measurements were conducted to examine the quality of supernatant water during the experiments. The change in supernatant turbidity in the deep tank semi-continuous dewatering system is presented in Figure 3-3 as a function of elapsed time, given as t/τ, where τ is residence time calculated as the effective volume (space between electrodes) over feed flow rate. Effluent samples of supernatant liquid were collected every 30 min during the operation. Supernatant turbidity, measured immediately after the sample was collected, is indicated as black squares. After settling in the sample cell, the turbidity dropped dramatically. After 24 hours, it was measured again and is

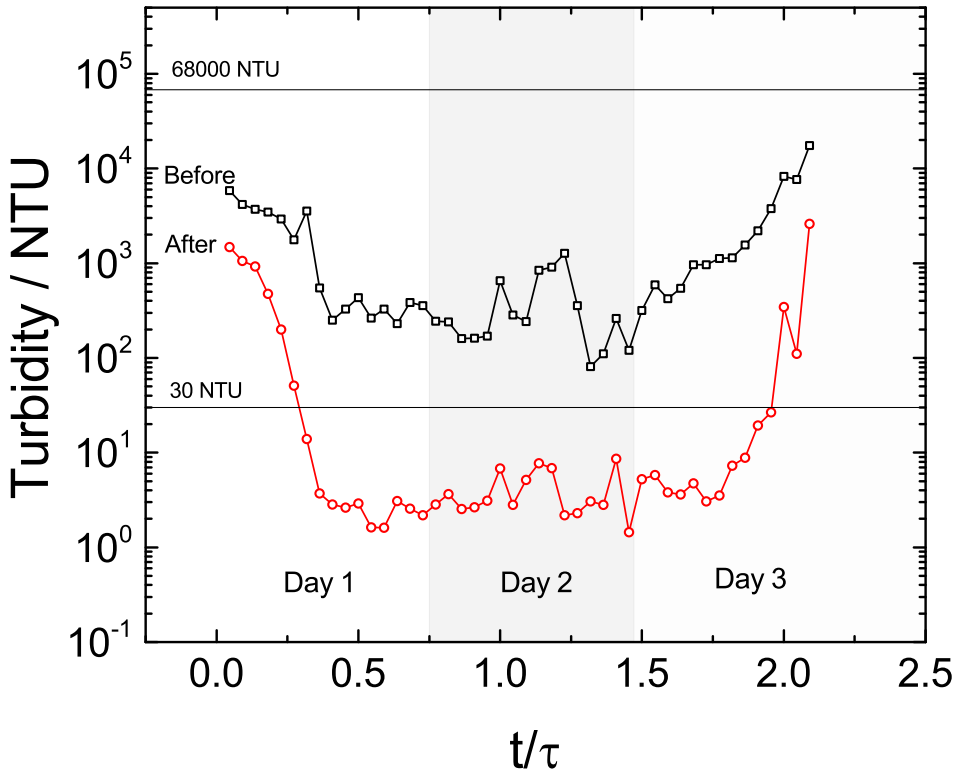

Figure 3-3. Turbidity of supernatant liquid as a function of scaled elapsed time for an electric field of 3 V/cm and a feed flow rate of 40 ml/min (τ=11 h): □ measured immediately after the sample was collected, and ○ measured 24 hours after the sample was collected. The electric field and flow was discontinued overnight.

indicated as red circles in Figure 3-3. The turbidity of the feed, shown as a horizontal line, was 68,000 NTU. The turbidity decreased sharply at the beginning of experiment, and reached a steady value after about 4 hours ($t/\tau = 0.3$). The turbidity remained at a steady and low level until $t/\tau > 1.8$. The operation between $0.3 < t/\tau < 1.8$ may be regarded to be under a pseudo-steady-state condition in which the supernatant turbidity, after settling for 24 hours, had a steady value less than 10 NTU and solids accumulated in the tank. For $t/\tau > 1.8$, the capability of the tank to hold solids was exceeded, and the solids content of the supernatant increased accordingly. The quality of the water produced during the pseudo-steady-state operation, with turbidity values lower than 30 NTU, was sufficient for recycling water to the beneficiation plant.

A representative series of images is presented in Figure 3-4 for supernatant samples

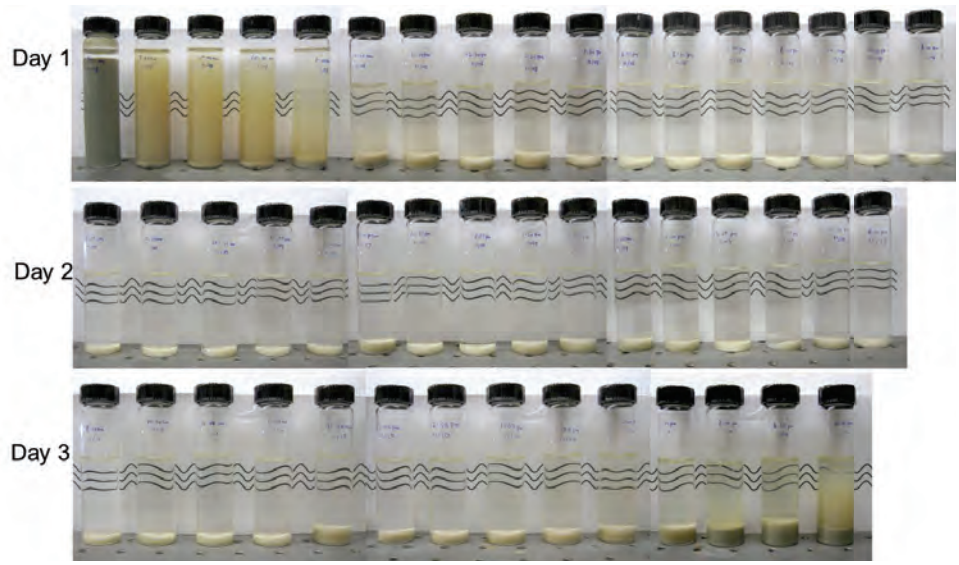

Figure 3-4. Representative images showing the supernatant samples 24 hours after collection (photograph by Rui Kong).

24 hours after collection. The turbidity is evidently quite large for the first 5 samples of Day 1, corresponding to the first 2.5 hours of operation, and the last samples of Day 3. These images are in good agreement with the turbidity reported in Figure 3-3. A thin layer of solids is visible at the bottom of the vials. These solids were entrained with the supernatant water and settled rapidly to the bottom of the vials.

The pH of the supernatant was measured and plotted in a similar manner. At $t = 0$, the pH of the cell contents was 7. As shown in Figure 3-5, the pH of the supernatant increased to 11.7 at the beginning of the experiment and remained stable around this value until the solids-storage capability of the container was exceeded. There was no significant difference between the pH measured immediately after the sample is collected and after 24 hours. The alkalinity of the supernatant liquid was a result of the electrochemical reaction at the cathode, dissociation of water to create hydrogen gas and hydroxide ions, OH^-.

3.2.4 X-Ray Diffraction

The results of X-Ray Diffraction analysis of the solids present in different samples are shown in Figure 3-6. The diffraction results indicate that smectite, mica, wavellite,

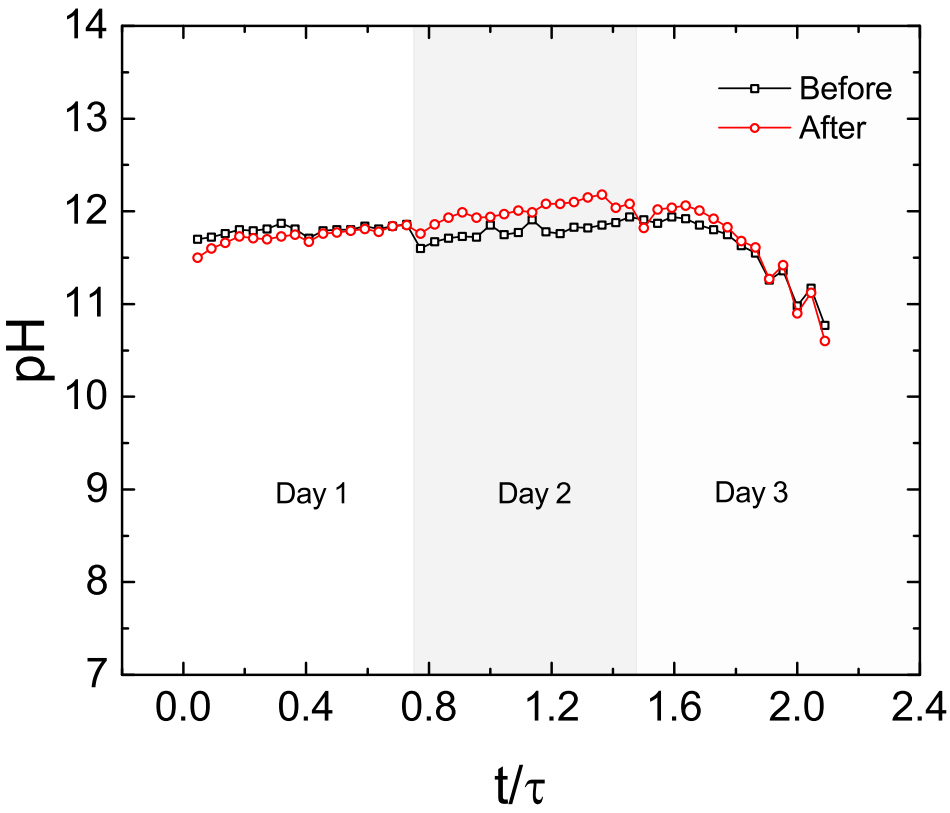

Figure 3-5. pH of supernatant liquid as a function of scaled elapsed time corresponding to the results presented in Figure 3-3.

quartz, kaolinite, apatite, and calcite comprise the solids present in the feed. The solids that settled from the supernatant water under pseudo-steady-state operation, i.e., for $t/\tau > 0.3$, were rich in calcite and also contained small amounts of smectite, quartz, kaolinite and apatite. The solids collected from the anode surface were found to have the same composition as initial suspensions. Thus, the electrokinetic dewatering process did not influence the solids composition and does not, therefore, provide a means for separation of the constituents of phosphatic clay.

3.2.5 Free-Settling Behavior

Free-settling of solids in the supernatant water was monitored by continuous measurement of turbidity at the midpoint of a cuvette. As solids settled and fell to the bottom of the cuvette, the turbidity measured in the central third of the cuvette decreased. A typical result is presented in Figure 3-7. The turbidity dropped quickly in

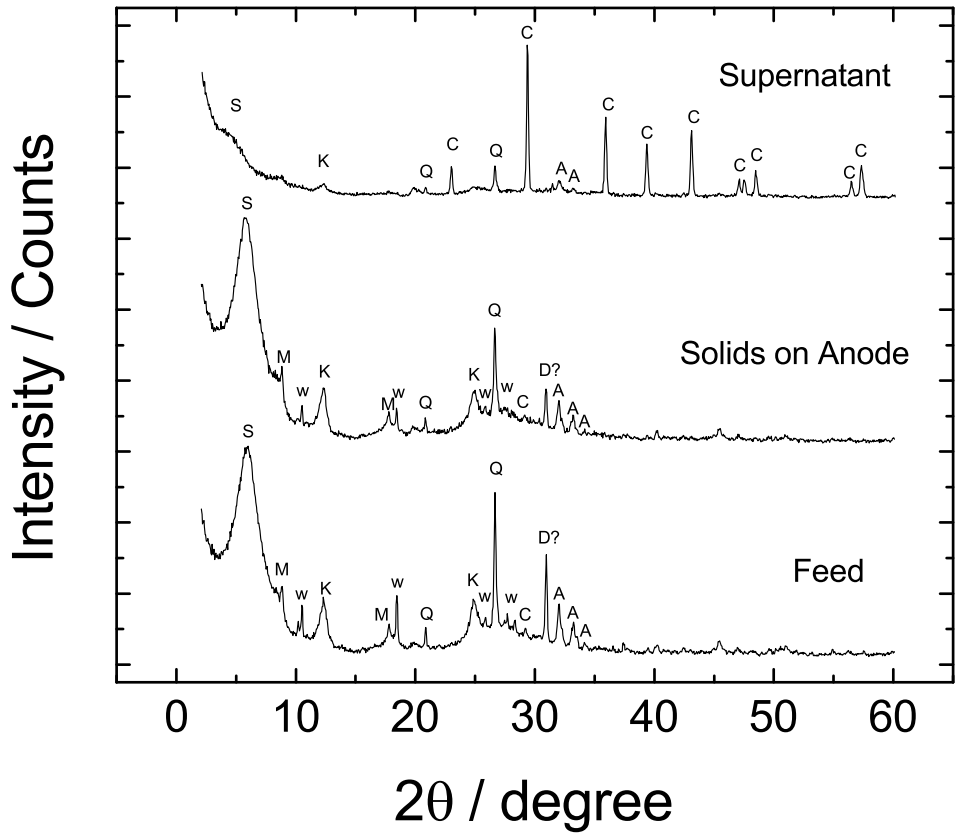

Figure 3-6. Identified XRD result of initial suspensions (bottom), solids collected from anode (middle), and solids settled from the supernatant water under pseudo-steady-state operation (top). S= smectite; M= mica; W= wavellite; Q= quartz; K= kaolinite; A= apatite (carbonate fluorapatite); D?= Dolomite(we think); C=Calcite; C?= Calcite(most likely)

the first 24 hours to a value lower than 10 NTU and changed slightly thereafter. The free settling behavior could be represented by

$$\log(T_{\mathrm{w}}) = p - q\log(t) \tag{3–2}$$

where T_{w} represents the turbidity in NTU, t represents the elapsed settling time in the cell, and p and q are parameters determined by specific operation conditions.

Application of Equation 3–2 is demonstrated in Figure 3-8 for samples collected during pseudo-steady-state operation after 2, 4, 6, and 8 hours of elapsed time. In each case, the settling behavior followed Equation 3–2. Turbidity levels lower than 10 NTU

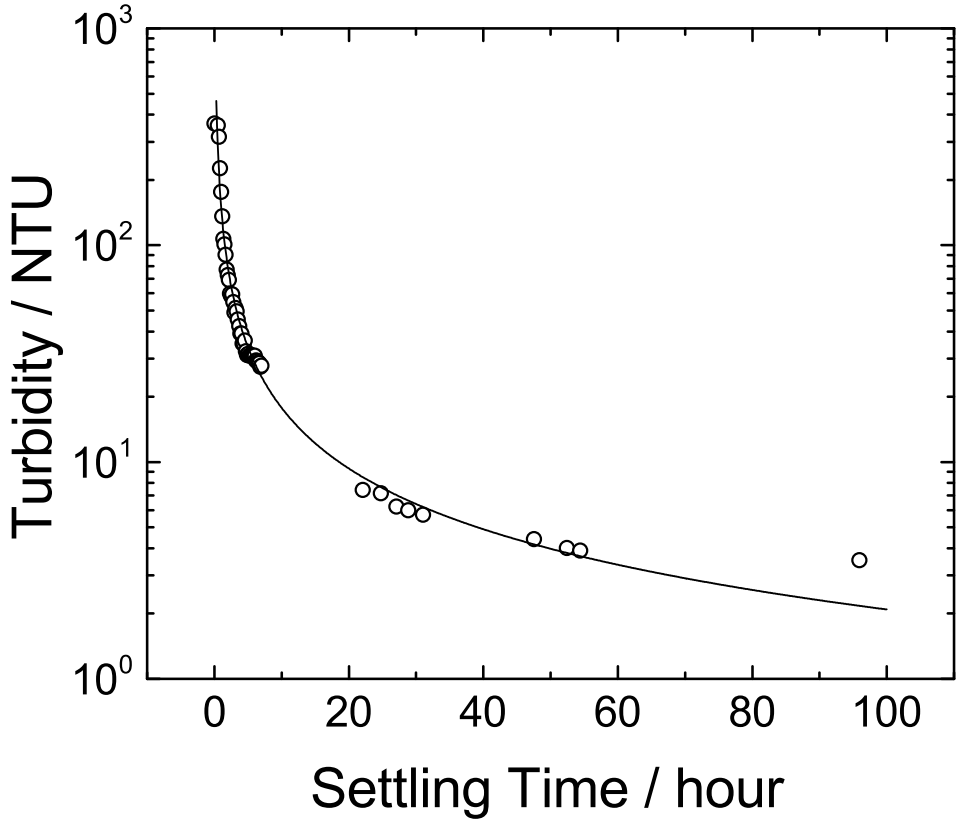

Figure 3-7. Turbidity measured in the middle of the cuvette as a function of elapsed free-settling time for a sample collected in the pseudo-steady-state region for an electric field of 2 V/cm and a feed rate of 30 ml/min (τ=14.7 h). The symbols represent measured values and the line is represented by Equation 3–2 with $p = 5.49$ and $q = 0.93$.

were achieved in less than 2-8 hours. While some variability was evident, the behavior for all four samples was quite similar.

In contrast, the feed flow rate had a much larger impact on free-settling characteristics, as seen in Figure 3-9 for an applied electric field of 2 V/cm. The samples were collected in the middle of the pseudo-steady-state regime. Interestingly, smaller turbidity levels were achieved for a flow rate of 40 ml/min (τ=11 h) as compared to either 30 ml/min (τ=14.7 h) and 60 ml/min (τ=7.3 h). Thus, the feed flow rate of 40 ml/min (τ=11 h) was considered to be optimal for the present configuration.

The influence of electric field on free-settling behavior of the supernatant can be seen in Figure 3-10 at the optimal feed flow rate of 40 ml/min (τ=11 h for 2 and

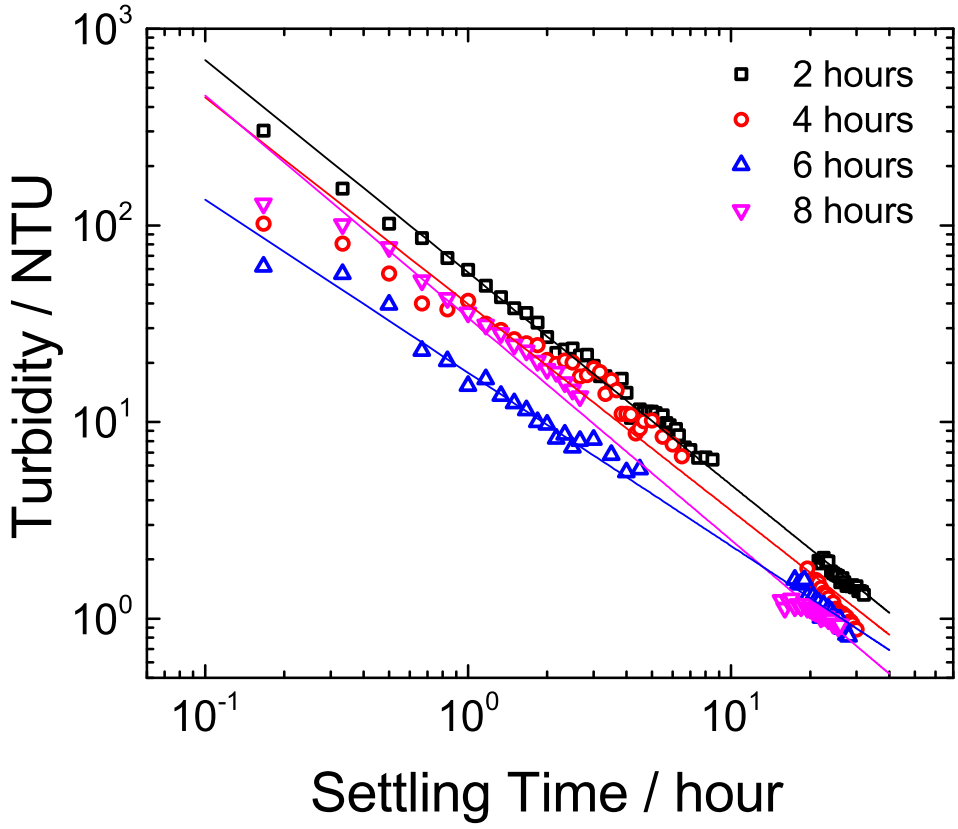

Figure 3-8. Turbidity measured in the middle of the cuvette as a function of elapsed free-settling time for a sample collected in the pseudo-steady-state region for an electric field of 3.3 V/cm and a feed rate of 40 ml/min (τ=6.6 h). The symbols represent measured values and the line is represented by Equation 3–2. $\square$ 2 hours with $p = 5.60$ and $q = 1.08$; $\circ$ 4 hours with $p = 5.33$ and $q = 1.05$; $\triangle$ 6 hours with $p = 5.55$ and $q = 1.13$; and $\triangledown$ 8 hours with $p = 4.38$ and $q = 0.88$.

3 V/cm, τ=6.6 h for 3.3 V/cm). The samples were collected in the middle of the pseudo-steady-state regime. The settling behavior of the supernatant liquids was independent of applied electric fields of 2 V/cm, 3 V/cm and 3.3 V/cm . In all examples shown in Figures 3-8, 3-9, 3-10, Equation 3–2 provided an excellent representation of the settling behavior.

3.2.6 Effect of Feed Flow Rate on Performance

Supernatant turbidity after settling is presented as a function of scaled time with flow rate as a parameter in Figure 3-11. With the highest feed flow rate of 60 ml/min (τ=7.3 h), the separation could not reach the pseudo-steady-state condition. For the feed

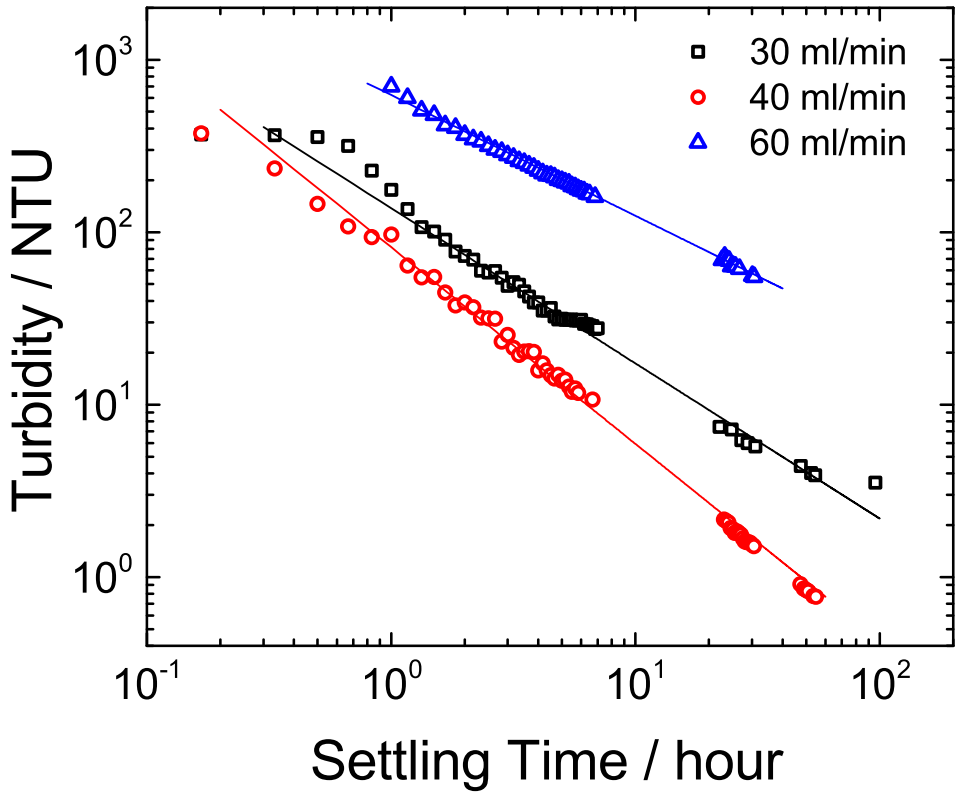

Figure 3-9. Turbidity measured in the middle of the cuvette as a function of elapsed free-settling time for samples collected in the pseudo-steady-state region for an electric field of 2 V/cm (200 V/m). The symbols represent measured values and the line is represented by Equation 3–2. □ 30 ml/min (τ=14.7 h) with $p = 5.34$ and $q = 0.90$; ∘ 40 ml/min (τ=11 h) with $p = 5.97$ and $q = 1.14$; △ 60 ml/min (τ=7.3 h) with $p = 5.28$ and $q = 0.70$.

flow rates of 30 ml/min (τ=14.7 h) and 40 ml/min (τ=11 h), the similarity of the shapes indicates that the supernatant turbidity increased after a quantity corresponding to the volume between the electrodes was treated. This suggests that fully-continuous operation should be capable of achieving turbidity levels below 30 NTU. The data suggest that the separation achieved the best result with flow rate of 40 ml/min (τ=11 h) in this specific configuration. The corresponding pH value is shown in Figure 3-12. The supernatant liquid from the system with the different flow rates maintained similar pH value during the operation.

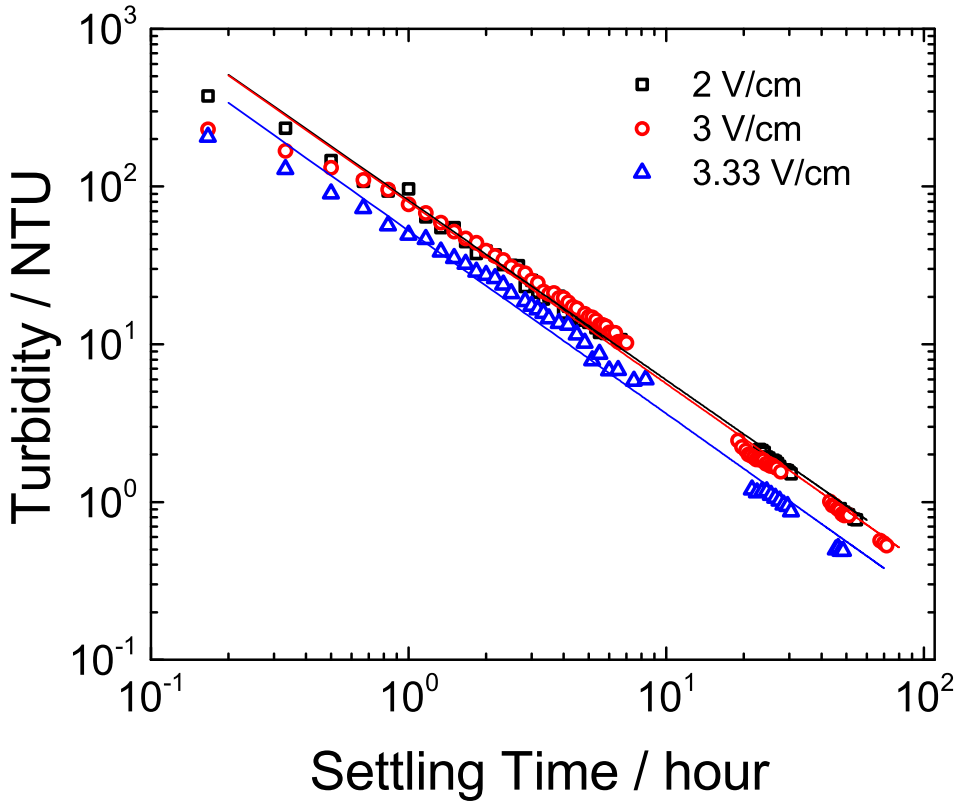

Figure 3-10. Turbidity measured in the middle of the cuvette as a function of elapsed free-settling time for samples collected in the pseudo-steady-state region for a flow rate of 40 ml/min (τ=11 h for 2 and 3 V/cm, τ=6.6 h for 3.3 V/cm). The symbols represent measured values and the line is represented by Equation 3–2. $\square$ 2 V/cm with $p = 5.97$ and $q = 1.14$; $\circ$ 3 V/cm with $p = 5.99$ and $q = 1.15$; $\triangle$ 3.3 V/cm with $p = 5.85$ and $q = 1.16$.

3.2.7 Effect of Electric Field and Electrode Separation on Performance

The effect of electric field was demonstrated by keeping the flow rate constant at 40 ml/min (τ=11 h) and increasing the electric field from 2 V/cm to 3 V/cm. As shown in Figure 3-13, the experiment reached the pseudo-steady-state condition faster with an increased electric field, and the duration of the pseudo-steady-state operation was increased for a given residence time. This result shows that the larger electric field increases the capacity for the system to store solids. The electric field of 3.3 V/cm was achieved by reducing the electrode separation from 10 cm to 6 cm. The decreased electrode spacing decreased the residence time proportionally. Thus, though the larger electric field allowed a more rapid approach to the pseudo-steady-state condition,

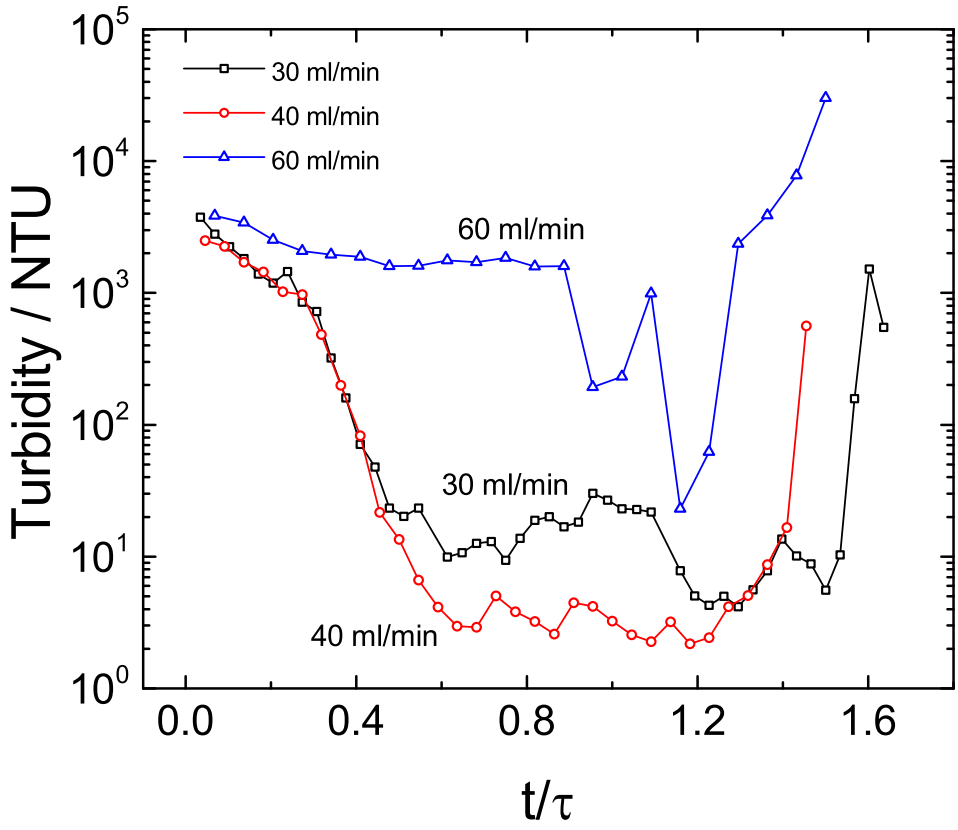

Figure 3-11. Turbidity of supernatant liquid as a function of scaled elapsed time for an electric field of 2 V/cm with flow rate as a parameter.

the duration of the pseudo-steady-state condition was shorter. The supernatant pH corresponding to the results presented in Figure 3-13 are shown in Figure 3-14. Under pseudo-steady-state operation, the pH remained on the order of 11.7, independent of applied electric field.

3.2.8 Effect of pH

To answer the question that whether the reduction of turbidity could be attributed to the increase in pH, a pair of experiments were performed. Two identical graduated cylinders were filled with same amount of untreated suspensions. One of the samples was adjusted by adding KOH solution to reach a pH value of 11.7, which is the same as observed for the supernatant liquid under semi-continuous operation. In the second cylinder, the pH was unchanged from the original value of 7.1. The samples were allowed

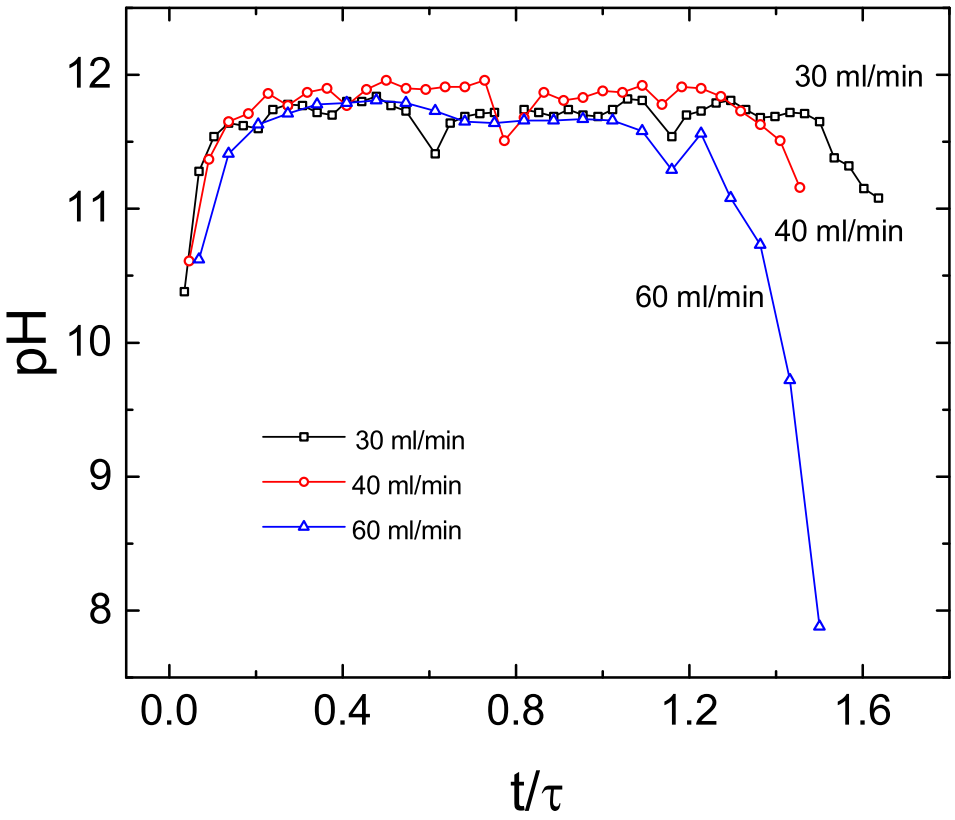

Figure 3-12. pH of supernatant liquid as a function of scaled elapsed time for an electric field of 2 V/cm with flow rate as a parameter.

to experience free-settling by gravity for a period of ten days. As shown in Figure 3-15, after 10 days, a layer of clear water was observed for both cylinders, in which the higher pH sample had thinner clear layer and higher water turbidity. This result indicates that alkaline property of the supernatant water did not assist in the dewatering process. The low turbidity of supernatant water could therefore be attributed to the electrokinetic process.

3.3 Discussion

The present semi-continuous system was designed for separation of a stream of clear supernatant water and for accumulation of solids. The discussion of results is presented here in terms of factors that influenced the quality of the supernatant water and the associated electrical and power requirements of the operation. Successful implementation of fully-continuous electrokinetic devices for separating phosphatic mine waste streams

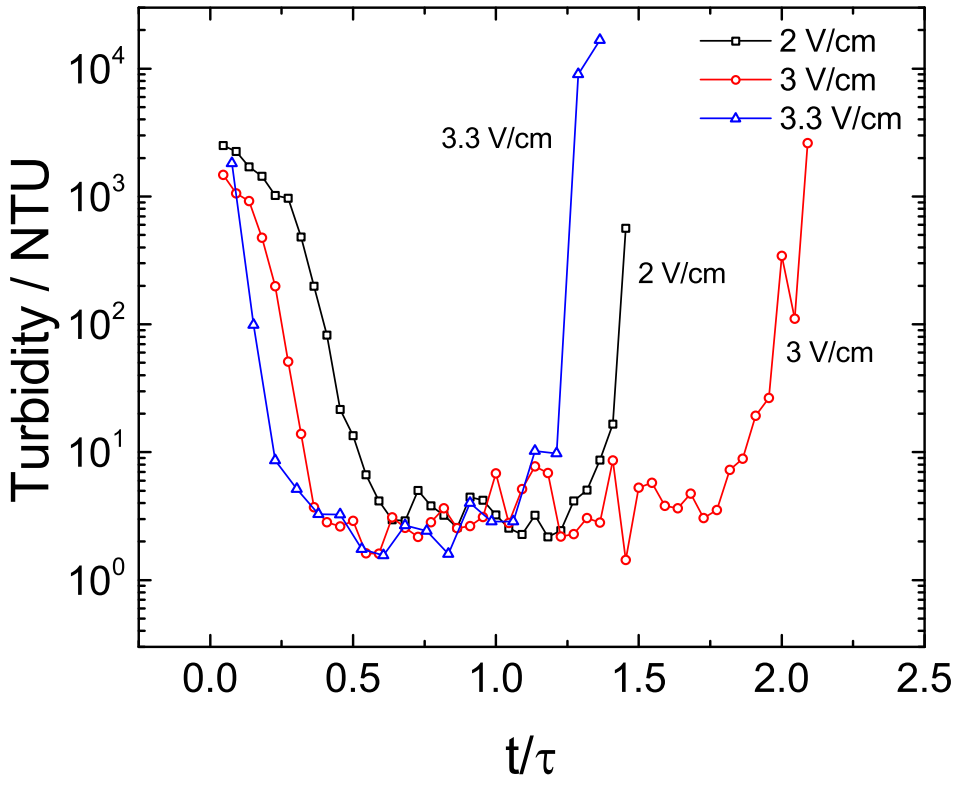

Figure 3-13. Turbidity of supernatant liquid as a function of scaled elapsed time for a flow rate of 40 ml/min (τ=11 h for 2 and 3 V/cm, τ=6.6 h for 3.3 V/cm) with electric field as a parameter.

will demand maximizing the solids content of the solids-rich effluent in combination with maintaining clarity of the supernatant liquid and minimizing energy and power requirements.

3.3.1 Supernatant Water Quality

The semi-continuous system presented here was designed to be a transition from batch to fully-continuous operation. It successfully separated water from phosphatic clay suspensions and produced concentrated solids. Thickened phosphatic clay was accumulated on the surface of the anode. The overflow clear water was collected on the opposite side of the feed. The pH value of the supernatant water remained around 11.7 throughout the experiment. The alkaline solution is the result of the hydrogen evolution reaction on the cathode. A separate experiment showed that the enhanced settling of

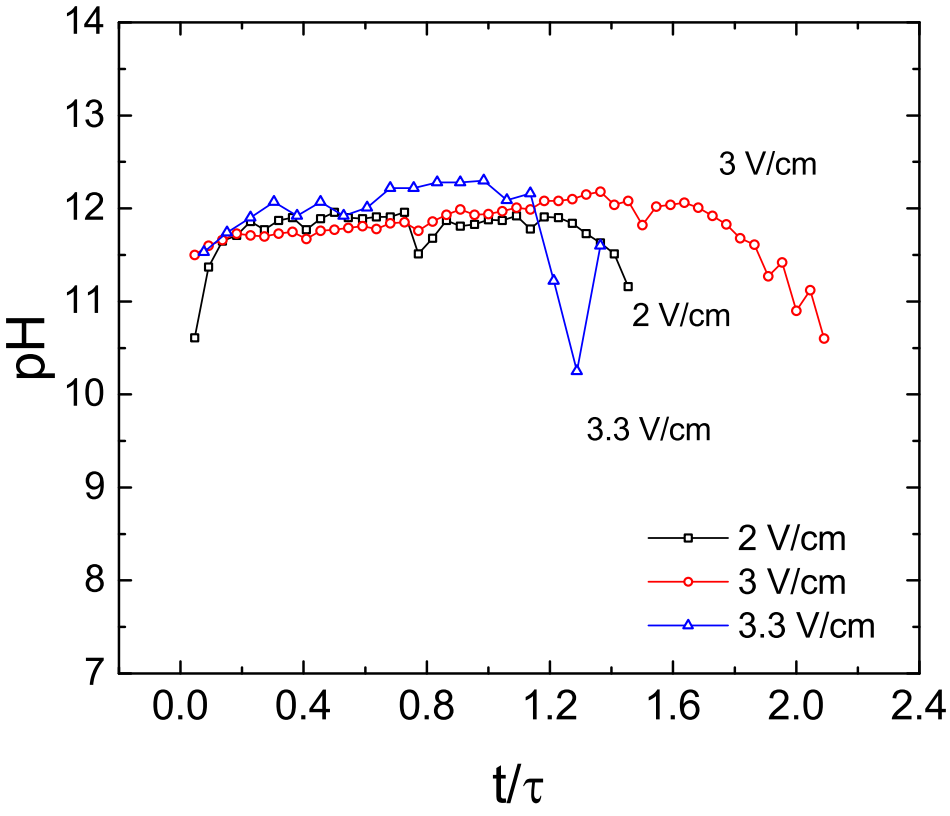

Figure 3-14. pH of supernatant liquid as a function of scaled elapsed time for a flow rate of 40 ml/min (τ=11 h for 2 V/cm and 3 V/cm, τ=6.6 h for 3.3 V/cm) with electric field as a parameter.

solids from the supernatant could not be attributed to the pH; thus, the electrokinetic process altered the solids content of the supernatant liquid, allowing settling to occur.

The turbidity of the supernatant liquid dropped quickly after it was collected. The free-settling behavior was similar for all operation conditions. Within 24 hours, values lower than 10 NTU were consistently observed. The XRD result showed that the supernatant deposits were rich in calcite. This result suggests that the fine clay mineral particles were attracted to the anode by the applied electric field, and the particles that remained in the supernatant water were larger and tended to settle quickly.

Results showed that increasing electric field increased the speed of achieving a pseudo-steady-state condition, while not affecting the supernatant turbidity value. The smaller residence time decreased the elapsed period of operation under a pseudo-steady

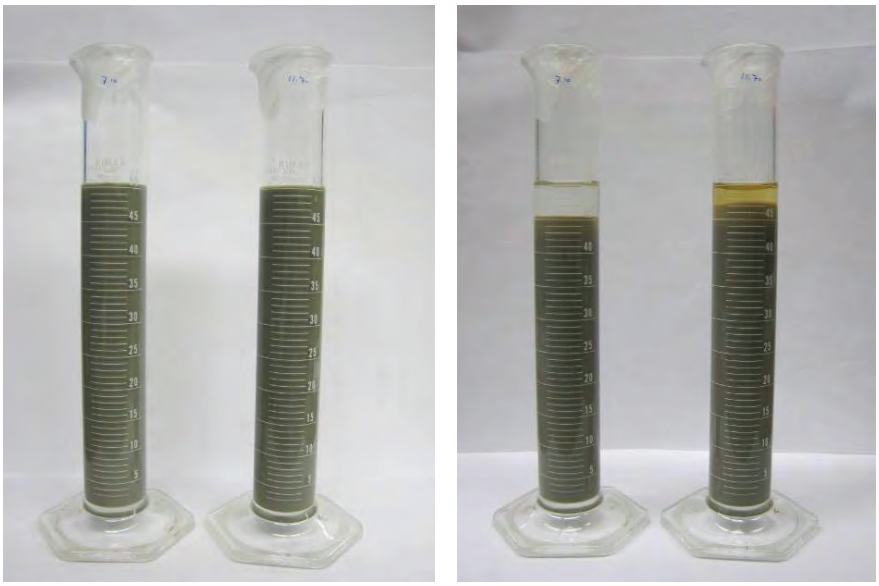

A B

Figure 3-15. Separation affected by pH. A) Initial clay samples with pH of 7.1(left) and pH of 11.7(right). B) 10 days later under only gravity sedimentation (photographs by Rui Kong).

state. For an electric field of 2 V/cm, a pseudo-steady-state condition was not achieved with flow rate of 60 ml/min (τ=7.3 h). The lowest flow rate gave a longest elapsed time of pseudo-steady-state operation; whereas, the flow rate of 40 ml/min (τ=11 h) reached the lowest turbidity during pseudo-steady-state operation.

These results suggest that a low-turbidity stream could be easily obtained by electrokinetic separation under a moderate electric field. An even lower turbidity (under 10 NTU) could be reached in 24 hours by subsequent free-settling. The free-settling zone could be designed as a separate unit operation for on-site implementation. The residence time required to achieve the highest water quality was on the order of 11 hours. It is expected that the optimal residence time would be smaller for a fully-continuous system that provides continuous removal of solids-rich and clear streams.

3.3.2 Energy and Power Requirements

In batch experiments, the power consumption can be expressed by

$$P_{\text{req}} = V_{\text{cell}} I \tag{3–3}$$

where P_{req} is power consumption (W), V_{cell} is the cell potential (V), and I is the current (A). For the semi-continuous system, the power consumption could be defined by the same equation. Since V_{cell} was controlled to be constant throughout the duration of the experiment and current changed with time, the power consumption could be plotted as a function of time as shown in Figure 3-16 with feed flow rate as a parameter. The

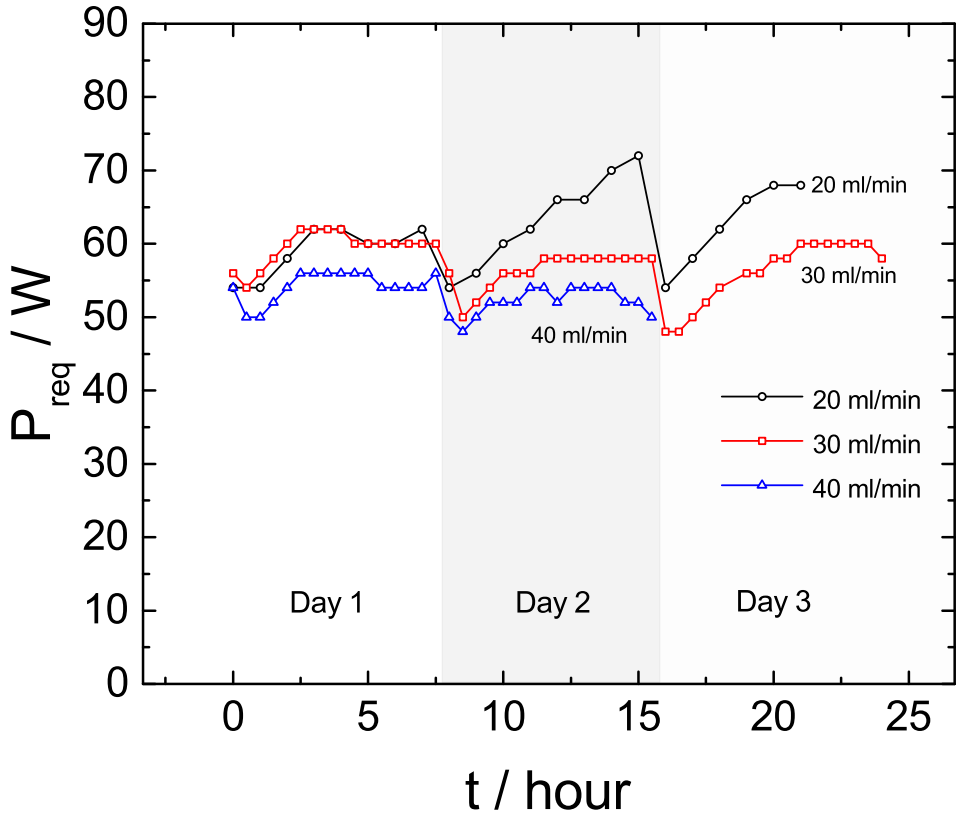

Figure 3-16. Power consumption as a function of operation time with feed flow rate as a parameter.

power consumption increased at the beginning of experiment until a pseudo-steady-state condition was achieved. After a rest overnight, power consumption fell to a lower

level. This pattern was repeated for the transition from Day 2 to Day 3. The power consumption tends to be lower with higher feed flow rate.

For batch experiments, the energy consumption can be expressed by

$$E_{\mathrm{req,w}} = \frac{V_{\mathrm{cell}} I t}{\Delta m_{\mathrm{w}}} \tag{3–4}$$

where $E_{\mathrm{req,w}}$ is energy consumption per kg of water removed ($\mathrm{Wh/kg_{H_2O}}$), V_{cell} is cell potential (V), I is current (A), t is operation time (hours), and Δm_{w} is mass of water removed (kg). Energy consumption in semi-continuous process was calculated based on the assumption of a pseudo-steady-state. Since the total volume of clay suspensions in the tank is conserved during pseudo-steady-state operation, the feed flow rate Q_{in} was equal to the effluent flow rate Q_{out}, which is the volumetric rate of supernatant water removed. The energy consumption in the semi-continuous system is then defined by

$$E_{\mathrm{req,w}} = \frac{P_{\mathrm{req}}}{\rho_{\mathrm{w}} Q_{\mathrm{out}}} \tag{3–5}$$

where ρ_{w} is the density of water. This equation represents the energy consumption in pseudo-steady-state operation under the assumption that P_{req} is the average power consumption during that period of time. The energy requirement is presented in Figure 3-17 as a function of applied electric field. The energy requirement increased with increasing electric field.

The energy analysis presented above is essential for developing an economic assessment of the viability of electrokinetic dewatering. McKinney and Orazem[70] showed that application of electrokinetic technology to dewatering of a clay settling area yielded energy costs that were competitive with alternate technologies, but the power requirement was excessive. The present work, as shown in Figure 3-17, yielded energy requirements that were in agreement with the batch experiments[69] and simulations[70] for a given electric field. The batch experiments showed that the solids content of the cake increased with the logarithm of electric field[69]; therefore, process optimization is governed by the

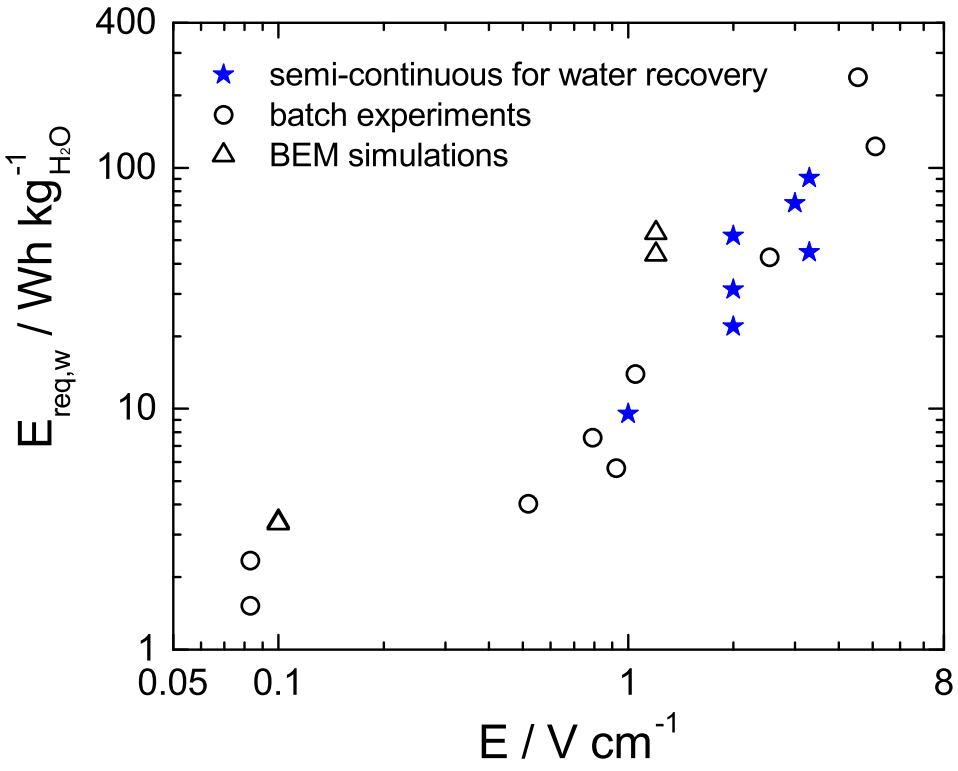

Figure 3-17. Energy requirement as a function of applied electric field. The batch experiments and CP3D simulation results were reported by McKinney and Orazem[69, 70]

compromise between desired cake water content and the energy and power consumption required to achieve it. In the batch and semi-continuous experiments, thickened clay was accumulated in the container, which reduced the dewatering efficiency over time. As shown in Chapter 5, the energy consumption is reduced in a well-designed fully-continuous prototype that continuously separates the supernatant water and the thickened clay.

CHAPTER 4
SEMI-CONTINUOUS PROTOTYPE FOR SOLIDS RECOVERY

The semi-continuous experiment for water recovery showed that the electrokinetic dewatering could be applied on semi-continuous operation to produce low-turbidity water stream from the phosphatic clay suspension. However, the thickened clay was accumulated in the tank during the operation. As the second step towards the fully continuous operation, an improvement was made on the semi-continuous prototype to remove the thickened clay, and the new prototype is called the semi-continuous prototype for solids recovery.

4.1 Experimental Setup

Three initial designs were proposed for the semi-continuous prototype aimed to remove the thickened clay, as shown in Figure 4-1. The first design as shown in Figure 4-1A represents a type of apparatus using scraper to remove solids. The tank is a traditional gravity thickener, and a pair of electrodes are suspended in the tank to conduct electrokinetic dewatering. One scraper is implemented above the anode and another one is placed at the bottom. Both scrapers are rotated at very low speed to remove the thickened clay accumulated on anode. The initial clay suspensions are fed from the top, and the thickened clay are discharged from the bottom. The second prototype shown in Figure 4-1B uses an rotating anode to remove the thickened clay. Instead of horizontal configuration, the electrodes are tilted with a small angle which allows one end of the electrode under suspension, and the other end exposed in air. The feed clay suspensions will be pumped into the tank from the lower end, the thickened clay will move with the rotating anode, and leave the tank from the higher end. The third prototype is similar as the seconde one, except that this design uses an plate anode, and adds one non-conductive rotating belt surround the anode to remove the thickened clay, as shown in Figure 4-1C. Due to the difficulty of construction and the potential disturbance of clay consolidation caused by the scraper, the first design was abandoned.

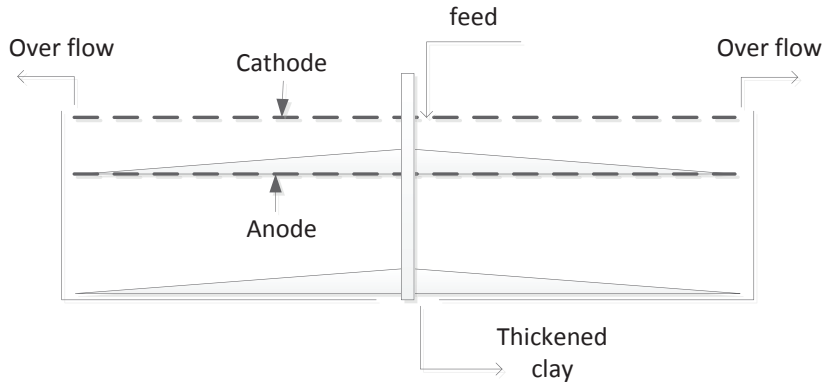

A

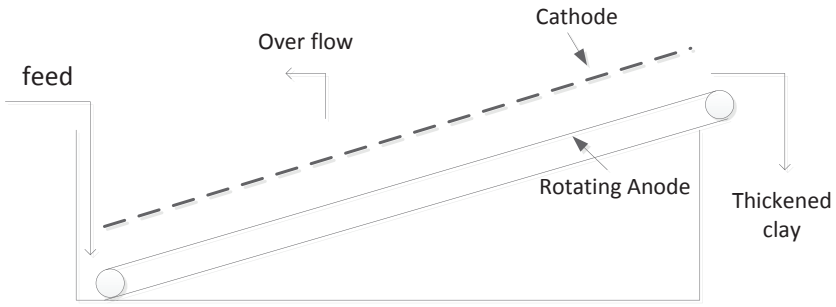

B

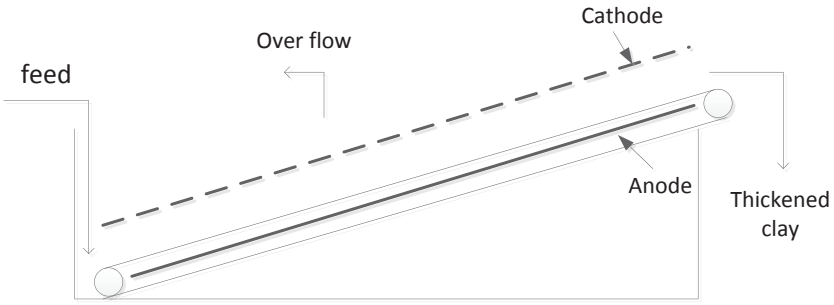

C

Figure 4-1. Three designs of prototypes for solids removal. A) Scraper. B) Rotating anode. C) Rotating belt.

In the second design, the difficulty is from the construction of the rotating anode. The anode used in the semi-continuous prototype of water removal was the dimensionally stable anode, which is titanium coated with a layer of IrO_2. The rotating anode needs to be flexible in structure, and a chain would be the best possible form. However, the IrO_2 coating on the chain structure would be very difficult to make, and the coating would be worn very easily by the friction after a period of usage. The titanium, as the substrate of the dimensionally stable anode, is known to be a good corrosion resistant metal. The difficulty of making rotating anode will be greatly reduced if titanium could be used as the replacement anode material. Thus, a series of experiments were conducted to test the feasibility of using titanium as the anode.

In the third design, the concern is from the non-conductive material of the conveyor belt placed between the electrodes. The belt material needs to be carefully selected to eliminate the energy loss caused by the potential drop across the belt. A good belt material needs to have a big open area that minimize the ohmic resistant across the belt, while still holding the thickened clay on belt. The experiments with different belt materials were conducted to evaluate the design of using conveyor belt.

4.1.1 Selection of Electrode

The tests on titanium as a replacement anode material were conducted on batch experiments with the cylindrical cell as shown in Figure 4-2. The phosphatic clay suspension with an initial solids content of about 10 wt% was placed in the cell. The cathode on the top is made of titanium with IrO_2 coating. The anode at the bottom is the titanium to be tested. The distance between cathode and anode was set at 6 cm for all experiments. A cell potential of 24 V was provided by a DC power supply which was connected directly to the cathode and anode. An electric field of 4 V/cm was applied for 4 hours. Two solid Ag/AgCl reference electrodes (In Vivo Metric, E201ML) were inserted in the suspension through the wall of cylinder, with a 3.2 cm distance apart from each other. The potential between the two reference electrodes and the total current

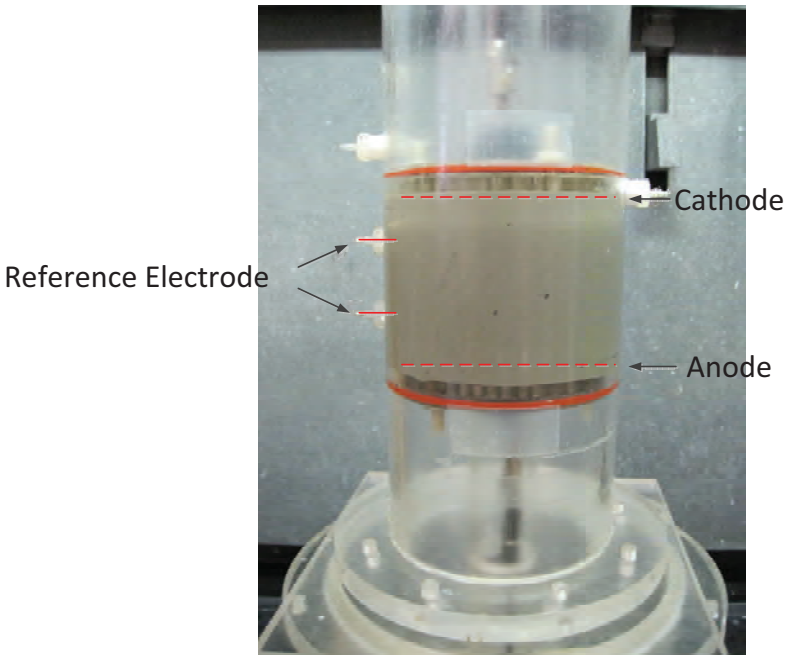

Figure 4-2. Cylindrical cell for belt and anode materials test (photograph by Rui Kong).

Table 4-1. Specifications of titanium mesh for replacement anode materials.

Titanium mesh type[a]	Wire diameter /mm	Open area /%	Δw /wt%
Ti 16×18 mesh 010 wire	0.25	70.6	3.62
Ti 32 mesh 010 wire	0.25	46.5	8.07
Ti 40 mesh 010 wire	0.25	36.0	9.78
Ti 20 mesh 014 wire	0.36	51.8	8.54
control experiment	N/A	N/A	9.83

[a] All titanium mesh materials provided by Cleveland Wire Cloth & Mfg. Co., Cleveland, Ohio, USA.

was measured in a 30-minute interval. After the experiment, the supernatant water was removed from the top and the thickened clay was collected to measure the final solids content. The solids content was calculated by Equation 3–1.

The titanium meshes with wire diameters of 0.25 mm and 0.36 mm and open areas from 36.0 % to 70.6 % were tested under the same experimental condition, as shown in Table 4-1. A total of five tests were conducted including four titanium mesh materials and one control experiment. In the control experiment both the anode and the cathode

were made of IrO_2 coated titanium. The increase of solids content for each experiment is listed in Table 4-1.

The control experiment produced the clay with the highest solids content, and the clay solids content from other experiments were very close to the control experiment, with the exception of Ti 16×18 mesh 010 wire. In the experiment using Ti 16×18 mesh 010 wire, the change in solids content was only 3.62 wt% as compared to others at about 9 wt%. From Table 4-1, Ti 16×18 mesh 010 wire is the titanium mesh sample with the biggest open area of 70.6 %. A big open area indicated a small effective electrode surface area, thereby reducing the efficiency of the electrokinetic dewatering. The normalized total current as a function of elapsed time for titanium anode is shown in Figure 4-3A. The normalized current was lower than 1 for all samples, indicating that the potential drop at the titanium anode surface was bigger than that at the dimensionally stable anode surface. The sample Ti 16×18 mesh 010 wire had the lowest cell current as compared to other titanium samples. The normalized potential between the reference electrodes as a function of elapsed time is shown in Figure 4-3B. For all the samples, the normalized potential was lower than 1, and the sample Ti 16×18 mesh 010 wire had the lowest normalized potential. The potential and current results are in agreement with each other, indicating that the increased open area for titanium mesh would decrease the electrokinetic dewatering efficiency. The best performance was obtained from the control experiment.

In addition to the reduced performance, significant corrosion was observed on the titanium mesh anodes. A photograph taken from a titanium mesh anode after one experiment is shown in Figure 4-4. An obvious white film appeared on the mesh surface, and a portion of the titanium wire was dissolved. The strong acidic environment at the anode accelerated the corrosion process. Due to the fast corrosion rate, the titanium mesh are not suitable anode materials for this system.

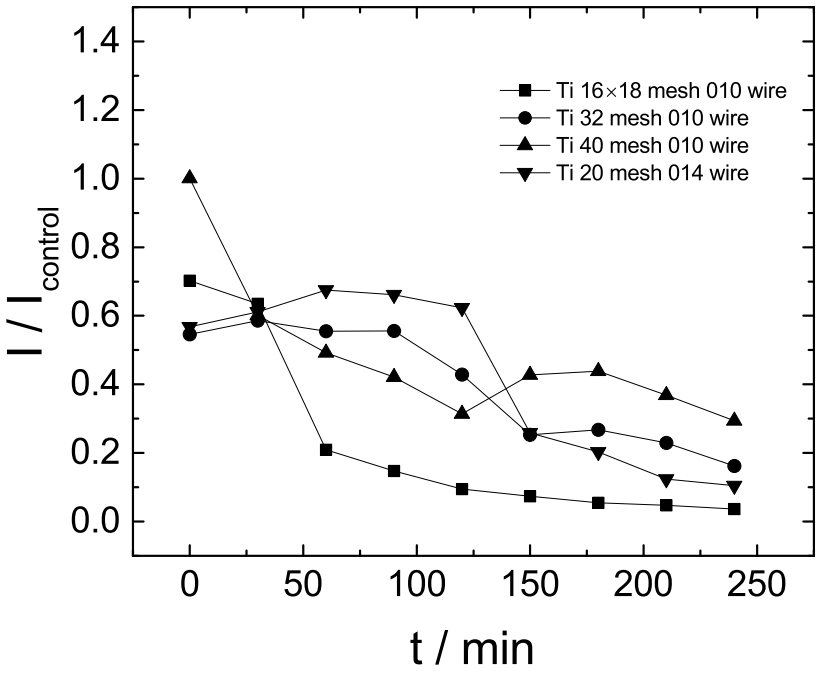

A

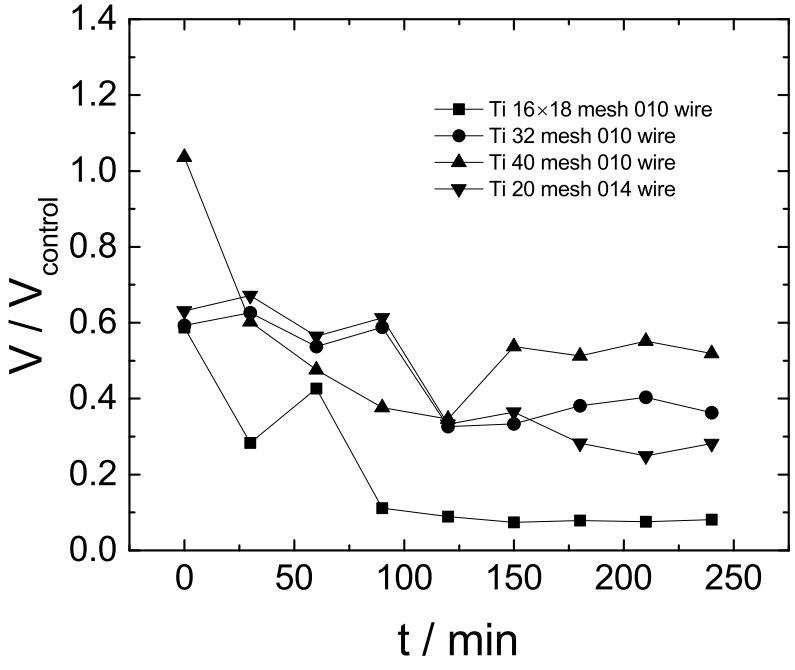

B

Figure 4-3. Normalized current and potential as a function of operation time using titanium mesh as a replacement anode. A) Normalized current as a function of elapsed time. B) Normalized potential drop between the reference electrodes as a function of elapsed time.

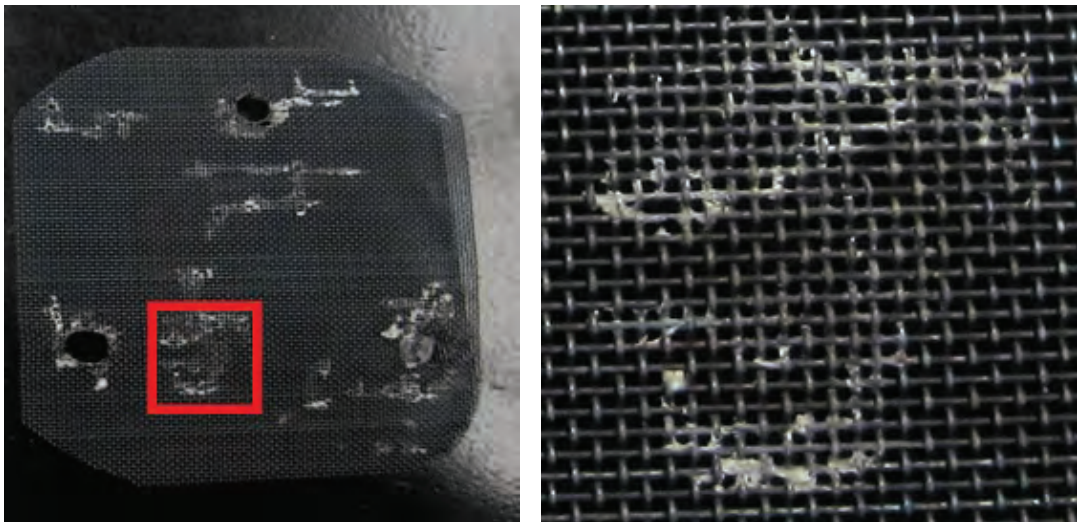

A B

Figure 4-4. Corrosion on a titanium mesh. A) The corrosion occurred on different locations on the mesh. B) Some wires disappeared due to the corrosion, and a white film was formed on the mesh surface (photographs by Rui Kong).

4.1.2 Selection of Belt Materials

In the design with the implementation of a rotating belt, the belt material needs to meet some requirements, including flexibility, electric non-conductivity, small potential drop across the belt, good change in solids content, and low cost. The filter cloth used in the filter press industry had the properties of flexibility, non-conductivity and low cost. The potential drop and change in solids content were obtained from tests conducted in the cylindrical cell. Five filters with various thickness and open areas were tested, as shown in Table 4-2. These filters were trimmed to be the same shape and size as the anode (Figure 4-5), and placed on top of the anode. The experiments were performed using the same approach as in the anode material tests, and one control experiment was conducted without the filter. The total current and local potential drop were recorded every 30 minutes during the operation, and the solids content of clay was measured before and after each experiment.

The increase of solids content Δw for each filter is shown in Table 4-2. The change in solids content for the experiments with filters was very close to that obtained from

Table 4-2. Specifications of filter fabric for belt materials.

Filter type[a]	Thickness / mm	Open area / %	Δw /wt%
Filter 530, U-CMY-530	0.37	50	13.8
Filter 06602	1.10	42.89	9.10
Filter 09452	0.88	33.71	9.61
Filter 18304	0.62	23	8.56
Filter 09502	0.90	24.97	9.49
control experiment	N/A	N/A	9.83

[a] Filter 530 was provided by Component Supply Co. USA. All other filters were provided by Fly Dragon Wire Mesh Co.,Ltd. P.R. China

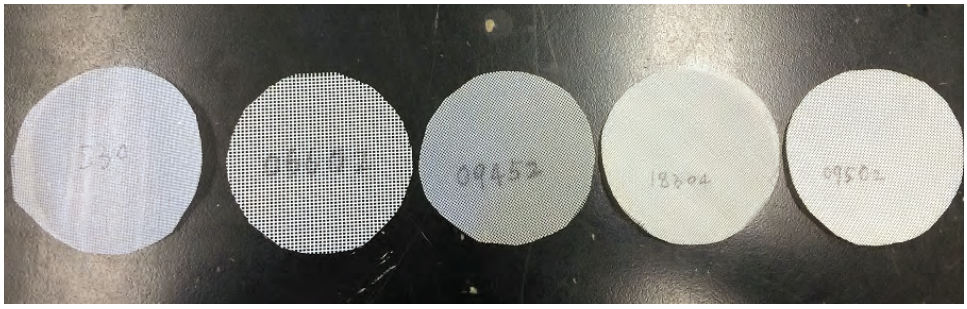

Figure 4-5. A photograph of the filters tested. From left to right: 530, 06002, 09452, 18304, 09502 (photograph by Rui Kong).

the control experiment, and the Filter 530 achieved the highest change in solids content of 13.8 wt%. From Table 4-2, the Filter 530 had the biggest open area of 50 % and smallest thickness of 0.37 mm. The lowest change in solids content was obtained from the experiment with Filter 18304, which had the smallest open area of 23 % and a larger thickness. This result suggests that the implemented filter caused a negligible influence on solids content, and a thin filter with a large open area is preferred. This is because the large open area and small thickness caused a small ohmic resistance across the filter; thus, the potential and energy loss across the filter was small. The result was confirmed by the cell current and the local potential drop as shown in Figure 4-6. The Filter 530 maintained the highest normalized current throughout the operation. The local potential was high at the beginning, and dropped slightly at the end of experiment. The normalized current and potential value was close to 1, indicating a very small difference from the control experiment.

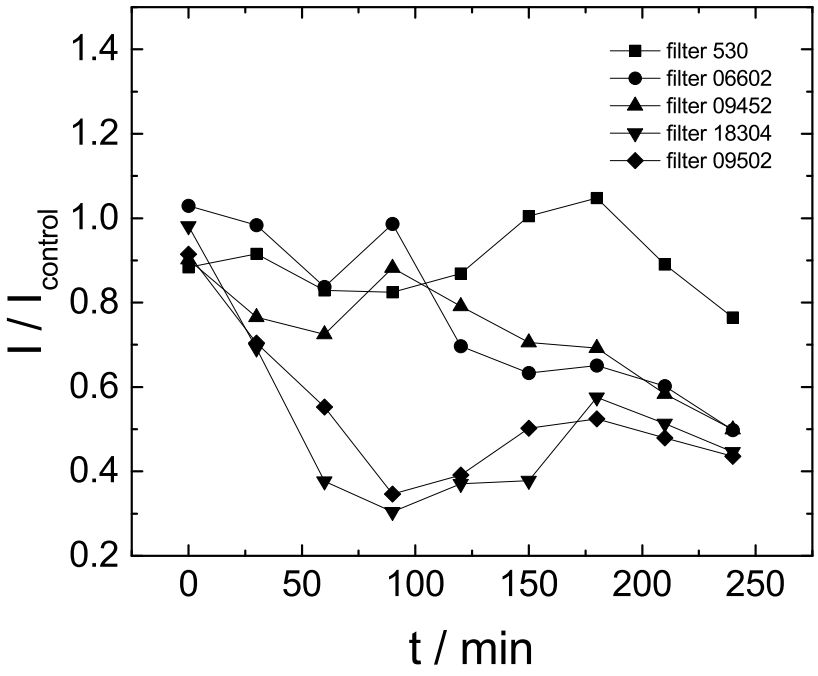

A

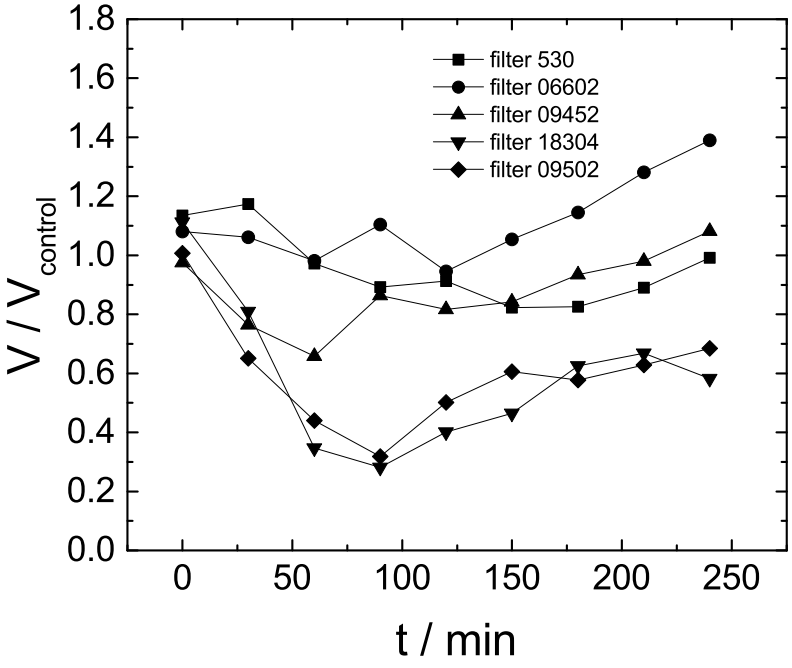

B

Figure 4-6. Normalized current and potential as a function of operation time with tested filter samples placed on the anode. A) Normalized current as a function of elapsed time. B) Normalized potential drop between the reference electrodes as a function of elapsed time.

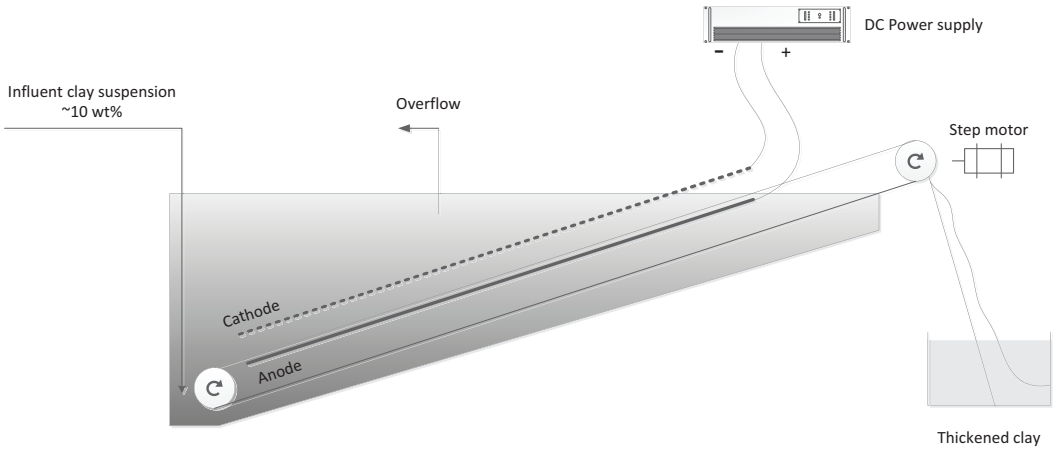

Figure 4-7. Schematic representation of semi-continuous prototype for solids removal.

In the cylindrical experiments for the titanium anode and the filter test, each material was evaluated by the change of solids content, cell current and local potential drop in bulk solution. This work suggests that the filters had minimal influence on the electrokinetic dewatering, and the Filter 530 with the biggest open area had the highest efficiency. Therefore, the design of rotating belt was selected for the semi-continuous prototype for solids removal, with the Filter 530 as the belt material.

4.1.3 Cell Design

The semi-continuous prototype for solids removal is represented in Figure 4-7. The concept was developed from the semi-continuous prototype for water removal, with an addition of conveyor belt to remove the thickened clay continuously. The tank was constructed with a triangular shape to accommodate the inclined electrode. The cathode and anode are made of the same material, the titanium coated with Iridium oxide (Water Star Inc.). The solid plate anode with a dimension of 64 cm $\times$ 36 cm $\times$ 0.16 cm was placed at the bottom, and the expanded mesh cathode with the same dimension was placed parallel above the anode, with an adjustable distance in between. The cathode was made of the expanded mesh to allow the passage of the hydrogen and oxygen gas generated by electrochemical reactions. The length of the cathode is 64 cm, with about

50 cm in the suspension which contacted the clay, and 14 cm outside of the tank and exposed in air. In this chapter, only the portion under water contributed to the effective length of electrode.

A rotating belt was placed surround the anode and held by two rollers on each end. One roller was at the left bottom of the tank close to the feeding position, and the other one was on the right top of the tank close to the thickened clay collection container.

A photograph of the assembled prototype is shown in Figure 4-8. A fish tank with the dimensions of 91 cm × 46 cm × 33 cm was used as the reservoir. The tank was made with transparent acrylic material for easy observation, and a ramp was added in the tank to reduce the dead volume and form the triangular zone. The belt and electrodes were constructed on the frame. The cathode was placed on a holder which screwed to the frame, and the distance between the cathode and anode could be adjusted from 3.2 cm to 18 cm by moving the cathode along the holder. A PVC tube that served as the water outlet channel was suspended on the cathode holder with an adjustable height.

A 10 wt% clay suspension was fed from the bottom left of the tank with a controlled the feeding speed. A DC power supply was connected to the cathode and anode to provide the cell potential. The rotating belt was driven by the upper roller which connected to a stepper motor. The belt controlling system included a frequency generator, a worm gear, and a stepper motor. The control system is illustrated in Figure 4-9. The frequency generator provided the frequency signals to control the speed of stepper motor. The stepper motor provided the driving force to rotate the roller. The worm gear was used to provide a sufficient torque to drive the belt.

After the clay cake was formed under the electric field, it would move with the belt, and drop in a plastic container, as shown in Figure 4-10. At the bottom of the tank, a drainage hole was drilled and connected with a hose, to drain out the suspension for cleaning.

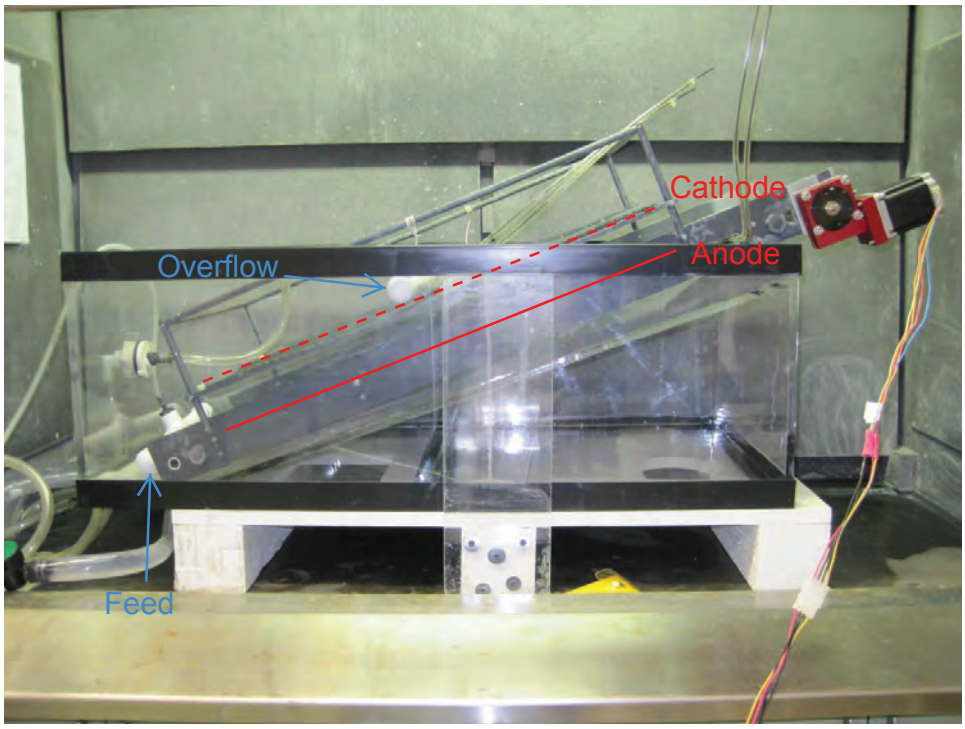

A

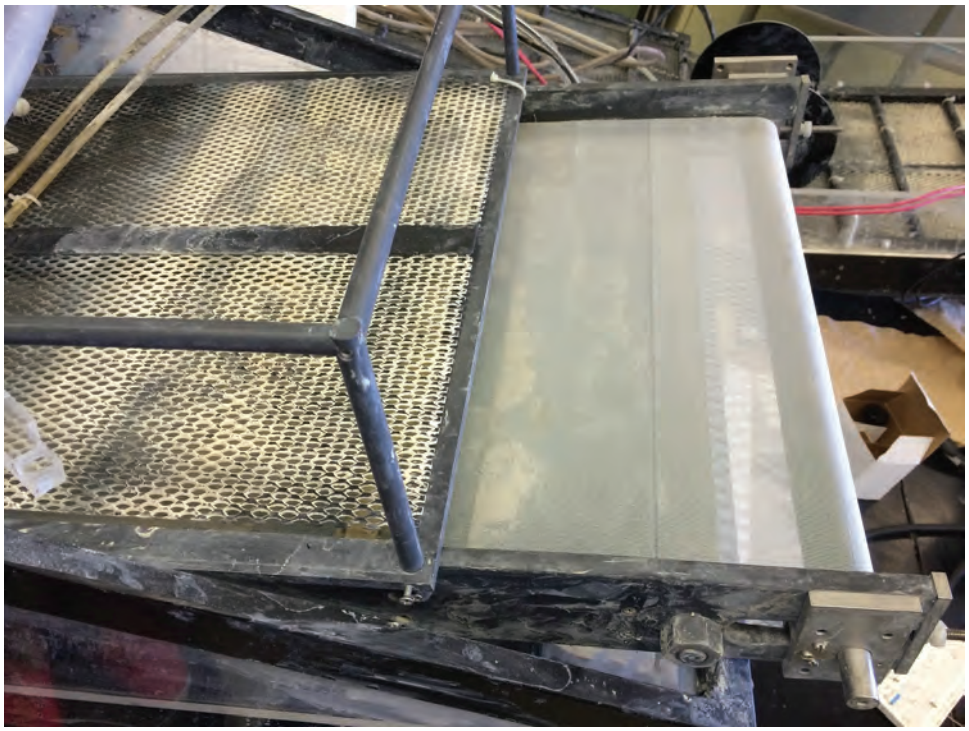

B

Figure 4-8. The assembled semi-continuous prototype for solids removal. A) A side view showing the positions of feed, overflow, cathode and anode. B) A top view showing the belt and cathode (photographs by Rui Kong).

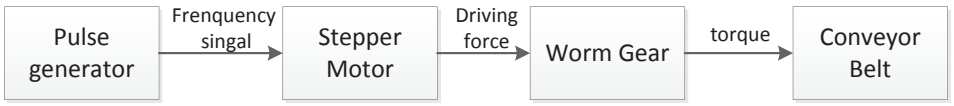

Figure 4-9. Representation of conveyor belt driving system.

Figure 4-10. A container for thickened clay collection (photograph by Rui Kong).

4.1.4 Experimental Protocol

The tank was filled with 10 wt% clay suspensions before the experiment, and the water overflow pipe was adjusted right on the liquid level. The power supply, water pump, and stepper motor were turned on at the same time to start the experiment. Under the influence of the electric field, the clay particles moved to the anode, and settled on the conveyor belt. The water moved to the cathode at the top and flowed out of the tank through the overflow pipe. As the system reached the pseudo-steady-state, a layer of thickened clay cake was produced on the belt. The clay cake was collected for more than one hour during the pseudo-steady-state. During the operation, the cell potential, total current, and feed flow rate were recorded every 15-30 minutes, depending on the belt

speed. The thickened clay mass production rate in the unit of kg/h was obtained by dividing the total weight of clay by the total collection time. The final solids content was obtained by Equation 3–1. The thickened clay was always mixed well for the measurement of solids content to ensure the result representing the average value.

4.1.5 Instrumentation

The DC voltage was provided by a Sorensen DCS60-18E DC Power Supply (Range: potential 0-60 V, current 0-18 A). The feed flow rate of the phosphatic clay suspension was controlled by a Masterflex Model 77202-60 digital pump (Cole-Parmer Instrument Company). The belt speed was controlled by a HEATHKIT Function Generator Model IG-1271. The belt driving force was provided by a SANYO DENKI Model 103H7126-5740 stepper motor and an Ondrives PF30-60NM Worm wheel gearbox, Nema Flange, 60:1.

4.2 Results

The performance of the semi-continuous prototype for solids removal was evaluated by measuring the turbidity of supernatant water and the final solids content of the thickened clay. The feeding speed was adjusted according to the operation conditions, varied from 50 ml/min to 500 ml/min. The distance between the cathode and anode was adjusted at 3.2 cm and 6.2 cm.

4.2.1 Proof of Concept

An electric field of 8 V/cm was applied on the semi-continuous prototype to treat the initial clay slurry with a solids content of 10 wt%. The thickened clay was collected after 3.3 hours of operation, and the clay cake had a strong solid structure as shown in Figure 4-11. The average solids content of the clay cake is about 24.4 wt%. During the operation, the 10 wt% clay slurry was continuously fed into the system, and the thickened clay was moved out by the conveyor belt. The semi-continuous prototype was shown to be capable of continuously producing the thickened clay by the electrokinetic dewatering.

Figure 4-11. A thickened clay cake with an average solids content of 24.4 wt% was produced under the electric field of 8 V/cm. The electrodes distance was 3.2 cm and the residence time was 3.3 h (photograph by Rui Kong).

4.2.2 Supernatant Water

Although the thickened clay was produced continuously, the supernatant water was difficult to obtain from the operation of this prototype. The difficulty of producing a clarified water characterized this prototype to be a semi-continuous process. Under a fully-continuous operation, the supernatant water was expected to form on the top layer of the suspension, as shown in Figure 4-12A. In the ideal case, the supernatant water was formed at the top layer, and the thickened clay was removed on the side of the tank. However, the clarified water zone was observed only when the operation was stopped for relaxation after several hours operation. The supernatant region during a steady-state operation of producing thickened clay cake is shown in Figure 4-12B. There was a vague boundary between the "supernatant water" and clay suspension. Under operating conditions, the triangular zone was found to contain a mixture of clarified water and unprocessed clay suspension, leading to the observed solids content of about 2-3 wt%.

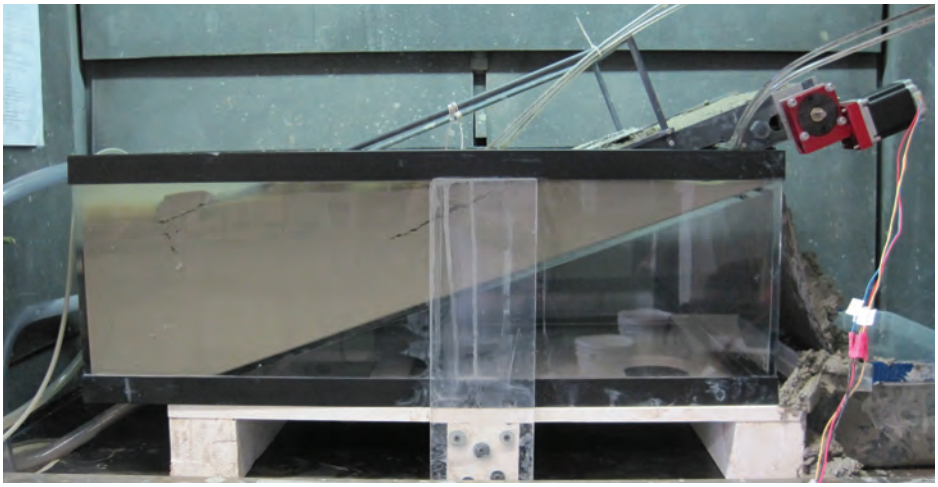

A

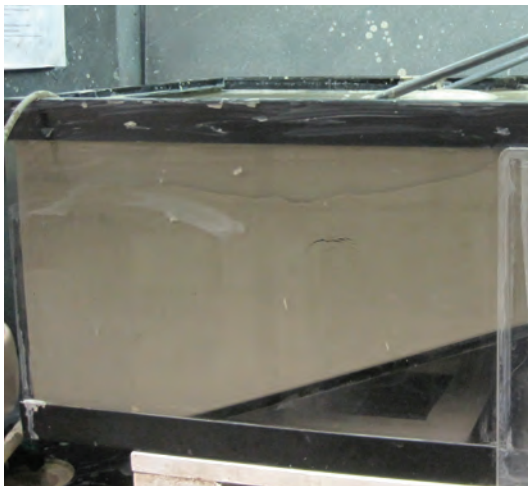

B

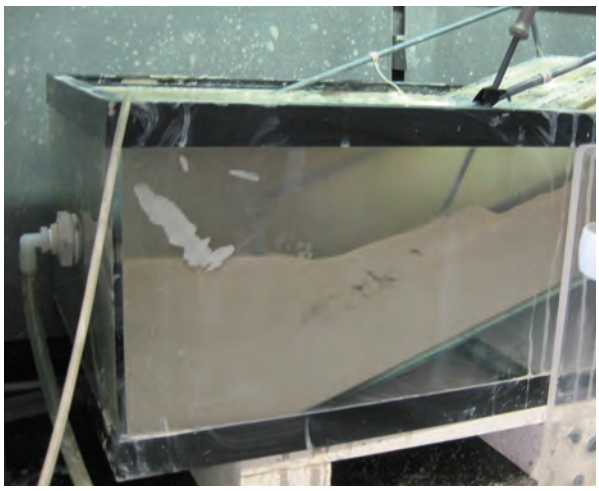

C

Figure 4-12. Supernatant water in semi-continuous prototype for solids removal. A) An ideal case where a layer of supernatant water was formed. B) The triangular zone was turbid during a steady-state operation. C) The triangular zone was clear when clay was depleted in tank (photographs by Rui Kong).

If the new clay was not fed into the tank, or fed at a very low speed, the clay suspension in the triangle zone would be diluted by the supernatant water gradually, and finally become clear as shown in Figure 4-12C. Although a clear water region was obtained, the process was not in a steady-state because the feeding speed was extremely low and only small quantity of clay cake with low solids content could be produced. Therefore, for

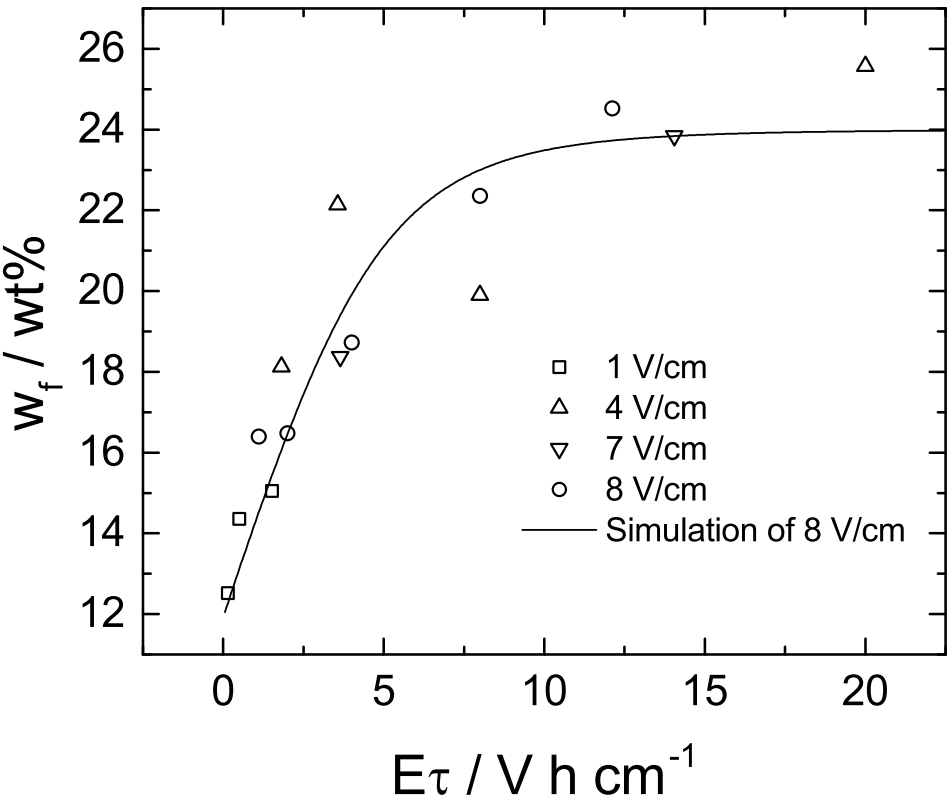

Figure 4-13. Final solids content as a function of Eτ with electric field as a parameter. The electrode spacing was 6.2 cm. The solid line represents a simulation of 8 V/cm by constitutive relationship.

the purpose of producing thickened clay cake with this semi-continuous prototype, the operation condition does not allow the existence of the supernatant water region.

4.2.3 Final Solids Content

A series of experiments with the electrode spacing of 6.2 cm was conducted to evaluate the final solids content influenced by the electric field and the residence time. The residence time τ is defined by

$$\tau = \frac{L}{v_{\text{belt}}} \tag{4–1}$$

where L represents the effective length of the electrode (the length of cathode under water, 50 cm), and v_{belt} represents the speed of the conveyor belt. The final solids content w_{f} of the thickened clay as a function of $E\tau$ is shown in Figure 4-13. The final solids content increased linearly as a function of τ in the short time, and reached a plateau at a long

time. For the experiment with an applied electric field of 8 V/cm, the final solids content increased to 24.5 wt% in the long time. For the experiment with an applied electric field of 1 V/cm, the maximum final solids content was only 15 wt%. The regression of the experiment results was in the form of the constitutive relationship derived by McKinney and Orazem[69], represented by

$$w_f = [(aE\tau + c)^{-n} + b^{-n}]^{-1/n} \tag{4–2}$$

where for an applied electric field of 8 V/cm, a=2.5, b=24, c=12, and n=5.

From the constitutive relationship, the final solids content increased with the increase of τ at the beginning, and reached a maximum value which depended only on the electric field. For a same residence time, the final solid content would increase with an increased electric field at the linear region of the curve. At the plateau region of the curve, the increase of the electric field would only increase the energy consumption. Therefore, the operation should be conducted at the point of inflection for best efficiency.

4.2.4 Effect of Electrode Spacing

The experiments were conducted with a reduced electrode spacing of 3.2 cm, and the final solids content as a function of $E\tau$ is shown in Figure 4-14. Similar to the results obtained from the 6.2 cm experiments, the final solids content at plateau was affected by the applied electric field. The final solids content was smaller than 15 wt% for an applied electric field of 1 V/cm. As the electric field increased to 10 V/cm, the final solids content increased to 25.8 wt%. The performance of the experiment with the 8 V/cm electric field was between the other two. The simulation result on the experiments with 8 V/cm was obtained from the constitutive relationship in Equation 4–2. The final solids content at the plateau from the experimental data (shown in circle) was higher than the simulation result. Since the simulation result was obtained from the 6.2 cm experiments, the difference of the simulation and 3.2 cm experiment results could be attributed to the change of the electrode spacing. There are two reasons for the better final solids

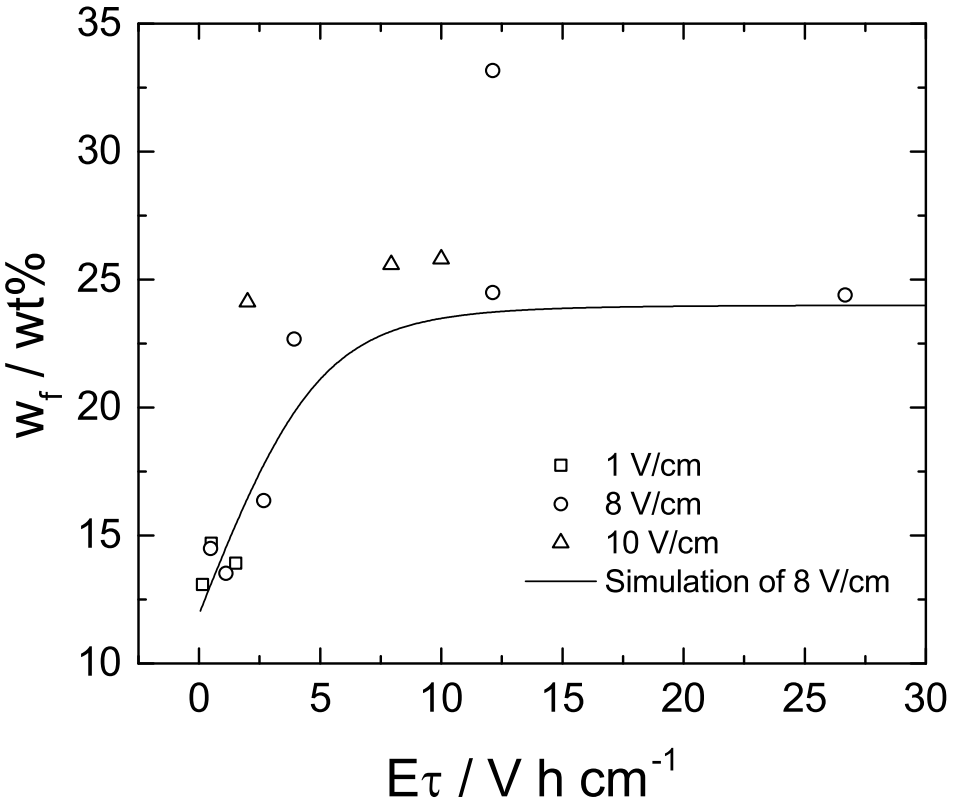

Figure 4-14. Final solids content as a function of Eτ with electric field as a parameter. The electrode spacing was 3.2 cm.

content obtained by the reduced electrode spacing. The first one was from the mechanical design of the prototype. As shown in Figure 4-8B, the cathode was placed on a frame was about 0.5 cm (the frame thickness) lower than the cathode. In the experiments with 6.2 cm electrode spacing, the frame did not cause a problem. But in the experiments with 3.2 cm spacing spacing, if a clay cake thicker than 2.7 cm was formed on the belt and moved with out of the water, the portion that was higher than 2.7 cm would be shaved off by the frame, leaving only the thickness of 2.7 cm clay cake passed through the frame. Photographs taken for the 6.2 cm and 3.2 cm experiments are shown in Figure 4-15. In Figure 4-15A, a clay cake thinner than 5.7 cm was formed between the electrodes with 6.2 cm spacing. As the clay cake moved out of the tank, the frame did not touch the clay, and the clay surface showed a non-uniform thickness distribution. In the experiment with 3.2 cm electrode spacing as shown in Figure 4-15B and Figure 4-11, the top layer of the

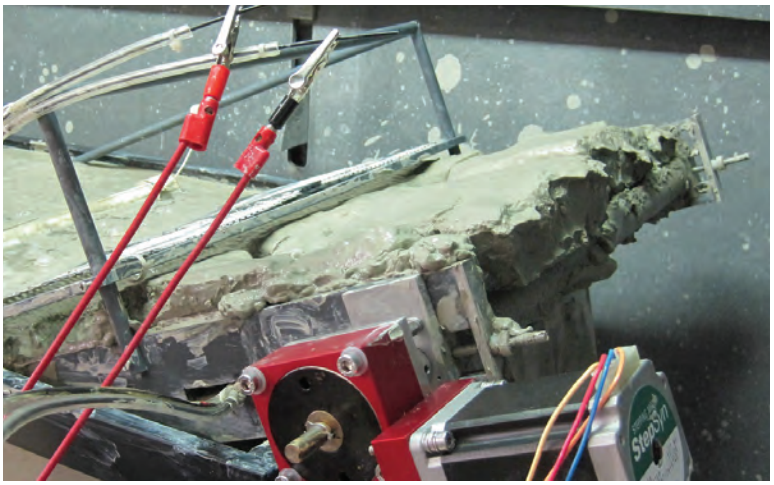

A

B

Figure 4-15. Shaving effect due to the reduced electrode spacing. A) With the electrode spacing of 6.2 cm, the clay cake was formed with a non-uniform surface. B) With the electrode spacing of 3.2 cm, the clay cake was sliced off by the cathode frame, leaving a flat clay surface (photographs by Rui Kong).

clay cake was shaved by the frame, and the produced clay had a perfect flat surface. Since the frame thickness of 0.5 cm was a fixed number, it was much easier for the shaving effect to happen in the 3.2 cm experiments than in the 6.2 cm experiments. In principle, the shaving effect would also exist in the 6.2 cm experiments if a very high electric field was applied for a very long τ. However, this phenomenon was not observed in our experiments. As the clay settled on the belt under the electric field, the solids content of the clay cake was not uniformly distributed in the vertical direction, and the top layer of the clay cake

tended to have lower solids content compared to the other layers. Therefore, the removal of the top layer by the cathode frame resulted in a higher average final solids content of the thickened clay.

The second reason for the high final solids content in the reduced electrode spacing is a combined result of the shaving effect and the presence of electrokinetic dewatering for the region of electrode that was out of water. Since the top layer of the clay cake was shaved by the cathode frame and filled the space between the cathode and anode, the clay cake had direct contact with the electrodes. The electric field remained in effect as the clay moved out of the suspension; thereby, increasing the solids content of the clay cake.

4.2.5 Effect of Intermittent Power

It was reported that the intermittent current increased the efficiency of electrokinetic dewatering on a bench-top cell[61]. To evaluate the influence of the intermittent power on the semi-continuous prototype, the experiments were conducted by controlling the DC power with a cycle duty of 2 minutes on/ 2 minutes off and 15 minutes on/ 15 minutes off. The other experimental conditions were remained the same. As shown in Figure 4-16A, the open circle represents the control experiment with the DC power. The system was operated under the 8 V/cm electric field and 3.2 cm electrode spacing. The filled symbol represents the experiment with the intermittent power. The residence time τ for the intermittent power was calculated by Equation 4–1. From Figure 4-16A, the final solids content of the experiments with intermittent power was very close to the final solids content of the experiments with the DC power. Since the effective time of the applied electric field was only half for intermittent power experiments compared to the DC power experiments, the total applied energy was greatly reduced by applying the intermittent power. However, the intermittent power did not necessarily save energy. As shown in Figure 4-16A, the experiment with the intermittent power was operated in the plateau region of the curve. If the residence time τ for the intermittent experiment was defined as the effective residence time for the clay exposed in the electric field, the points would

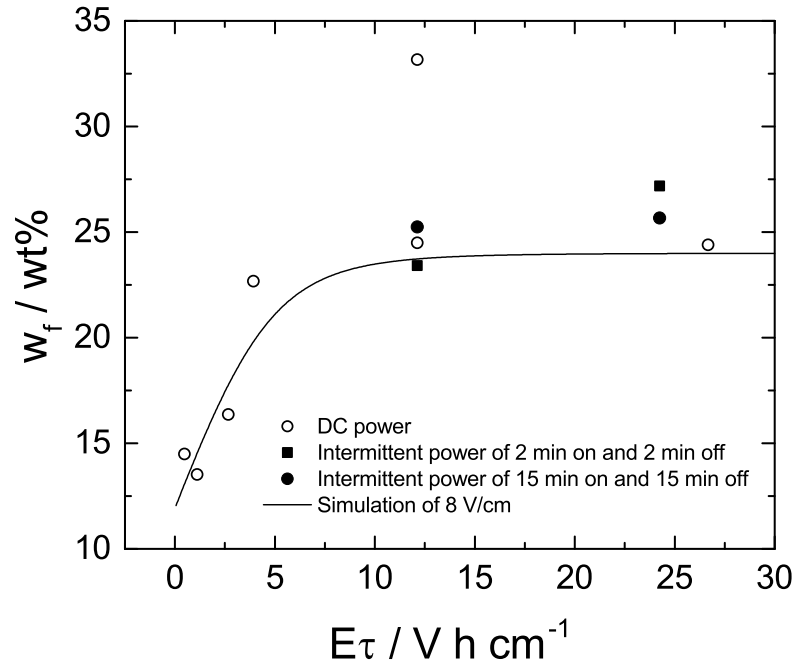

A

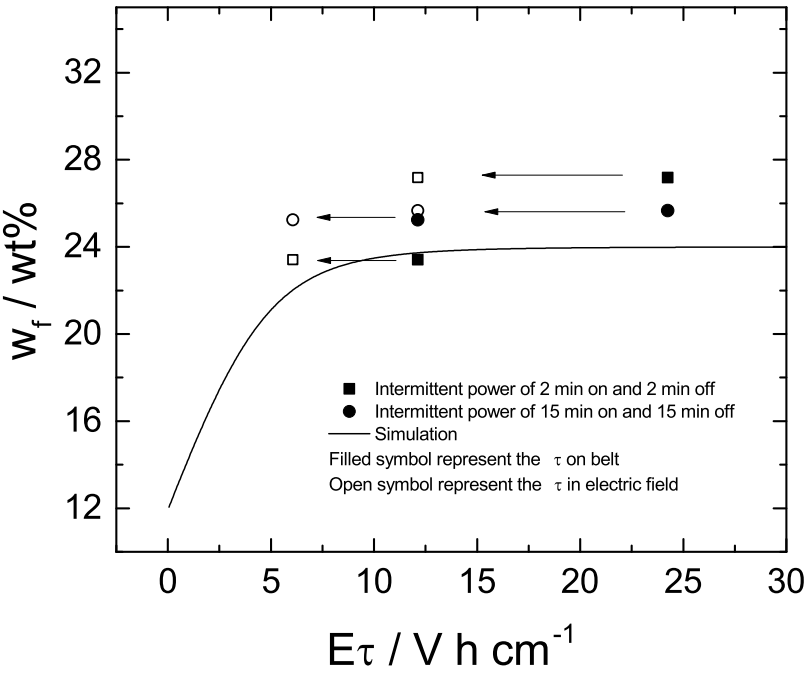

B

Figure 4-16. Final solids content as a function of $E\tau$ under the influence of intermittent power. A) Final solids content as a function of $E\tau$ with DC power and intermittent power. The experiments were conducted under an electric field of 8 V/cm and 3.2 cm electrode spacing. B) The points shifted if τ was defined as the effective residence time for the clay exposed in the electric field.

shift to the smaller $E\tau$ side as shown in Figure 4-16B. The shifted points still followed the constitutive relationship, and the corresponding energy consumption would be similar to the DC power experiment.

From the result of the experiment with the intermittent power, the applied intermittent power with half time on and half time off did not reduce the energy consumption. Because the experiments were conducted on the plateau region, the system was under the inefficient operation condition. Future experiments should be designed carefully to be near or before the interception point for the evaluation of the influence of intermittent power.

4.3 Discussion

The semi-continuous prototype for solids recovery was developed to remove the thickened clay formed by electrokinetic dewatering. The solids content of clay increased from 10 wt% to 24 wt% within 2 hours, under an electric field of 8 V/cm. The experiment result showed that the increase of the electric field increased the final solids content. In this section, the energy consumption is discussed in terms of final solids content and electric field.

4.3.1 Energy Consumption

The energy consumption in the semi-continuous prototype intended to remove solids could be defined as

$$E_{\mathrm{req,w}} = \frac{V_{\mathrm{cell}} I}{Q_{\mathrm{m,w}}} \tag{4–3}$$

where $E_{\mathrm{req,w}}$ represents the energy consumption per mass of water removed ($\mathrm{Wh/kg_{H_2O}}$), V_{cell} represents the cell potential (V), I represents the total current (A), and $Q_{\mathrm{m,w}}$ represents the mass flow rate of the supernatant water (kg/h). The value of $Q_{\mathrm{m,w}}$ was determined from the mass balance,

$$Q_{\mathrm{m,w}} = Q_{\mathrm{m,f}} \left(\frac{w_{\mathrm{f}}}{w_{\mathrm{in}}} - 1 \right) \tag{4–4}$$

where w_{in} represents the initial solids content of the clay slurry, w_f represents the final solids content of the thickened clay, and $Q_{m,f}$ represents the mass production rate of the thickened clay.

The energy consumption is shown in Figure 4-17A as a function of the electric field for the semi-continuous prototype of solids recovery and the results from previous prototypes. The energy consumption increased with the increase of the applied electric field. For each electric field, the value of $E_{req,w}$ depended on the operation conditions, such as the residence time and the electrode spacing. At 1 V/cm, the energy consumption was only about 0.16 Wh/kg_{H_2O}, but the final solids content was also very low, only about 14.7 wt%. When only experiment results with final solids content greater than 20 wt% are retained, as shown in Figure 4-17B, the lowest energy consumption increased to 18.7 Wh/kg_{H_2O}, and the applied electric field was higher than 4 V/cm.

The relationship of the energy consumption and the final solids content in the prototype dedicated for solids removal is presented in Figure 4-18. The energy consumption increased as the final solids content increased from 13 wt% to 20 wt%. For final solids content higher than 20 wt%, the energy consumption varied in a range of 20-500 Wh/kg_{H_2O}, depending on the operation conditions. The lowest value of energy consumption was obtained under the optimum operation condition, which was the infection point on the curve of constitutive relationship.

4.3.2 Heating Issue

The semi-continuous prototype intended for solids removal was evaluated with operation conditions including the residence time and electric field. The final solids content of more than 20 wt% could be achieved for an electric field higher than 4 V/cm. If the required final solids content increased to 25 wt%, the applied electric field has to be increased to 8 V/cm. During the operation under an electric field of 8 V/cm, the temperature of the bulk suspension increased from 24 °C to 40 °C in four hours. The clay was heated by the current, and the efficiency of electrokinetic dewatering was greatly

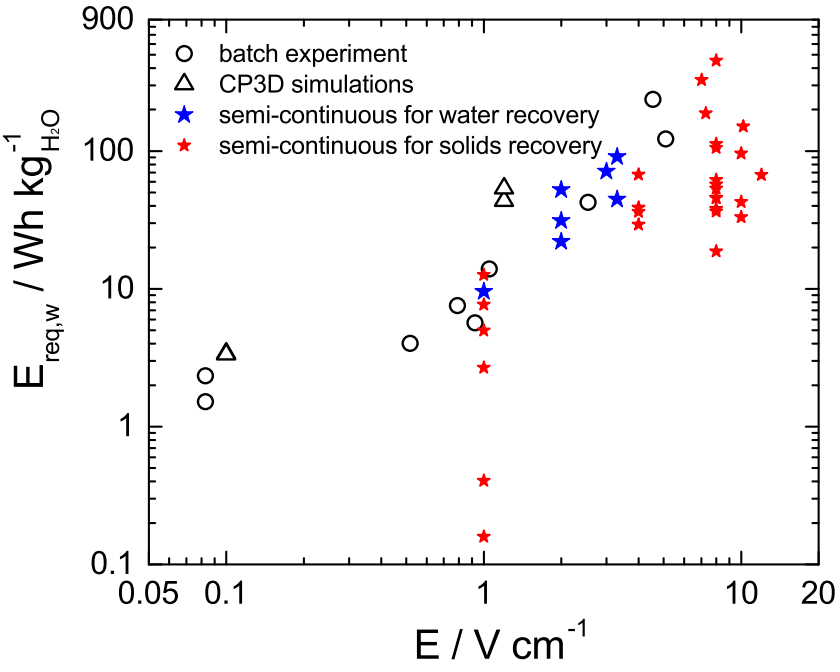

A

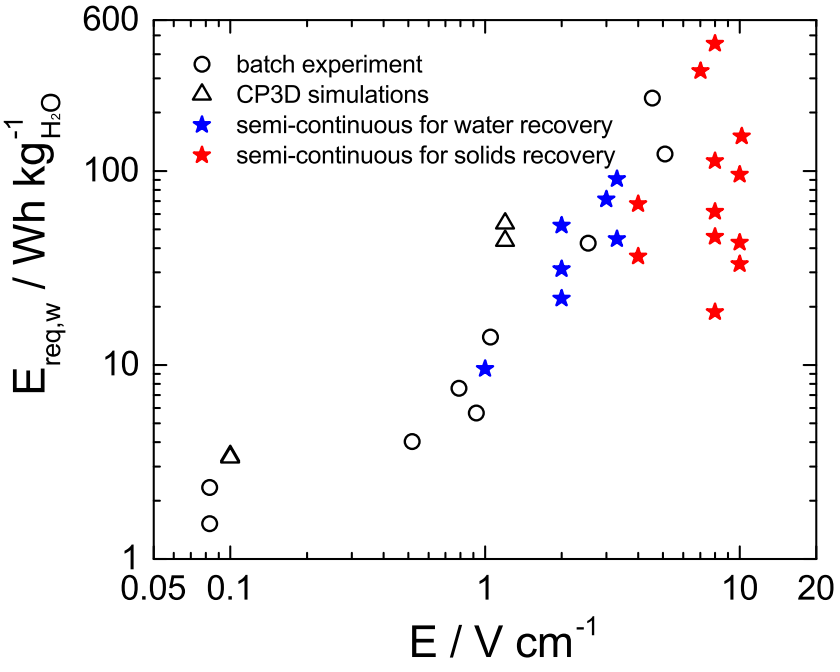

B

Figure 4-17. Energy requirement as a function of applied electric field. The batch experiments and CP3D simulation results were reported by McKinney and Orazem[69, 70]. A) Experimental results obtained from semi-continuous prototype for solids recovery in comparison to the results from previous prototypes. B) Only experimental results with final solids content higher than 20 wt% are shown in semi-continuous prototype for solids recovery.

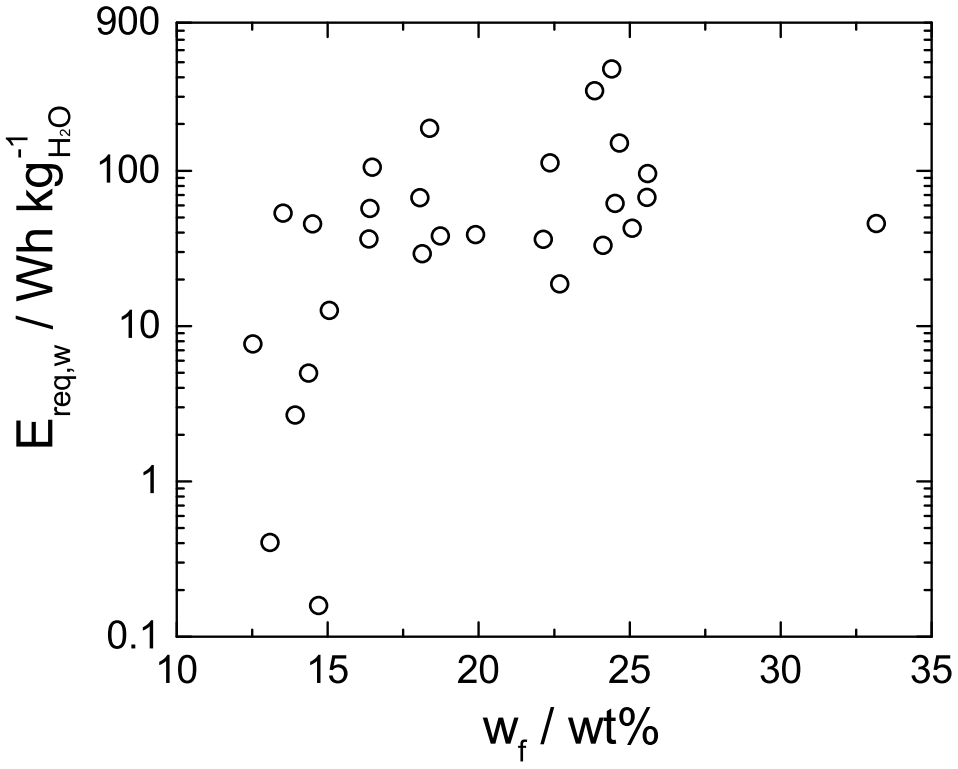

Figure 4-18. Energy consumption as a function of final solids content in semi-continuous prototype for solids recovery.

reduced. The increased temperature could also reduce the life span of the electrode. Since the heating issue was not observed with the electric field lower than 8 V/cm, an applied electric field of 8 V/cm is the recommended highest value for this configuration.

CHAPTER 5
FULLY-CONTINUOUS PROTOTYPE

The semi-continuous experiment for removing solids successfully generated thickened clay with solids content of about 25 wt% under appropriate operation conditions. However, the triangular space above the cathode caused re-mixing of water with the feed slurry. As a result, a stream of clear supernatant water could not be generated during the operation. In this chapter, a fully-continuous prototype is presented that was designed to produce continuously thickened clay and supernatant water and, thereby, maximize the separation efficiency.

5.1 Experimental

The concept is to combine the design of prototype for water recovery and the prototype for solids recovery. The fully-continuous prototype includes a horizontal part aimed to generate clear water, and an angled part for solids removal. The first generation was designed and constructed as shown in Figure 5-1. A pair of parallel electrodes were placed horizontally in a shallow tank. The clay cake was formed under an applied electric field in the horizontal part, and removed by the moving belt in the angled region. A few preliminary tests were conducted on this prototype with operation parameters similar to that of semi-continuous prototype, but the final solids content of thickened clay was not satisfactory. As the clay was moving out of the space between horizontal electrodes and entered into the angled part, it was still under water, possibly causing the rehydration of clay cake. Therefore, an improvement was made by adding a pair of electrodes to the angled region of the first prototype. This new design was termed the second generation of the fully-continuous prototype. Unless stated otherwise, all the discussions on the fully-continuous prototype in this dissertation refer to the second generation of prototype.

5.1.1 Cell Design

The concept of the second generation of fully-continuous prototype is illustrated in Figure 5-2. A shallow tank with dimensions of 1.3 m $\times$ 0.5 m $\times$ 0.15 m made with

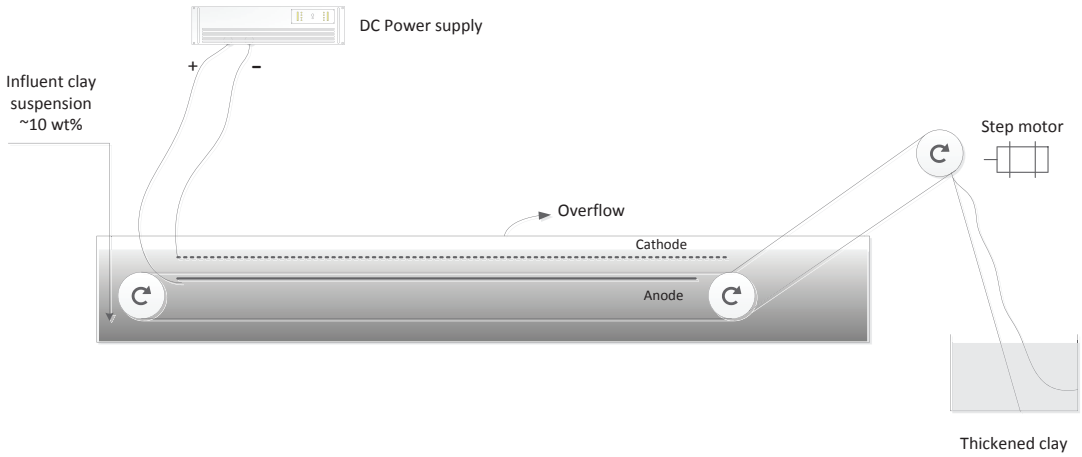

A

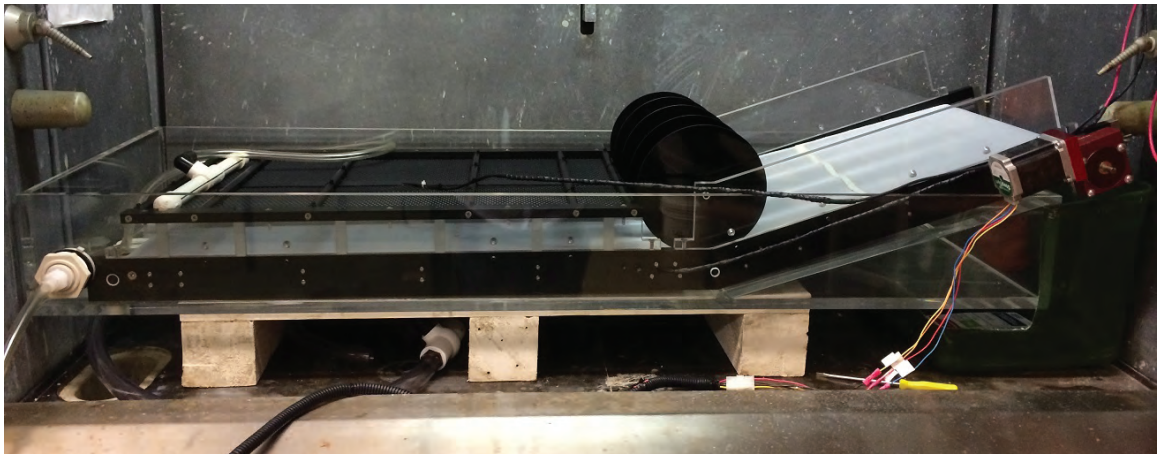

B

Figure 5-1. The first generation of fully-continuous prototype. A) Schematic representation of the first generation of fully-continuous prototype. B) A photograph of the first generation of fully-continuous prototype (photograph by Rui Kong).

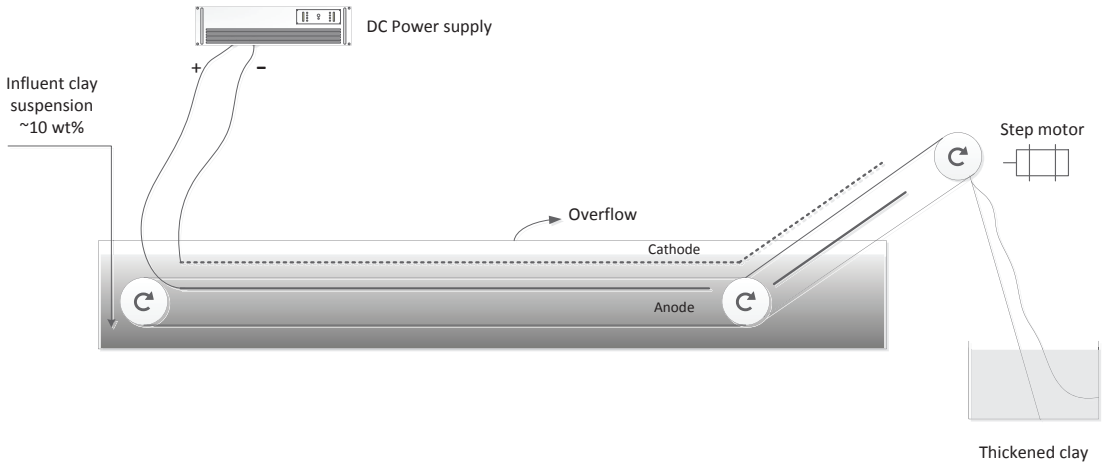

Figure 5-2. Schematic representation of the second generation of fully-continuous prototype.

acrylic material was used as reservoir. The electrodes (titanium with iridium oxide coating from Water Star Inc.) and the conveying belt (U-CMY-530, Component Supply Co.) were constructed on a frame which was fitted in the shallow tank. The prototype was composed of two functional regions: a cake formation zone (horizontal part) and a cake dewatering zone (angled part). In each zone, a pair of electrodes were placed in a parallel configuration, and the two zones were connected by the conveyor belt surrounding the anode. In the horizontal zone, the distance between cathode and anode could be adjusted between 3.2 cm and 6.2 cm. A lot of effort was taken to make a reliable connection of the belt, including the test of the epoxy glues of major brands. All of the epoxy glues failed after about a week of constant use in the aqueous environment with the strong tension on belt, but the belt connected by sewing, as seen in Figure 5-3, worked very well. The electrodes in the horizontal zone had dimensions of 0.73 m $\times$ 0.38 m, and the electrodes in the angled zone had dimensions of 0.45 m $\times$ 0.38 m. The anodes were made of solid plate, and the cathodes were made of expanded mesh plate to facilitate easy passage of gas and liquid. The combination of a stepper motor and a worm gear was used to provide enough driving force to move the belt, and the belt speed was controlled between 0.3 m/hour and

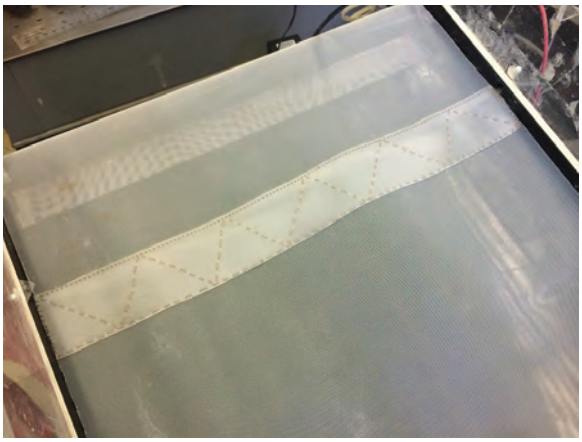

Figure 5-3. The connection of conveyor belt by sewing (photograph by Rui Kong).

2 m/hour. The cell potential was provided by a DC power supply, which was connected to the cathode and anode using copper wires. The cathodes in horizontal zone and angled zone were connected to each other, and the anodes in horizontal zone and angled zone were also connected to each other. The configuration was selected to eliminate unnecessary current flow in the horizontal direction.

A photograph of the assembled prototype is shown in Figure 5-4. During operation, the 10 wt% phosphatic clay suspension was fed at a controlled flow rate from the beginning (left) of horizontal zone. The liquid level was maintained at about 5 mm above the cathode by aspiration using a peristaltic pump. In the horizontal zone, electrophoresis was the major electrokinetic phenomenon, under which the solid particles moved to the anode to form a clay cake under the influence of an electric field. The horizontal zone is also called the cake formation zone.

As the clay cake was generated in the cake formation zone and moved towards the angled zone, the belt made a slight turn without affecting the already formed clay cake. The change in direction was realized by two designs which provided a uniform force on belt: five wheels were placed above the belt to provide the bending force on belt, and two nylon fishing lines were placed across the belt to distribute the bending force. The fishing line chosen for this application was Zebco Omniflex monofilament 30 lb. test (0.023 inch

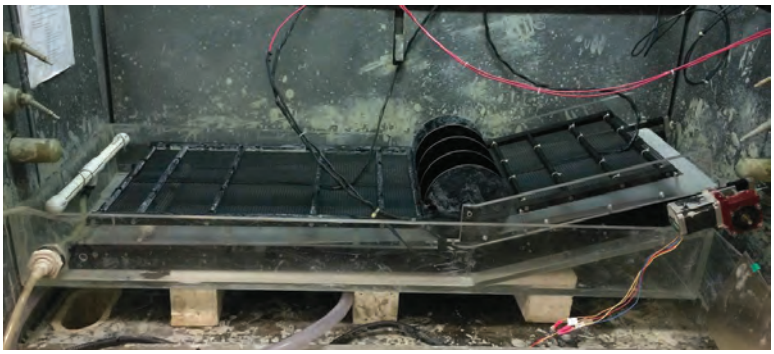

A

B

Figure 5-4. Experimental setup of fully-continuous prototype. A) Empty device. B) Device in operation (photographs by Rui Kong).

diameter). The line was strong enough to hold the force, and thin enough to keep the clay cake undisturbed.

The angled zone had two functions: applying electrokinetic dewatering on clay cake and pulling thickened clay cake out of tank. As the clay cake exited the horizontal zone and entered the angled zone, it was still under an applied electric field. The electro-osmosis was the major electrokinetic phenomenon in the angled zone, and the water was squeezed out by electric force, and flowed back to the tank. This region is also called the cake dewatering zone. For the best dewatering efficiency, the cathode in the angled zone was placed lightly on the clay to maximize the contacting area between clay cake and electrode. The height of the cathode was adjustable to accommodate this requirement. During the steady-state operation, the clay cake was formed in cake

Figure 5-5. The collection tray of fully-continuous prototype (photograph by Rui Kong).

formation zone, thickened in cake dewatering zone, and collected after been dropped from the tank into a collection tray, as shown in Figure 5-5.

5.1.2 Experimental Protocol

At the beginning of the experiment, the tank was filled with the phosphatic clay suspension with a concentration of about 10 wt% solids. The belt speed was controlled by a frequency generator, and the cell potential was provided by a DC power supply. At the angled zone, the cathode was elevated such that the distance between the cathode and the anode was not smaller than the distance between the two electrodes in horizontal region. This preliminary configuration was selected to ensure that the clay cake did not contact cathode, as shown in Figure 5-6A. After the clay cake was formed on belt, the screws on the cathode in the angled zone were released and the cathode was allowed to float on the clay cake, as shown in Figure 5-6B. As the steady state was achieved, the collection of the thickened clay cake started. The total mass of thickened clay was measured and

A B

Figure 5-6. The cake dewatering zone of fully-continuous prototype with the cathode lifted up and released. A) The cathode was lifted at the beginning of the experiment. B) The cathode was released to float on the clay cake during steady-state operation (photographs by Rui Kong).

recorded as m_{total}, and the wet clay production rate $Q_{\text{m,f}}$ was calculated by m_{total}/t, where t is length of time for collection. The average solids content w_{f} was calculated as discussed in Section 3.1.3. During the operation, the cell current and potential were recorded with a time interval of 30 minutes. The supernatant water samples were collected from horizontal zone every 30 minutes. The turbidity and pH value of supernatant were measured immediately when the water samples were collected, and a second measurement was conducted after one day of in cell free settling by gravity.

5.1.3 Instrumentation

The cell potential was provided by an Agilent Technologies N8759A DC Power Supply (Shown in Figure 5-7. Range: potential 0-100 V, current 0-50 A). The feed flow rate of phosphatic clay suspensions was controlled by a Masterflex Model 77202-60 digital peristaltic pump (Shown in Figure 5-8, Cole-Parmer Instrument Company). This pump was also used to evacuate supernatant water. The turbidity of supernatant water was measured using a HACH 2100Q Portable Turbidimeter (range: 0-1000 NTU). The frequency which controlled the belt speed was generated by a HEATHKIT Function

Figure 5-7. DC power supply of fully-continuous prototype (photograph by Rui Kong).

Figure 5-8. Water pump of fully-continuous prototype (photograph by Rui Kong).

Generator Model IG-1271. The belt driving force was provided by a SANYO DENKI Model 103H7126-5740 stepper motor and Ondrives PF30-60NM Worm wheel gearbox, Nema Flange, 60:1.

5.2 Results

The performance of the fully-continuous prototype was evaluated by measuring the quality of supernatant water, the final solids content of the thickened clay, and the power and energy consumption during the operation.

5.2.1 Supernatant Turbidity

Since the turbidity of supernatant was very similar for all experiments under different operation parameters, the experiment with an electric field of 4 V/cm and a residence time of 2.4 h (belt speed of 0.5 m/h) is used here to illustrate the turbidity of supernatant water generated from the fully-continuous prototype. The change in supernatant turbidity in the fully continuous system is presented in Figure 5-9 as a function of elapsed time, given as t/τ, where τ is residence time calculated by the total length of electrode divided by belt speed. The residence time was 2.4 hours in the present case. The black square represents the measured turbidity immediately after the water sample was collected, and the red circle represents the supernatant turbidity after one day of free settling. The supernatant water turbidity was relatively stable during the operation. The turbidity was between 100 and 1000 NTU when measured immediately after the sample water was collected, and dropped dramatically after one day of free settling in the cell, reaching a value as low as 1 NTU. This behavior was very similar to that obtained by the semi-continuous prototype for water removal (as shown in Figure 3-3). As a smaller NTU was achieved using the semi-continuous prototype for water recovery, the electric field likely separated most of the clay particles from the suspension, but the bubbles generated by the electrochemical reactions brought some particles to the upper layer that were mixed with the supernatant water. These particles were mainly composed of calcite which has a bigger diameter than clay particles, and settled very quickly by gravity. Thus,

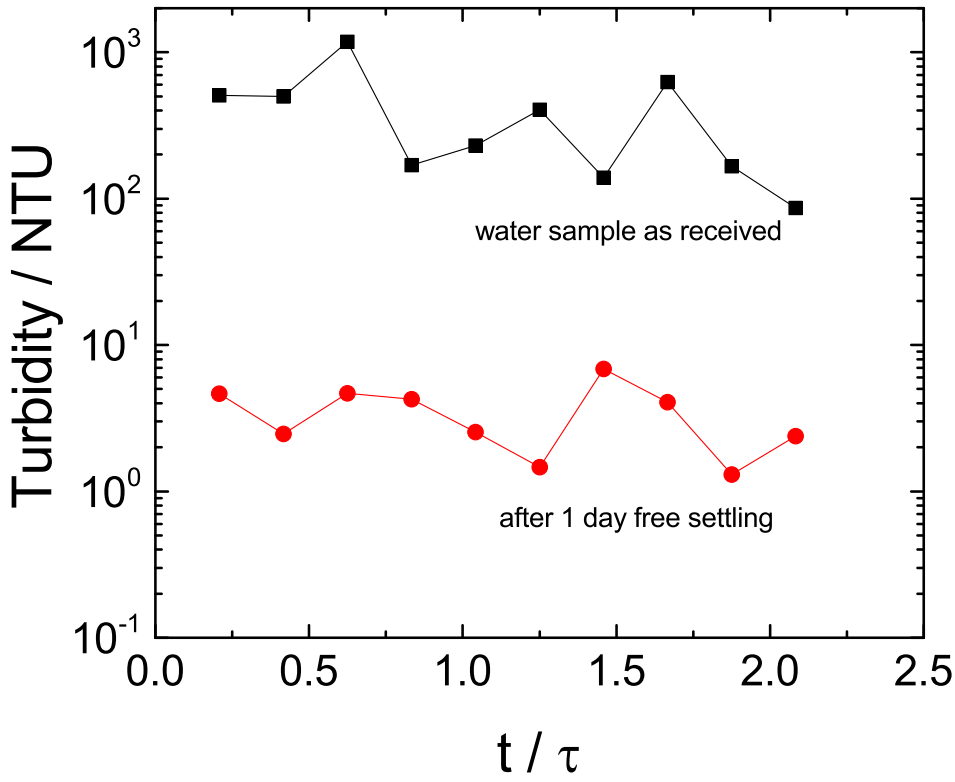

Figure 5-9. Turbidity of supernatant liquid as a function of scaled elapsed time for an electric field of 4 V/cm and a belt speed of 0.5 m/h (τ=2.4 h): ■ measured immediately after the sample was collected, and ● measured 24 hours after the sample was collected. The electrode spacing was 6.2 cm.

the supernatant with the high turbidity caused by the coarse particles was easily clarified by free settling.

The corresponding pH value of the water samples in Figure 5-9 is presented in Figure 5-10. The supernatant pH varied from 11.5 to 13 during the operation due to the products of electrochemical reaction in Equation 6–5. The pH remained around 12 after one day free settling.

Under fully continuous operation, the entire system is in a dynamic balance. Although the supernatant turbidity decreases and pH increases as a general trend, the measured value could be very different from one location to another, indicating that the position of the clear water region was changed during the operation. The current method of supernatant water collection was used to show the capability of generating supernatant

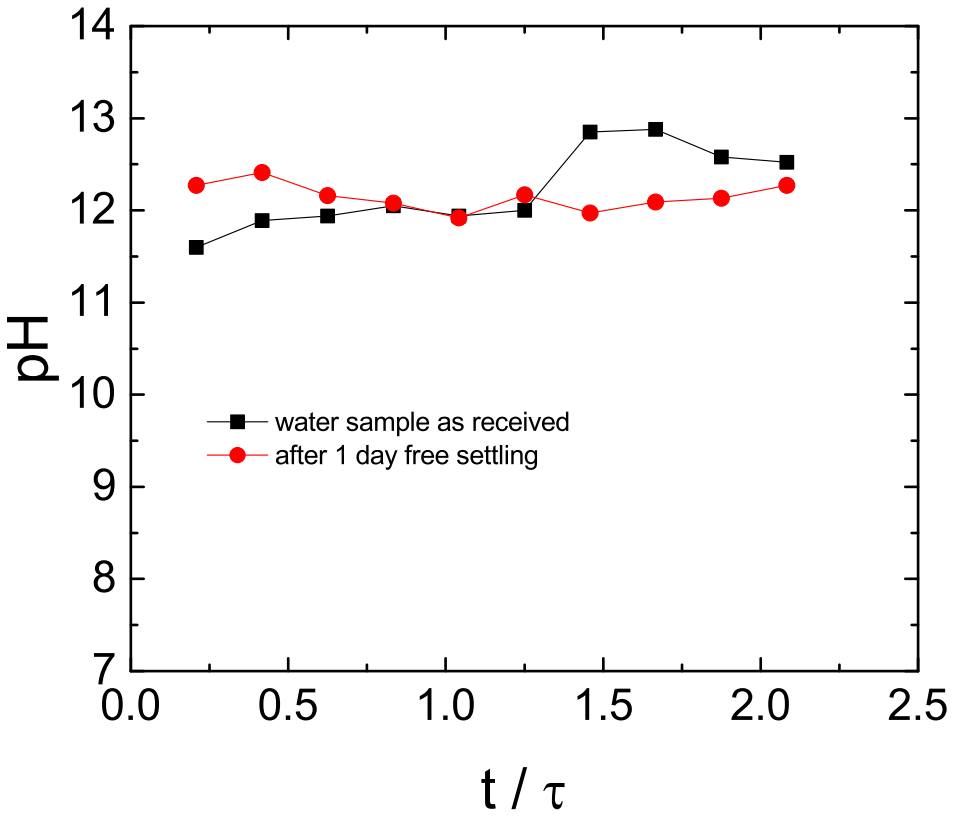

Figure 5-10. pH of supernatant liquid as a function of scaled elapsed time corresponding to the results presented in Figure 5-9.

clear water with the fully-continuous prototype. However, in the on-site implementation, an improved water collection method will be needed to collect supernatant water of consistent quality.

5.2.2 Final Solids Content

A series of experiments with electrode spacing of 6.2 cm and electric field of 4 V/cm were conducted with residence time ranging from 0.59 h to 2.4 h (belt speed from 0.5 m/h to 2 m/h). The final solids content is shown in Figure 5-11 as a function of $E\tau$. For τ smaller than 1.2 h, the final solids content increased with the increase of $E\tau$, from 20 wt% to 32 wt%. The final solids content reached the plateau with τ larger than 1.2 h. At the region where τ is larger than 3 h, the final solids content appeared to decrease. The solid line in Figure 5-11 is the fitting result from the constitutive relationship (Equation 4–2) with parameters of a=3.5, b=32, c=14, and n=5. The simulation curve is in good

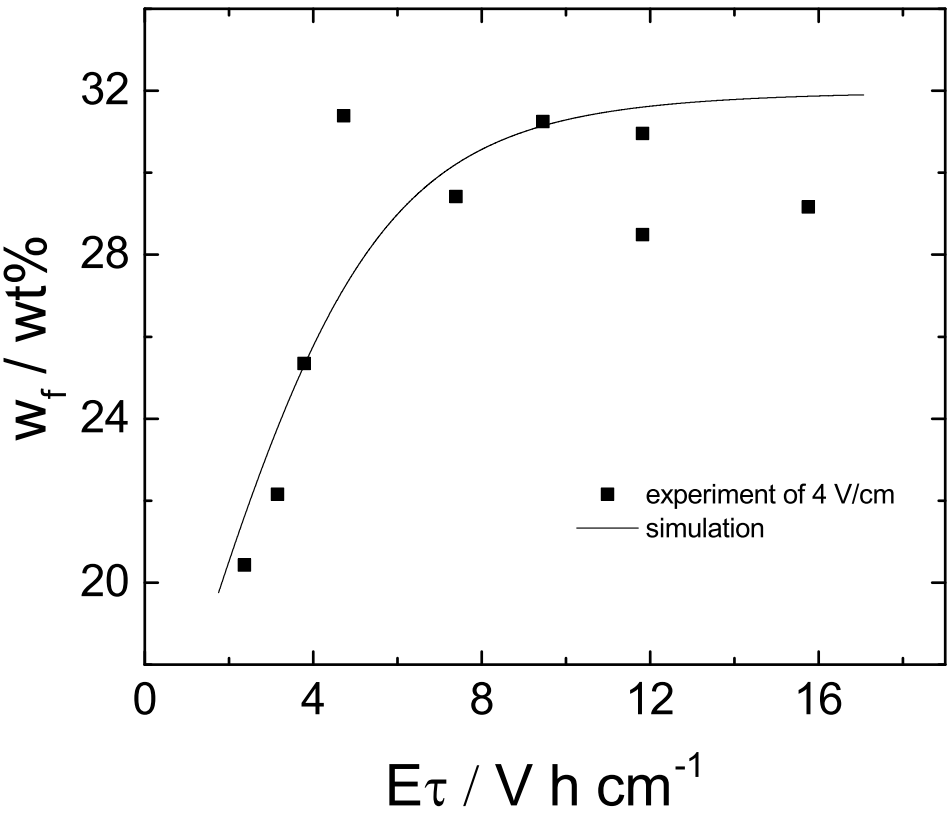

Figure 5-11. Final solids content as a function of $E\tau$ under an electric field of 4 V/cm. The scatters represent the experimental results, and the solid line represents the simulation result (obtained from Equation 4–2 with a=3.5, b=32, c=14, n=5).

agreement with experimental results, with the exception when τ is larger than 3 h. A photograph taken from the wheels region of the prototype at τ=3 h suggests an explanation for the discrepancy between measured and predicted solids content values, as is shown in Figure 5-12. With a 4 V/cm electric field and a very slow belt speed, an obvious build-up of solids appeared at the wheels region, which blocked the movement of the thickened clay. The high-solids content clay was blocked at the wheel region, and the clay that traversed the wheel region and could be collected had a lower solids content. Thus, the average final solids content was underestimated. Since the reduced solids content was caused by the mechanical design instead of the principle of electrokinetic dewatering, it could be improved by a future design of the prototype.

Figure 5-12. Excessive build-up of deposit in the cake formation zone caused solids dam at wheels. E=4 V/cm, τ=3 h (photograph by Rui Kong).

From this fully-continuous prototype, the experiments with τ longer than 3 h in 4 V/cm electric field were not suitable to evaluate the performance of electrokinetic dewatering. The final solids content from experiments with observed blocking issues are not considered in the following discussion.

In order to explore the influence of the applied electric field on the final solids content, experiments were conducted for electric fields of 1 V/cm and 2 V/cm. The reduced electric field was achieved by reducing the cell potential and keeping the same electrode spacing in the horizontal zone. The electrode spacing in the angled zone was equal to the clay cake thickness, which is always controlled by the system itself. The final solids content is shown in Figure 5-13 as a function of $E\tau$ with electric fields of 1 V/cm, 2 V/cm, and 4 V/cm. In a few experiments at 1 V/cm, the cathode in the angled zone did not properly contact the clay cake: these results are labeled as "1 V/cm poor contact" in the plot. In these experiments, the effective electrokinetic dewatering area was reduced due to the poor contact, and the produced clay had a lower solids content.

From the results of batch and semi-continuous prototypes, the increase of electric field increased the final solids content of thickened clay. However, this statement is not

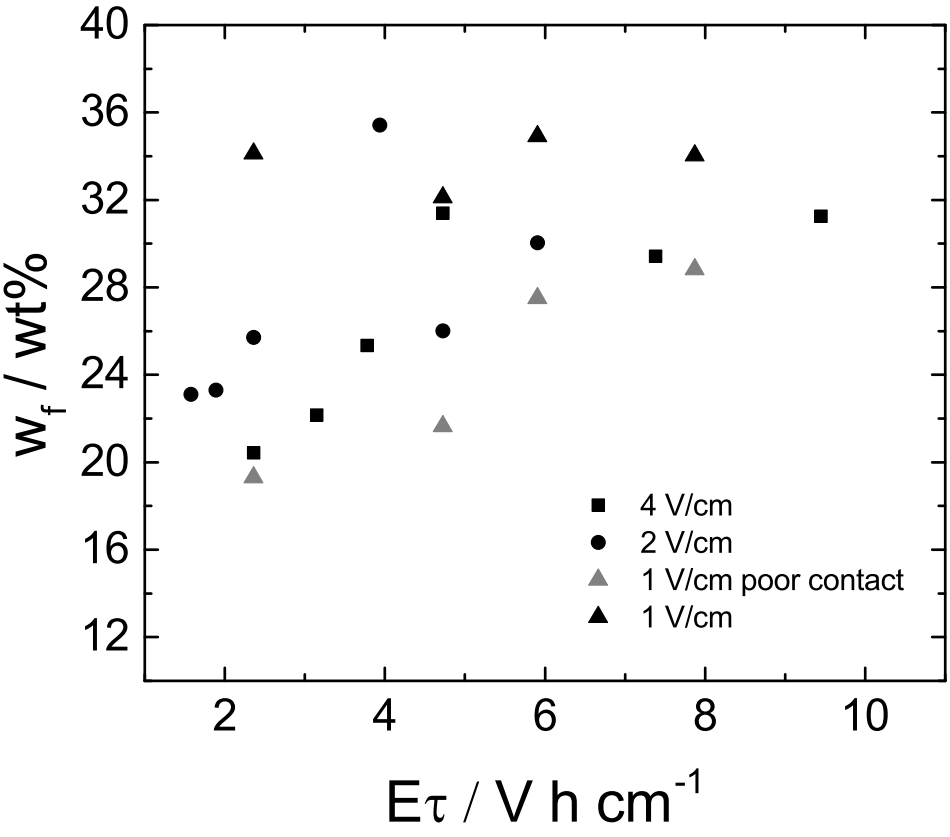

Figure 5-13. Final solids content as a function of $E\tau$ with electric field as a parameter.

true for the fully-continuous prototype. As shown in Figure 5-13, the experiments with an electric field of 1 V/cm produced the clay with a final solids content up to 35 wt%, and the experiments with electric field of 4 V/cm produced the clay with the final solids content only about 32 wt%, given a long enough time. This result suggests that the applied electric field of 1 V/cm is high enough for the fully-continuous prototype.

5.2.3 Energy Consumption

The power consumption in the fully-continuous experiment is defined by Equation 3–3, which is the same as in batch and semi-continuous experiments. In the field of clay dewatering, the energy consumption could be evaluated by the energy consumption per unit mass of removed water $E_{\mathrm{req,w}}$, defined by

$$E_{\mathrm{req,w}} = \frac{P_{\mathrm{req}}}{Q_{\mathrm{m,w}}} \tag{5–1}$$

where $E_{\text{req,w}}$ is the energy consumption per kg of water removed ($\text{Wh/kg}_{\text{H}_2\text{O}}$), P_{req} is the power consumption (W), and $Q_{\text{m,w}}$ is the effluent mass flow rate of supernatant water (kg/h). The energy consumption per unit mass of produced dry solids is given by

$$E_{\text{req,s}} = \frac{P_{\text{req}}}{Q_{\text{m,s}}} \tag{5–2}$$

where $E_{\text{req,s}}$ is the energy consumption per kg of dry clay produced ($\text{Wh/kg}_{\text{solids}}$) and $Q_{\text{m,s}}$ is mass production rate of dry clay (kg/h).

The effluent mass flow rate of supernatant water is calculated from the materials balance, i.e.,

$$w_{\text{f}} Q_{\text{m,f}} = w_{\text{in}} (Q_{\text{m,w}} + Q_{\text{m,f}}) \tag{5–3}$$

Equation 5–3 can be expressed as

$$Q_{\text{m,w}} = Q_{\text{m,f}} \left(\frac{w_{\text{f}}}{w_{\text{in}}} - 1 \right) \tag{5–4}$$

where w_{in} is the initial solids content of clay suspension, w_{f} is the final solids content of the thickened clay, and $Q_{\text{m,f}}$ is the mass production rate of the thickened wet clay. The production rate of dry clay is calculated from

$$Q_{\text{m,s}} = w_{\text{f}} Q_{\text{m,f}} \tag{5–5}$$

The energy consumption per kg of removed water is presented in Figure 5-14 as a function of applied electric field for experiments ranging from batch to the fully-continuous prototype. The red squares represent the fully-continuous experimental results under various operation conditions with electric field of 1 V/cm, 2 V/cm, and 4 V/cm. The results shows that, in the fully-continuous experiments, the increase of applied electric field increased the energy consumption. This trend is in agreement with all previous experiments. Under the same electric field, the fully-continuous operation had the lowest energy cost as compared to other experiments.

The final solids content is shown in Figure 5-15 as a function of energy consumption

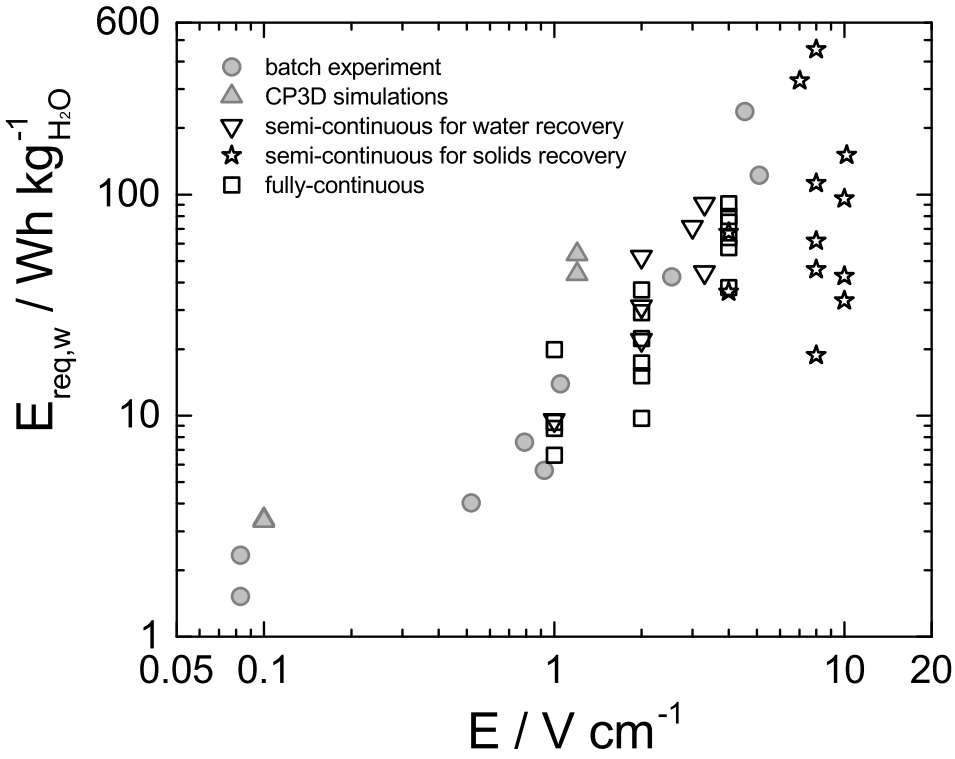

Figure 5-14. Energy consumption as a function of applied electric field. The batch experiments and CP3D simulation results were reported by McKinney and Orazem[69, 70]

with electric field as a parameter. The corresponding residence time is labeled for each point. The applied electric field varied from 1 V/cm to 4 V/cm, and τ varied from 0.59 h to 3.9 h. As shown in Figure 5-15, the lower electric field is favorable for fully continuous operation. With the electric field of 1 V/cm and residence time of 3.0 h, the solids content w_f reached 35 wt% with the energy cost $E_{req,w}$ smaller than 10 Wh/kg_{H_2O}. As the electric field increased to 4 V/cm, the energy of at least 63 Wh/kg_{H_2O} was consumed to achieve the final solids content of 32 wt%. The experiments with 2 V/cm had a performance between the experiments at 1 V/cm and 4 V/cm. The experiments with poor contact cathode reduced the final solids content, but the energy consumption was not reduced.

5.3 Discussion

The fully-continuous prototype was designed and constructed, and the performance of fully continuous operation was evaluated by measuring the turbidity of supernatant water

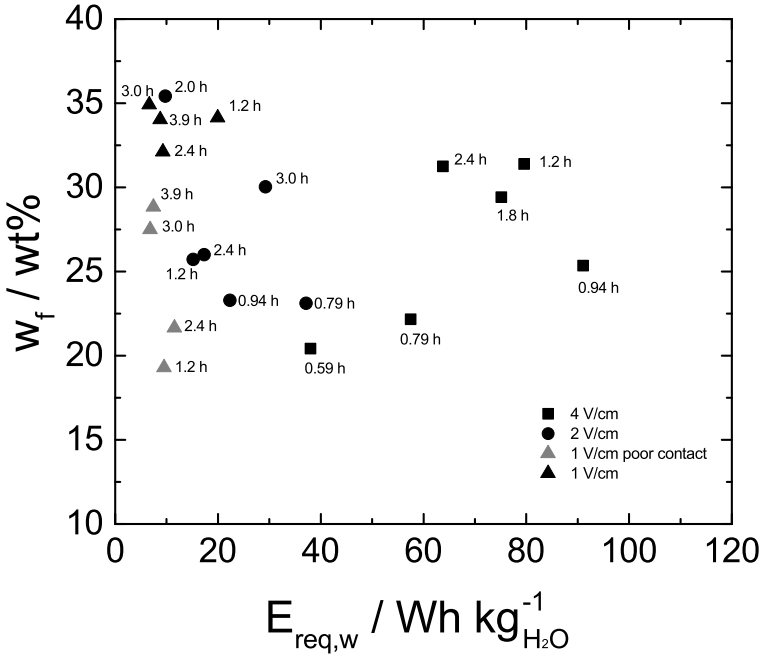

A

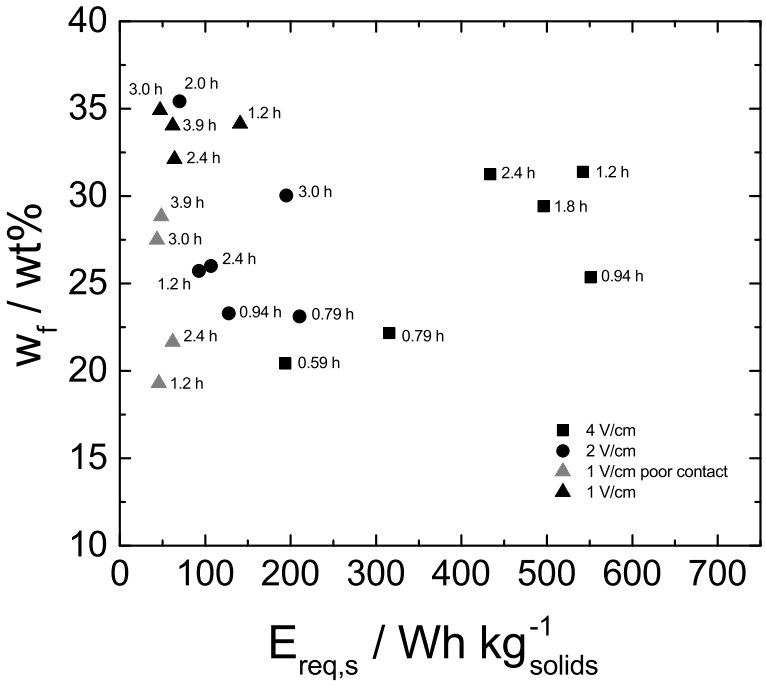

B

Figure 5-15. Relationship between final solids content and energy consumption of fully-continuous prototype. A) Energy consumption evaluated by mass of water removed. B) Energy consumption evaluated by mass of dry clay produced.

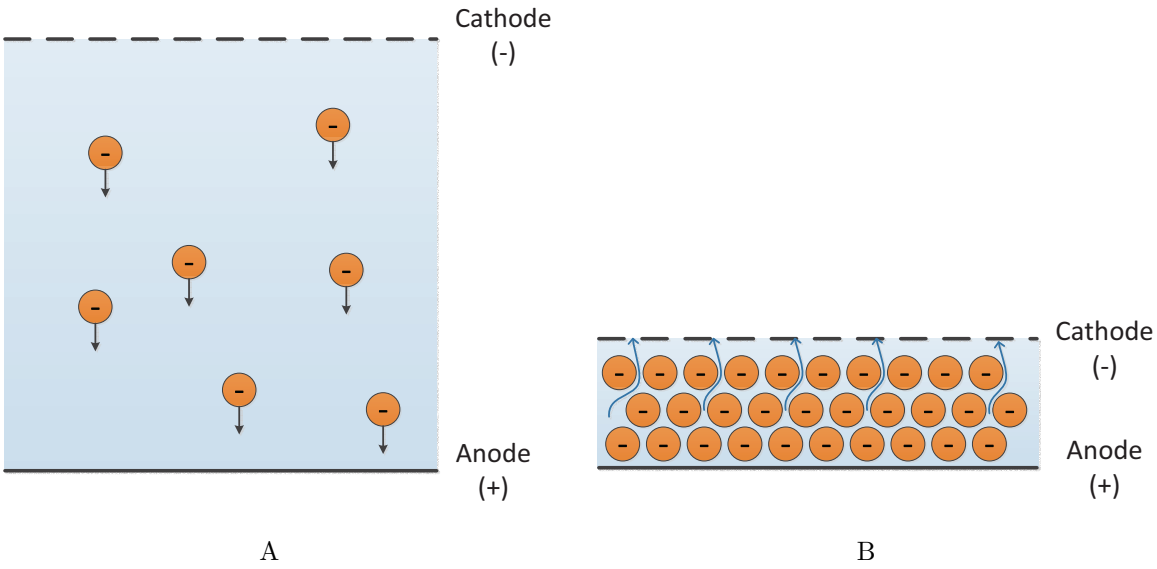

Figure 5-16. An illustration of the cake formation zone and the cake dewatering zone. A) Cake formation zone. B) Cake dewatering zone.

and the final solids content of thickened clay. A stream of low turbidity (10 NTU after settled) supernatant water was continuously generated, and the thickened clay with the solids content up to 35 wt% was continuously produced. Even with a smaller electric field, the system produced higher solids content while consuming less energy. The reason for the good performance with a small electric field is discussed in the present section, and the performance is compared between prototypes from batch to fully continuous.

5.3.1 Cake Formation Zone and Cake Dewatering Zone

In order to explain the good performance using a small electric field under fully continuous operation and to provide guidance for future improvement, the mechanism of the fully continuous system was investigated. The system is composed a cake formation zone and a cake dewatering zone with the wheels region as the boundary. The cake formation zone is the horizontal zone, fed by the initial clay slurry with the solids content of 10 wt%. Influenced by the applied electric field, the clay particles migrate to the anode (bottom) and accumulate on the slowly moving conveyor belt, as shown in Figure 5-16A. The thickness of the clay cake increases with time. Under the optimum operation condition, the clay cake builds up and fills the space between the cathode and anode at

the end of the cake formation zone, with the solids content high enough to maintain the solid state, and a thickness small enough to be able to move past the wheels. In the cake formation zone, the electrokinetic separation is mainly in the form of electrophoresis, represented by the movement of solids in the suspension.

As the clay cake passes the wheels and moves to the cake dewatering zone, as shown in Figure 5-16B, the extra water flows back to the tank and the clay cake is exposed in air. The cathode is placed loosely on the clay cake to maximize the contact area between cathode and clay, and fixed on the frame along the direction of belt motion. In the cake dewatering zone, the supernatant water is extracted from the porous structure of clay cake, and moved to the cathode. The movement of water in the porous clay cake can be described by the phenomenon of electro-osmosis. The clay dewatering zone is like a power squeezer which effectively squeezes the water from the clay cake.

The electric field in cake formation zone differs from the electric field in cake dewatering zone. The whole system is powered by a constant DC voltage V_{cell}, and the potential is equal for both cathodes in cake formation zone and cake dewatering zone, as well as anode. The distance between cathode and anode d in cake formation zone is fixed, and the electric field is defined by V_{cell}/d, which is maintained at a constant value during the operation. The electrode distance in the cake dewatering zone is equal to the thickness of clay cake $\delta(x)$, and $\delta(x)$ is a function of location x. The electric field in the cake dewatering zone is represented by $V_{\text{cell}}/\delta(x)$. Because the cake thickness decreases with the increase of solids content, $\delta(x)$ decreases along the belt moving direction, as shown in Figure 5-17. In the experiments, the electric field of 1 V/cm, 2 V/cm, and 4 V/cm represent the electric field in the cake formation zone. In the cake dewatering zone, the electric field increases as a result of the decreased electrode spacing, which is controlled by the system itself. If a thin layer of clay cake is formed in cake formation zone due to a low electric field, the electrode spacing in cake dewatering zone will be small, the electric field in cake dewatering zone will be large, and a clay cake with the high solids

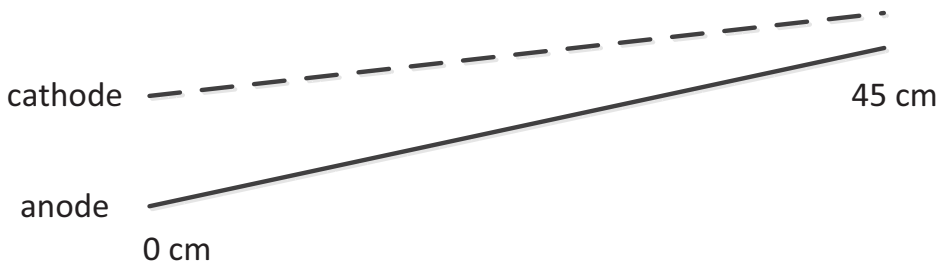

Figure 5-17. Illustration of clay sampling positions in cake dewatering zone.

content will be produced. This explains that the 1 V/cm experiments produced higher solids content w_f as compared to experiments using 2 V/cm and 4 V/cm.

A local measurement of clay thickness and solids content was conducted on clay dewatering zone to show the variation of electric field along the belt moving direction. As shown in Figure 5-17, the left edge of anode is defined to have a position at 0 cm, and the total length of electrode is 45 cm. Seven points were selected along the anode, at the position of 10 cm, 14 cm, 21 cm, 27 cm, 32 cm, 39 cm, and 45 cm. At each sampling point, the average clay thickness was measured, and the average solids content was determined. The electric field and solids content is represented in Figure 5-18 as a function of position. The position is represented by x, in unit of cm, and the value of x from 0 cm to 10 cm represents the wheels region. There is no sampling point between 0 cm to 10 cm because it is very difficult to collect sample, and even if collected, the result is not reliable due to the existence of wheels. At x=10 cm, the electric field was 2 V/cm, twice that of the electric field in cake formation zone. At the end of cake dewatering zone, the electric field increased to 13 V/cm, which is 13 times of the electric field in cake formation zone. The dramatic increase of electric field explains the result obtained from Figure 5-18B, where the solids content increased from 23 wt% to 31 wt% in the cake dewatering zone.

Inspired by the exploration of cake formation zone and cake dewatering zone, the optimization of fully continuous operation is considered to be a balance between the two regions. The cake formation zone initiates the formation of clay cake and needs to be long

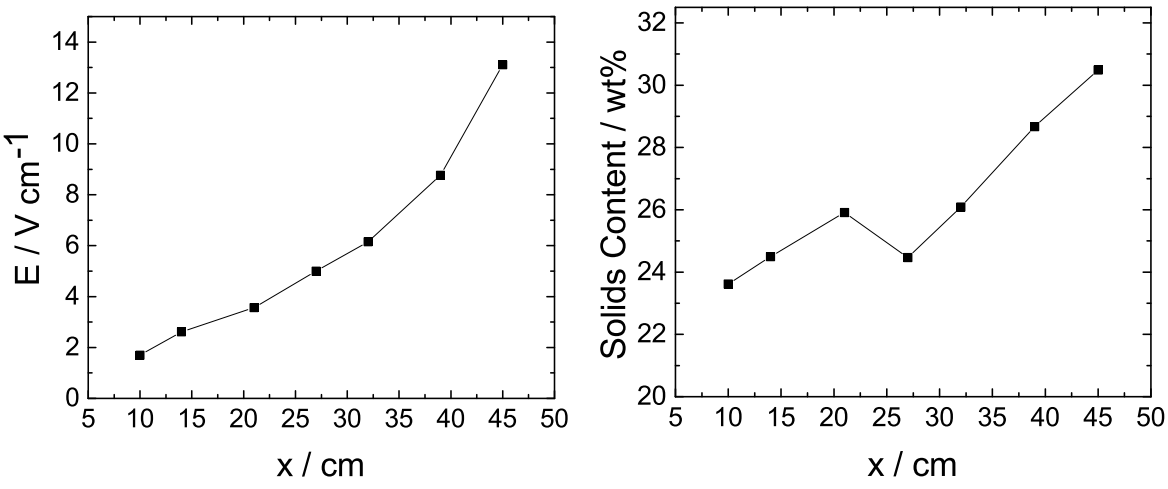

Figure 5-18. Changes of electric field and solids content in the cake dewatering zone. The experiment was conducted under an applied electric field of 1 V/cm, electrode spacing of 6.2 cm, and residence time of 1.2 h. A) Electric field as a function of position. B) Solids content as a function of position.

enough to form the solid clay cake, yet short enough to avoid wasting energy. The cake dewatering zone is the second part of the continuous electrokinetic dewatering system, and the dramatically increased electric field extensively squeezes the water from the clay cake. The final solids content w_f of the thickened clay is controlled by the combination of cake formation zone and dewatering zone.

5.3.2 Economic Assessment

An economic assessment for on-site implementation was conducted based on the results obtained from semi-continuous and fully-continuous prototypes and compared to the simulation results obtained by McKinney and Orazem[70]. The results are shown in Table 5-1. McKinney and Orazem evaluated the power and energy consumption of electrokinetic dewatering based on the batch operation for an one square mile clay settling pond at the Mosaic Four Corners Mine in central Florida. The predicted energy consumption was 41.3 Wh/kg_{H_2O} for the increase of solids content from 10 wt% to 25 wt% under an applied electric field of 1.2 V/cm. A power consumption of 44,000 MW was predicted for the treatment of the entire clay settling pond.

Table 5-1. Economic analysis for on-site implementation.

E	w_f/wt%	T_w/NTU	τ/h	P_{req}/MW	E_{req}	Electricity Cost[d]
1 V/cm[a]	35	9.1	3.0	29	47 Wh/kg_{solids}	$\$2.9/10^3 kg_{solids}$
					6.6 Wh/kg_{H_2O}	$\$0.41/10^3 kg_{H_2O}$
2 V/cm[a]	35	4.2	2.0	43	70 Wh/kg_{solids}	$\$4.3/10^3 kg_{solids}$
					9.7 Wh/kg_{H_2O}	$\$0.60/10^3 kg_{H_2O}$
4 V/cm[a]	31	3.5	2.4	269	434 Wh/kg_{solids}	$\$27/10^3 kg_{solids}$
					103 Wh/kg_{H_2O}	$\$6.4/10^3 kg_{H_2O}$
10 V/cm[b]	26	N/A	1.0	141	210 Wh/kg_{solids}	$\$13/10^3 kg_{solids}$
					42.7 Wh/kg_{H_2O}	$\$2.6/10^3 kg_{H_2O}$
1.2 V/cm[c]	25	N/A	19	44,000	248 Wh/kg_{solids}	$\$15.4/10^3 kg_{solids}$
					41.3 Wh/kg_{H_2O}	$\$2.56/10^3 kg_{H_2O}$

[a] Fully-continuous prototype
[b] Semi-continuous prototype for solids removal
[c] Batch experiments[70]
[d] Electrical cost based on industrial rates of \$0.062/kWh

The on-site evaluation with semi-continuous and fully continuous operation was conducted assuming a continuous treatment of the output clay slurry from Mosaic Four Corners Mine, which is 130,000 GPM phosphatic clay slurry with solids content of 2 wt%. The influent flow rate was converted to 26,000 GPM for clay slurry with solids content of 10 wt%. The applied electric field, final solids content, residence time, and thickened clay production rate were obtained from the best experimental result. The power requirement was scaled up by the influent flow rate. A detailed calculation is presented in Chapter 6. The best result from the semi-continuous operation was obtained using an electric field of 10 V/cm. The on-site evaluation shows that an energy consumption of 42.7 Wh/kg_{H_2O} and a power consumption of 141 MW would be required to produce 26 wt% clay. In the fully continuous operation, a lower electric field is preferred, and the experiment with an electric field of 1 V/cm produced a thickened clay with solids content of 35 wt% and an energy consumption only about 6.6 Wh/kg_{H_2O}. The corresponding on-site implementation requires the input power of only 29 MW for the treatment of 26,000 GPM (10 wt%) phosphatic clay slurry. When the electric field was increased to 4 V/cm, a final solids content of only 31 wt% was obtained even with a much higher energy consumption.

As compared to the results from the semi-continuous operation, the electric field needed to achieve a final solids content of 26 wt% or higher, was greatly reduced by the fully-continuous operation, and the energy consumption was reduced from 42.7 Wh/kg_{H_2O} to 6.6 Wh/kg_{H_2O}. Compared with the batch experiment, the fully-continuous prototype increased the final solids from 25 wt% to 35 wt%, reduced the energy consumption from 41.3 Wh/kg_{H_2O} to 6.6 Wh/kg_{H_2O}, and dramatically reduced the power consumption from 44,000 MW to 29 MW.

5.3.3 Limitations of the Fully-Continuous Prototype

Although the fully continuous experiment achieved a final solids content of 35 wt% with a residence time of 3 hours and an energy consumption of 6.6 Wh/kg_{H_2O}, with applied electric field of only 1 V/cm, the performance of the fully-continuous prototype can be improved. The room for improvement is evident from the already observed issues associated with the current version of prototype.

5.3.3.1 Poor Contact in the Cake Dewatering Zone

In the cake dewatering zone, the cathode floats on the clay cake. If the clay thickness were uniformly distributed, the cathode would be in good contact with the clay everywhere on the surface. However, the clay cake was not generated uniformly, and the contact was poor at the thin part of the clay cake. Without contacting the cathode, the electrokinetic dewatering did not happen, and the average final solids content of clay was greatly reduced. The influence of non-uniform clay thickness existed in all fully continuous experiments, and was especially obvious in the experiments of low final solids content. The variability of solids content is shown in Figure 5-19, where the open symbols represent the average final solids content and the filled symbols represent the maximum local value in the same experiment. In the 2 V/cm experiment, the local solids content was 41 wt%, and the average final solids content was only about 35 wt%. In the 1 V/cm experiment, the local solids content was 32 wt%, and the average final solids content was

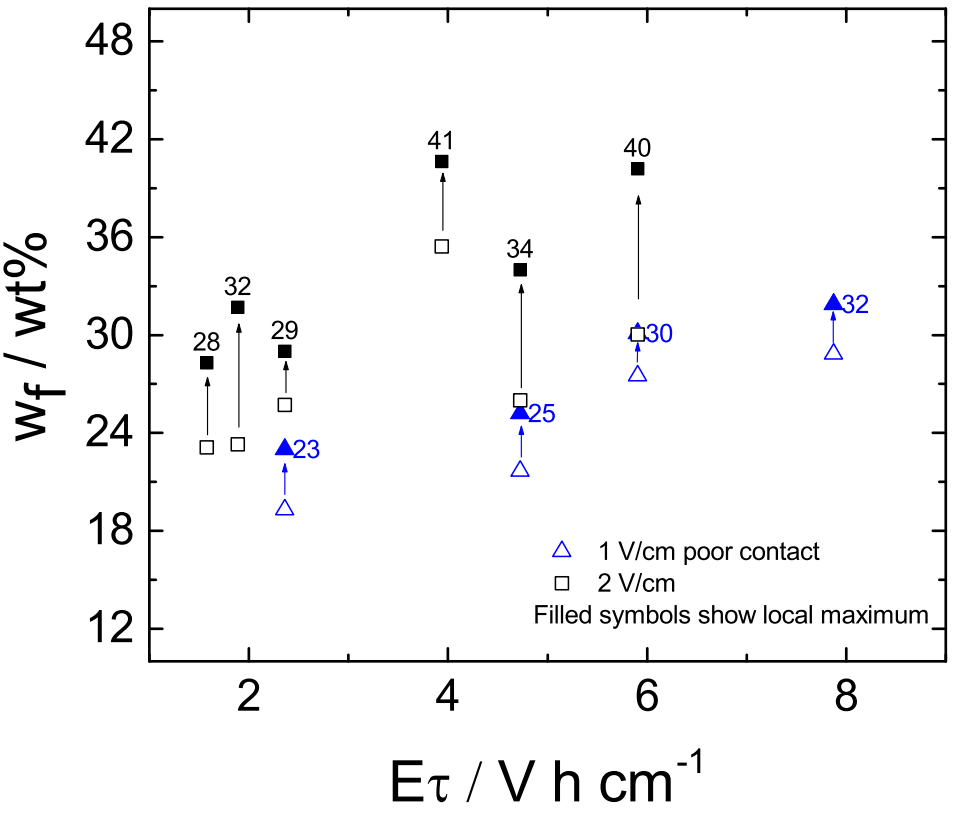

Figure 5-19. Average final solids content and local maximum final solids content under electric field of 2 V/cm and 1 V/cm poor contact.

only about 29 wt%. Under optimal operation, the average final solids content should be the same as the maximum local value.

5.3.3.2 Supernatant Water Collection

Although the low-turbidity supernatant water was produced from the fully-continuous prototype, it was still difficult to collect. The current method of removing water is by aspiration from the surface. The water produced by this method usually contained a mixture of supernatant and solids entrained by gas bubbles rising from the anode, thereby increasing the water turbidity. Another problem is from the non-uniform distribution of the surface clarified water. Because the clear water region always moved during the operation, the water collection location needed to move as well. When the water was not collected in the best location, the turbidity measurement result did not reflect the best value achievable by the system. In the future improvement, it is suggested to add a weir at

the wall of the tank, and to create a space that will allow settling of the suspended solids before removing the supernatant water from the tank.

CHAPTER 6
HYDROGEN EMISSION AND ECONOMIC ASSESSMENT

The fully-continuous prototype developed for electrokinetic dewatering produced low turbidity water and thickened clay. A by-product from this process is the hydrogen and oxygen gas generated on the electrode surface from the electrochemical reactions. The hydrogen and oxygen, continuously generated during the operation, are released immediately into the atmosphere, and hence represent a potential flammability hazard. The concentration of hydrogen was calculated for the lab prototype and estimated for a full-scale on-site installation, and both were found to be below the lower flammable limit. The power and energy consumption for Mosaic's Four Corners plant was predicted using data generated from the model of fully-continuous prototype. The assumptions and procedures used for estimating the hydrogen concentration and economic assessment for mine site treatment is discussed below.

6.1 Material Balance for Fully-Continuous Steady-State Operations

In a fully developed steady-state operation, the weight of solids in the feed suspensions is equal to the weight of solids in the produced thickened clay, represented by

$$w_{\text{in}}\rho_{\text{in}}Q_{\text{in}} = w_{\text{f}}Q_{\text{m,f}} \tag{6–1}$$

Thus, the volumetric feed rate Q_{in} of clay slurry is represented by

$$Q_{\text{in}} = \frac{w_{\text{f}}Q_{\text{m,f}}}{w_{\text{in}}\rho_{\text{in}}} \tag{6–2}$$

where Q_{in} is the influent volumetric flow rate, in m^3/s; w_{f} is the final solids content of the thickened clay, in percent solids; $Q_{\text{m,f}}$ is the mass production rate of the thickened clay, in kg/s; w_{in} is the solids content of the influent clay slurry, in percent solids; and ρ_{in} is the density of the influent clay slurry, in kg/m^3.

6.2 Hydrogen Emission in Lab Prototype and On-Site Implementation

During electrokinetic dewatering, current is carried by ions in the solution and by electrons in the metal electrode. At the interface between the bulk solution and electrode, the electrons are exchanged via the electrochemical reaction. In the electrokinetic dewatering of phosphatic clay suspensions, the major electrochemical reactions at the anode are

$$2H_2O \rightarrow O_2 + 4H^+ + 4e^- \tag{6–3}$$

and, for non-noble electrode M

$$M \rightarrow M^{n+} + ne^- \tag{6–4}$$

At the cathode, the reaction is

$$2H_2O + 2e^- \rightarrow H_2 + 2OH^- \tag{6–5}$$

As shown in Equation 6–3, the oxygen evolution reaction occurs at the anode, and the pH of the solution is decreased by the generation of H^+. The anode material must be very corrosion resistant, because the anode can corrode as shown in Equation 6–4. The anode, in all the prototypes discussed in this paper was a dimensionally stable anode, which contains a layer of IrO_2 deposited on the titanium substrate. This anode is very stable during the oxygen evolution reaction, and thus the corrosion reaction represented by Equation 6–4 was not considered to exist in the system. As shown in Equation 6–5, the hydrogen evolution reaction occurs at the cathode, and the pH of the solution is increased from the generation of OH^-. The hydrogen and oxygen generated at the electrode surface would accumulate if the system is operated in an enclosed space, and could result in an explosion in extreme circumstances. Therefore, the electrokinetic dewatering process must operate with ample ventilation, which means a fume hood in the lab model, and necessary ventilation during plant operations.

Table 6-1. Constants for calculating hydrogen concentration.

Symbol	Parameter	Value
n_e	number of electrons transferred in the reaction	2
M_{H_2}	molecular weight of hydrogen gas	2×10^{-3}kg/mol
F	Faradays constant	96487 C/equiv
R	Universal gas constant	8.3143 J/mol K
T	temperature	298.15 K
P	pressure	101325 N/m^2
k_1	nonideal mixing factor-lab	0.5
k_2	nonideal mixing factor-plant	1/7

Table 6-2. Parameters for calculating hydrogen concentration and energy consumption.

Symbol	Parameter	Unit
$Q_{in,1}$	influent volumetric flow rate - lab	m^3/s
$Q_{in,2}$	influent volumetric flow rate - plant	m^3/s
w_f	solids content of effluent clay cake	wt%
$Q_{m,f}$	mass production rate of the thickened clay	kg/s
w_{in}	solids content of influent clay slurry	wt%
ρ_{in}	density of influent clay slurry	kg/m^3
$Q_{m,1}$	hydrogen evolution rate - lab	kg/s
$Q_{m,2}$	hydrogen evolution rate - plant	kg/s
I_1	total current-lab	A
I_2	total current-plant	A
$Q_{v,1}$	fume hood ventilation rate	m^3/s
$Q_{v,2}$	plant ventilation rate	m^3/s
A_1	duct cross-sectional area - lab	m^2
A_2	duct cross-sectional area - plant	m^2
$\overline{u}_1$	average wind velocity - lab	m/s
$\overline{u}_2$	average wind velocity - plant	m/s
$C_{ppm,1}$	hydrogen concentration - lab	ppm
$C_{ppm,2}$	hydrogen concentration - plant	ppm
V_{cell}	cell potential	V
P_{req}	power consumption	W
$E_{req,w}$	energy consumption	Wh/kg$_{H_2O}$

The quantitative estimation of hydrogen concentration for the lab prototype and on-site operations are illustrated separately, under the assumption of an ideal gas. The constants used are listed in Table 6-1, and the terms are defined in Table 6-2.

For the lab-scale prototype, the hydrogen evolution rate is represented by

$$Q_{m,1} = \frac{I_1 M_{H_2}}{n_e F} \tag{6–6}$$

where $Q_{\mathrm{m},1}$ is hydrogen evolution rate, in kg/s; I_1 is the total current, in A; $\mathrm{M}_{\mathrm{H}_2}$ is the molecular weight of the hydrogen gas, in kg/mol; n_{e} is number of electrons transferred in the reaction; R is universal gas constant, 8.3143 J/mol K; T is temperature, in K; F is Faraday's constant, 96487 C/equiv; and P is pressure, in $\mathrm{N/m^2}$.

The fume hood ventilation rate is represented by

$$Q_{\mathrm{v},1} = A_1 \overline{u}_1 \tag{6–7}$$

where $Q_{\mathrm{v},1}$ is fume hood ventilation rate, in $\mathrm{m^3/s}$; A_1 is duct cross-sectional area, in $\mathrm{m^2}$; and $\overline{u}_1$ is the average air velocity in the fume hood, in m/s.

The concentration of hydrogen gas in fume hood is the balance between hydrogen evolution and ventilation, represented by[73]

$$C_{\mathrm{ppm},1} = \frac{Q_{\mathrm{m},1}\mathrm{R}T}{\mathrm{k}_1 Q_{\mathrm{v},1} P \mathrm{M}_{\mathrm{H}_2}} \times 10^6 \tag{6–8}$$

where $C_{\mathrm{ppm},1}$ is hydrogen concentration in the fume hood, in ppm; k_1 is the nonideal mixing factor in the fume hood (ranges between 0 and 1). The term k_1 was assumed to be 0.5 in these calculations.

For the on-site implementation, the hydrogen evolution rate is proportionally scaled by the feed flow rate, represented by

$$Q_{\mathrm{m},2} = \frac{Q_{\mathrm{m},1} Q_{\mathrm{in},2}}{Q_{\mathrm{in},1}} \tag{6–9}$$

where the subscript 1 denotes the lab-scale prototype and 2 denotes the on-site implementation. The ventilation rate and hydrogen concentration are defined similarly to the lab-scale prototype, represented by

$$Q_{\mathrm{v},2} = A_2 \overline{u}_2 \tag{6–10}$$

and

$$C_{\mathrm{ppm},2} = \frac{Q_{\mathrm{m},2}\mathrm{R}T}{\mathrm{k}_2 Q_{\mathrm{v},2} P \mathrm{M}_{\mathrm{H}_2}} \times 10^6 \tag{6–11}$$

where the subscript 2 denotes the on-site prototype operation, and $\overline{u}_2$ is the wind velocity.

6.3 Cost Estimation for On-Site Operations

For on-site implementation, calculations were performed under the assumption that the electrode distance and electric field are similar to the lab prototype and that the increased treatment capacity is achieved by a proportional increase in the electrode surface area. Under this assumption, the total current for on-site operations is proportionally increased by an increase in the feed flow rate, represented by

$$I_2 = \frac{I_1 Q_{\text{in},2}}{Q_{\text{in},1}} \tag{6–12}$$

The total power consumption is defined as

$$P_{\text{req}} = I_2 V_{\text{cell}} \tag{6–13}$$

and the total energy consumption is defined as

$$E_{\text{req,w}} = \frac{P_{\text{req}}}{Q_{\text{m,w},2}} \tag{6–14}$$

or

$$E_{\text{req,s}} = \frac{P_{\text{req}}}{Q_{\text{m,s},2}} \tag{6–15}$$

where $Q_{\text{m,w},2}$ and $Q_{\text{m,s},2}$ could be obtained from Equations 5–4 and 5–5, respectively. Using an estimated industrial electric power rate of \$0.062/kWh, the total operating cost for on-site operations is calculated to be

$$\text{cost} = E_{\text{req}} \times \$0.062/\text{kWh} \tag{6–16}$$

Equation 6–16 provides the operating cost for electrical power. The annualized capital expenditure is not included in these calculations.

6.4 Example for a Fully-Continuous Operation

A representative experiment operating fully continuously is used as an example for the estimation of hydrogen concentration and energy consumption for on-site operations. This experiment was conducted using an applied electric field of 1 V/cm with 6.2 cm

Table 6-3. Input parameters

Symbol	Value
$Q_{\text{in},2}$	1.64 m^3/s
w_{f}	35 wt%
$Q_{\text{m,f}}$	2.46×10^{-4} kg/s
w_{in}	10 wt%
ρ_{in}	1050 kg/m^3
I_1	2.35 A
A_1	1.16 m^2
$\overline{u}_1$	0.508 m/s
$\overline{u}_2$	1.5 m/s
V_{cell}	6.2 V

Table 6-4. Calculation results

Symbol	Value
$Q_{\text{in},1}$	8.19×10^{-7} m^3/s
$Q_{\text{m},1}$	2.44×10^{-8}kg/s
$Q_{\text{m},2}$	4.88×10^{-2}kg/s
$Q_{\text{v},1}$	0.59 m^3/s
$Q_{\text{v},2}$	4273 m^3/s
A_2	2848 m^2
$C_{\text{ppm},1}$	3.2 ppm
$C_{\text{ppm},2}$	896 ppm
P_{req}	29 MW
E_{req}	6.6 Wh/kg_{H_2O}
operation cost	\$ $0.41/10^3 kg_{H_2O}$

electrode spacing and 3 hours residence time. From the experimental results, the thickened clay's production rate was 0.884 kg/h, the final solids content was 35 wt%, the cell potential was 6.2 V, and the average total current was 2.35 A. The on-site projection was based on the Mosaic Four Corners Mine, in which 130,000 GPM clay slurry is produced at a solids content of 2 wt%. The clay flow rate was converted to 26,000 GPM and a solids content of 10 wt% was used in the model. At the mine, ventilation is expected to be produced from wind, and the dewatering areas are anticipated to be covered by a roof structure 3 meters high. Following EPA recommendation for a worst case analysis, a wind velocity of 1.5 m/s was used for the calculations[73]. The relevant parameters are listed in Table 6-3, and the calculated results are listed in Table 6-4. The hydrogen generated

by the electrochemical reaction produces a concentration of 3.2 ppm (0.00032 %) for lab operations, and 900 ppm (0.09 %) for on-site operations. Since the lower flammability limit of hydrogen gas is 4 % by volume of air, the hydrogen concentration generated by the electrokinetic dewatering process is much lower than that required for combustion. Thus, the process should not represent an explosion hazard. As hydrogen is a greenhouse gas, it should be collected and combusted to form water.

CHAPTER 7
CONCLUSIONS

The current design of the electrokinetic dewatering process required three stages of development towards a fully-continuous operation. This involves the semi-continuous prototype for water recovery, the semi-continuous prototype for solids recovery, and the fully-continuous prototype. The experimental results from the water recovery prototype showed that the combination of electrokinetic treatment followed by gravity settling can produce low-turbidity water (pH 11.7) as solids accumulated within the cell. This free-settling observed with the supernatant water could not be achieved by changing the pH and was therefore attributed to changes in the solids characteristics caused by the electrokinetic treatment. The result suggests that fully continuous separation should provide a steady stream of low-turbidity water. This work also suggests that the most effective separation occurred at a flow rate of 40 ml/min (τ=11 h). The pseudo-steady-state condition could not be achieved if the flow rate was increased to 60 ml/min (τ=7.3 h). The energy requirement for the process was competitive with other dewatering strategies, but the power requirement remained high.

The second semi-continuous prototype focused on the removal of the solids in the phosphatic clay suspensions. A 0.37 mm thick conveyor belt with a 50% open area was used to remove the thickened clay. The final solids content of the clay increased with an increase in electric field and residence time, reaching a plateau, given sufficient residence time. The maximum final solids content with extended residence time was dependent only on applied electric field. The relationship between final solids content and $E\tau$ could be described by a empirical equation, which is the constitutive relationship derived by McKinney and Orazem[69] from batch experiments. The optimum operation condition was identified to be at the inflection point for the constitutive relationship. In addition to the electrokinetic dewatering effect, the mechanical design also influenced the final solids content. The final solids content increased as the electrode spacing was reduced from

6.2 cm to 3.2 cm. This reduced spacing caused the top layer of the clay cake to be sliced off, which increased the average solids content of the remaining clay.

The fully-continuous prototype was designed and constructed using the knowledge obtained from the semi-continuous prototypes. The experimental results showed that the fully-continuous prototype was efficient in producing simultaneously low turbidity supernatant water and thickened clay. The supernatant turbidity approached 10 NTU and the clay cake achieved a final solids content of 35 wt% when subjected to an applied electric field of 1 V/cm, and a corresponding energy consumption of 47 Wh/kg_{solids}. A cake formation zone and a cake dewatering zone were identified in the prototype. In the future, the performance of the fully-continuous prototype may be improved by optimizing the cake formation and cake dewatering processes.

CHAPTER 8
SUGGESTIONS FOR FUTURE WORK

The performance of the fully-continuous prototype showed the economic feasibility of electrokinetic dewatering for industrial applications. The energy consumption could be further reduced with improvement to the operational parameters and the mechanical design. The future work is proposed to focus on two aspects: improvement of the fully-continuous prototype and the investigation of using capacitive electrokinetic dewatering.

8.1 Improvements on the Fully-Continuous Prototype

In the fully-continuous prototype, the rigid mesh cathode in the cake dewatering zone produced non-uniform solids content if the thickness of the clay cake was not uniform in the cake formation zone. The average final solids content was thereby reduced due to a rigid mesh cathode. One idea is to use an alternative material for the cathode which possesses flexibility yet still maintains high hydrogen evolution kinetics to produce a small surface over potential at the electrode surface. This flexible cathode would have to be corrosion resistant and inexpensive. Carbon cloth may be a potential alternate cathode material.

The wheels located at the boundary between the cake formation zone and cake dewatering zone provided a simple and efficient design for the proof of concept. However, in some operation conditions under which a high solids content was achieved, the clay cake was blocked between adjacent wheels. This resulted in a reduction in clay production. One suggestion is to remove all the wheels and to insert guider on the sides of the frame to guide the direction of belt movement.

Another potential improvement involves the supernatant water collection region. Addition of a weir around the circumference of the tank would allow collection of the clarified water while blocking entrained large particles. A weir was implemented successfully in the design of the semi-continuous prototype for water recovery.

8.2 Capacitive Electrokinetic Dewatering

The constant DC voltage would be replaced by an intermittent voltage source to reduce the Faradic current associated with the electrochemical reactions. The electrokinetic separation would occur from the effects of both a charging current and a Faradic current. By reducing the Faradic current a reduction in the energy for water electrolysis will result. The ion concentration near the electrode could also be reduced, and the energy consumption decreased by the associated increased resistivity of the suspension. This approach, using intermittent power to reduce the Faradic current, is termed capacitive electrokinetic dewatering.

REFERENCES

[1] F. F. Reuss, "Notice sur un Nouvel Effet de l'électricité Galvanique," *Mémoires de la Société Impériale des Naturalistes de Moscou*, **2** (1809) 327–337.

[2] U. S. Geological Survey, "Phosphate Rock," in *Mineral Commodity Summaries* (U.S. Geological Survey, 1996) 122–123.

[3] U. S. Geological Survey, "Phosphate Rock," in *Mineral Commodity Summaries* (U.S. Geological Survey, 1997) 124–125.

[4] U. S. Geological Survey, "Phosphate Rock," in *Mineral Commodity Summaries* (U.S. Geological Survey, 1998) 124–125.

[5] U. S. Geological Survey, "Phosphate Rock," in *Mineral Commodity Summaries* (U.S. Geological Survey, 1999) 126–127.

[6] U. S. Geological Survey, "Phosphate Rock," in *Mineral Commodity Summaries* (U.S. Geological Survey, 2000) 124–125.

[7] U. S. Geological Survey, "Phosphate Rock," in *Mineral Commodity Summaries* (U.S. Geological Survey, 2001) 120–121.

[8] U. S. Geological Survey, "Phosphate Rock," in *Mineral Commodity Summaries* (U.S. Geological Survey, 2002) 122–123.

[9] U. S. Geological Survey, "Phosphate Rock," in *Mineral Commodity Summaries* (U.S. Geological Survey, 2003) 124–125.

[10] U. S. Geological Survey, "Phosphate Rock," in *Mineral Commodity Summaries* (U.S. Geological Survey, 2004) 122–123.

[11] U. S. Geological Survey, "Phosphate Rock," in *Mineral Commodity Summaries* (U.S. Geological Survey, 2005) 122–123.

[12] U. S. Geological Survey, "Phosphate Rock," in *Mineral Commodity Summaries* (U.S. Geological Survey, 2006) 124–125.

[13] U. S. Geological Survey, "Phosphate Rock," in *Mineral Commodity Summaries* (U.S. Geological Survey, 2007) 120–121.

[14] U. S. Geological Survey, "Phosphate Rock," in *Mineral Commodity Summaries* (U.S. Geological Survey, 2008) 124–125.

[15] U. S. Geological Survey, "Phosphate Rock," in *Mineral Commodity Summaries* (U.S. Geological Survey, 2009) 120–121.

[16] U. S. Geological Survey, "Phosphate Rock," in *Mineral Commodity Summaries* (U.S. Geological Survey, 2010) 118–119.

[17] U. S. Geological Survey, "Phosphate Rock," in *Mineral Commodity Summaries* (U.S. Geological Survey, 2011) 118–119.

[18] U. S. Geological Survey, "Phosphate Rock," in *Mineral Commodity Summaries* (U.S. Geological Survey, 2012) 118–119.

[19] U. S. Geological Survey, "Phosphate Rock," in *Mineral Commodity Summaries* (U.S. Geological Survey, 2013) 118–119.

[20] U. S. Geological Survey, "Phosphate Rock," in *Mineral Commodity Summaries* (U.S. Geological Survey, 2014) 118–119.

[21] U. S. Geological Survey, "Phosphate Rock," in *Mineral Commodity Summaries* (U.S. Geological Survey, 2015) 118–119.

[22] R. C. Specht, "Disposal of Wastes from the Phosphate Industry," *Journal (Water Pollution Control Federation)*, **32** (1960) 964–974.

[23] U. S. Geological Survey, "Phosphate Rock," *Minerals Yearbook. U.S. Geological Survey*, (2011) 56.1–56.11.

[24] M. T. Brown, "Landscape Restoration Following Phosphate Mining: 30 Years of Co-Evolution of Science, Industry and Regulation," *Ecological Engineering*, **24** (2005) 309–329.

[25] C. Barnett, "Mine Field," *Florida Trend: The Magazine of Florida Business*, (2008) 84–90.

[26] S. J. Van Kauwenbergh, J. B. Cathcart, and G. H. McClellan, *Mineralogy and Alteration of the Phosphate Deposits of Florida*, U.S.geological survey bulletin 1914 (U.S. Geological Survey, 1990).

[27] M. Wilson and E. A. Hanlon, *Florida Reclaimed Phosphate Mine Soils: Characteristics, Potential Uses, and Management Considerations*, Technical Report SL370, Soil and Water Science Department, Florida Cooperative Extension Service, Institute of Food and Agricultural Sciences, University of Florida. (2012).

[28] B. M. Moudgil, *Enhanced Recovery of Coarse Particles During Phosphate Flotation*, Technical report, Florida Institute of Phosphate Research (1992).

[29] P. M. Tyler and W. M. H. Waggaman, "Phosphatic Slime," *Industrial and Engineering Chemistry*, **46** (1954) 1049–1056.

[30] T. Tripathy and B. R. De, "Flocculation : A New Way to Treat the Waste Water," *Journal of Physical Sciences*, **10** (2006) 93–127.

[31] M. K. Abd-El Rahman, "Dewatering of Phosphatic Clay Waste by Flocculation," *Chemical Engineering & Technology*, **23** (2000) 457–461.

[32] M. J. Pearse, S. Weir, S. J. Adkins, and G. M. Moody, "Advances in Mineral Flocculation," *Minerals Engineering*, **14** (2001) 1505–1511.

[33] L. Lu, Z. Pan, N. Hao, and W. Peng, "A Novel Acrylamide-Free Flocculant and Its Application for Sludge Dewatering," *Water Research*, **57** (2014) 304–312.

[34] P. A. Vesilind, "The Role of Water in Sludge Dewatering," *Water Environment Research*, **66** (1994) 4–11.

[35] J. Vaxelaire and P. Cézac, "Moisture Distribution in Activated Sludges: A Review," *Water Research*, **38** (2004) 2215–2230.

[36] EPA, *Biosolids Technology Fact Sheet Belt Filter Press*, Technical Report EPA 832-F-00-057, United States Environmental Protection Agency (2000).

[37] J. T. Novak, "Dewatering of Sewage Sludge," *Drying Technology*, **24** (2006) 1257–1262.

[38] EPA, *Biosolids Technology Fact Sheet Centrifuge Thickening and Dewatering*, Technical Report EPA 832-F-00-053, United States Environmental Protection Agency (2000).

[39] H. G. Snyman, P. Forssman, A. Kafaar, and M. Smollen, "The Feasibility of Electro-Osmotic Belt Filter Dewatering Technology at Pilot Scale," *Water Science & Technology*, **41** (2000) 137–144.

[40] B. Peeters, "Mechanical Dewatering and Thermal Drying of Sludge in a Single Apparatus," *Drying Technology*, **28** (2010) 454–459.

[41] A. Mahmoud, J. Olivier, J. Vaxelaire, and A. F. A. Hoadley, "Electro-Dewatering of Wastewater Sludge: Influence of the Operating Conditions and Their Interactions Effects," *Water Research*, **45** (2011) 2795–2810.

[42] A. Volta, "On the Electricity Excited by the Mere Contact of Conducting Substances of Different Kinds. in a Letter From Mr. Alexander Volta, FRS Professor of Natural Philosophy in the University of Pavia, to the Rt. Hon. Sir Joseph Banks, Bart. KBPRS," *Philosophical Transactions of the Royal Society of London*, **90** (1800) 403–431.

[43] W. Horwitz, "The Theory of Electrokinetic Phenomena," *Journal of Chemical Education*, **16** (1939) 519–535.

[44] S. Speil and M. R. Thompson, "Electrophoretic Dewatering of Clay," *Journal of The Electrochemical Society*, **81** (1942) 119–145.

[45] S. Wall, "The History of Electrokinetic Phenomena," *Current Opinion in Colloid & Interface Science*, **15** (2010) 119–124.

[46] D.-H. Kim, B.-G. Ryu, S.-W. Park, C.-I. Seo, and K. Baek, "Electrokinetic Remediation of Zn and Ni-Contaminated Soil," *Journal of Hazardous Materials*, **165** (2009) 501–505.

[47] P. R. Buchireddy, R. M. Bricka, and D. B. Gent, "Electrokinetic Remediation of Wood Preservative Contaminated Soil Containing Copper, Chromium, and Arsenic," *Journal of Hazardous Materials*, **162** (2009) 490–497.

[48] K. Baek, D.-H. Kim, S.-W. Park, B.-G. Ryu, T. Bajargal, and J.-S. Yang, "Electrolyte Conditioning-Enhanced Electrokinetic Remediation of Arsenic-Contaminated Mine Tailing," *Journal of Hazardous Materials*, **161** (2009) 457–462.

[49] X. Mao, J. Wang, A. Ciblak, E. E. Cox, C. Riis, M. Terkelsen, D. B. Gent, and A. N. Alshawabkeh, "Electrokinetic-Enhanced Bioaugmentation for Remediation of Chlorinated Solvents Contaminated Clay," *Journal of Hazardous Materials*, **213** (2012) 311–317.

[50] Y. Guo and J. Q. Shang, "A Study on Electrokinetic Dewatering of Oil Sands Tailings," *Environmental Geotechnics*, **1** (2014) 121–134.

[51] S. Bourgès-Gastaud, G. Stoltz, P. Dolez, E. Blond, and N. Touze-Foltz, "A Laboratory Device to Characterize Electrokinetic Geocomposites for Fluid Fine Tailings Dewatering," *Canadian Geotechnical Journal*, (2014).

[52] A. B. Fourie, D. G. Johns, and C. J. F. P. Jones, "Dewatering of Mine Tailings Using Electrokinetic Geosynthetics," *Canadian Geotechnical Journal*, **44** (2007) 160–172.

[53] J. Lamont-Black, C. J. F. P. Jones, S. Glendinning, D. T. Huntley, and A. B. Fourie, "Laboratory Evaluation of the Potential for Electrokinetic Belt Filter Press Dewatering of Kimberlite Slimes," in *Paste* (2007) 147–152.

[54] J. Q. Shang and E. Mohamedelhassan, "Electrokinetic Dewatering of Eneabba West Mine Tailings: A Laboratory Experimental Study," in *Soft Ground Technology* (American Society of Civil Engineers, 2001) 346–357.

[55] O. Bayat, O. Kilic, B. Bayat, M. Anil, H. Akarsu, and C. Poole, "Electrokinetic Dewatering of Turkish Glass Sand Plant Tailings," *Water Research*, **40** (2006) 61–66.

[56] T. J. Johnson and E. J. Davis, "Experimental Data and Theoretical Predictions for the Rate of Electrophoretic Clarification of Colloidal Suspensions," *Environmental Science & Technology*, **34** (2000) 1806–1812.

[57] T. J. Johnson and E. J. Davis, "Electrokinetic Clarification of Colloidal Suspensions," *Environmental Science & Technology*, **33** (1999) 1250–1255.

[58] T. J. Johnson and E. J. Davis, "An Analysis of Electrophoresis of Concentrated Suspensions of Colloidal Particles," *Journal of Colloid and Interface Science*, **215** (1999) 397–408.

[59] J. Q. Shang, "Electrokinetic Sedimentation: A Theoretical and Experimental Study," *Canadian Geotechnical Journal*, **34** (1997) 305–314.

[60] J. Q. Shang, "Electokinetic Dewatering of Clay Slurries as Engineered Soil Covers," *Canadian Geotechnical Journal*, **34** (1997) 78–86.

[61] J. Q. Shang and K. Y. Lo, "Electrokinetic Dewatering of a Phosphate Clay," *Journal of Hazardous Materials*, **55** (1997) 117–133.

[62] S. Glendinning, J. Lamont-Black, and C. J. F. P. Jones, "Treatment of Sewage Sludge Using Electrokinetic Geosynthetics," *Journal of Hazardous Materials*, **139** (2007) 491–499.

[63] C. J. F. P. Jones, J. Lamont-Black, and S. Glendinning, "Electrokinetic Geosynthetics in Hydraulic Applications," *Geotextiles and Geomembranes*, **29** (2011) 381–390.

[64] S. Glendinning, C. K. Mok, D. Kalumba, C. D. F. Rogers, and D. V. L. Hunt, "Design Framework for Electrokinetically Enhanced Dewatering of Sludge," *Journal of Environmental Engineering*, **136** (2010) 417–426.

[65] M. Y. Ho and G. Chen, "Enhanced Electro-Osmotic Dewatering of Fine Particle Suspension Using a Rotating Anode," *Industrial & Engineering Chemistry Research*, **40** (2001) 1859–1863.

[66] S. Hwang and K.-S. Min, "Improved Sludge Dewatering by Addition of Electro-Osmosis to Belt Filter Press," *Journal of Environmental Engineering and Science*, **2** (2003) 149–153.

[67] M. H. M. Raats, A. J. G. van Diemen, J. Lavén, and H. N. Stein, "Full Scale Electrokinetic Dewatering of Waste Sludge," *Colloids and Surfaces A: Physico-chemical and Engineering Aspects*, **210** (2002) 231–241.

[68] A. B. Fourie and C. J. F. P. Jones, "Improved Estimates of Power Consumption During Dewatering of Mine Tailings Using Electrokinetic Geosynthetics (EKGs)," *Geotextiles and Geomembranes*, **28** (2010) 181–190.

[69] J. P. McKinney and M. E. Orazem, "A Constitutive Relationship for Electrokinetic Dewatering of Phosphatic Clay Slurries," *Minerals & Metallurgical Processing*, **28** (2011) 49–54.

[70] J. P. McKinney and M. E. Orazem, "Electrokinetic Dewatering of Phosphatic Clay Settling Areas: Numerical Simulation and Economic Assessment," *Minerals & Metallurgical Processing*, **28** (2011) 71–76.

[71] R. Kong and M. E. Orazem, "Semi-Continuous Electrokinetic Dewatering of Phosphatic Clay Suspensions," *Electrochimica Acta*, **140** (2014) 438–446.

[72] J. P. McKinney, *Design of Electrolytic Dewatering Systems for Phosphatic Clay Suspensions*, Ph.D. dissertation, University of Florida (2010).

[73] D. A. Crowl and J. F. Louvar, *Chemical Process Safety: Fundamentals with Applications* (Pearson Education, 2001).

BIOGRAPHICAL SKETCH

Rui Kong graduated from China University of Petroleum (East China) with a Bachelor of Science degree in materials chemistry, in July of 2009. She entered graduate school in August of 2009, at the University of Florida, into the Master of Engineering program in Chemical Engineering. Then, she joined Professor Mark E. Orazem's research group for advanced study on the project of phosphatic clay suspension dewatering, sponsored by Mosaic Fertilizer, LLC. She received her M.S. from the University of Florida in the summer of 2011. In August of 2011, she joined the PhD program and continued her research under Professor Orazem's supervision. Rui obtained her PhD in May 2015.